An Intercomparison of Line-by-Line Radiative Transfer Codes for Simulating HIRS Radiances

by

D.S. Turner[a], F. Chevallier[b], L. Garand[c], P. Rayer[d],

N. Scott[e], and P. van Delst[f]

Meteorological Service of Canada

Atmospheric and Climate Science Directorate

Internal Report 01-002

March 2001

a Meteorological Service of Canada (MSC), Downsview, Ontario, Canada

b European Centre for Medium-Range Weather Forecasts (ECMWF), Reading, United Kingdom

c Meteorological Service of Canada (MSC), Dorval, Quebec, Canada

e Centre National de Recherche Scientifique/Laboratoire de Météorologie Dynamique (CNRS/LMD), Palaiseau, France

f Cooperative Institute for Meteorological Satellite Studies/National Oceanic and Atmospheric Administrative/National Center for Environmental Prediction (CIMSS/NOAA/NCEP), Washington, D.C., U.S.A.

ABSTRACT:

This report presents an intercomparison of five line-by-line radiative transfer (LBL) infrared models: 4A, FLBL, GENLN2, LBLRTM and SYNSATRAD. This exercise aims at evaluating the differences between fast models that are due to employing different line-by-line models to construct them. Indeed it was motivated by a comparison of the fast forward models used to process data from the High resolution Infrared Radiation Sounder (HIRS) on board the National Oceanic and Atmospheric Administration's polar orbiting satellites.

A brief description of each of the contributing LBL models is presented, followed by a detailed set of graphs and tables comparing the top of the atmosphere brightness temperatures, the water vapour, ozone and total transmittance profiles, and the water vapour, ozone and temperature Jacobian profiles for a diverse set of 42 profiles and seven HIRS channels (HIRS 2, 5, 9, 10, 11, 12 and 15).

Overall the LBL models agree fairly well, although there is room for improvement. With few exceptions, the LBL radiances for all channels agree to within .5K. Transmittance and Jacobian profiles also tend to agree to within a few percent. As the intercomparison was set up for fast models, it is difficult to ascertain the nature of many of the differences between the LBL models as insufficient information was requested for this purpose.

ABSTRAIT

Ce rapport présente une comparaison de cinq modèles de rayonnement raie-par-raie (RPR) dans l'infrarouge: 4A, FLBL, GENLN2, LBLRTM et SYNSATRAD. Cet exercice vise à évaluer l'impact de l'utilisation de différents modèles RPR pour générer des modèles rapides. Il est motivé par une comparaison de modèles rapides utilisés pour traiter les données de l'instrument HIRS (High resolution Infrared Radiation Sounder) embarqué sur les satellites polaires de la NOAA (National Oceanic and Atmospheric Administration).

Les modèles RPR participants sont présentés. Ensuite, une série de tableaux et de figures détaillent les comparaisons effectuées sur une base de données variée de 42 profils atmosphériques pour sept canaux HIRS (HIRS 2, 5, 9, 10, 11, 12, 15): - températures de brillance au sommet de l'atmosphère, -profils de transmission de la vapeur d'eau, de l'ozone, et profils de transmission totaux, - profils des Jacobiens de vapeur d'eau, d'ozone et de tempéature.

Les modèles RPR sont en bon accord les uns avec les autres, même si des améliorations sont souhaitables. Les luminances des RPR diffèrent en général de moins de 0.5K, quelque soit le canal. Le désaccord entre les transmissions et celui entre les Jacobiens sont inférieurs à quelques pour cent. Comme le protocole de comparaison a été défini pour des modèles rapides, il est difficile de déterminer la nature de plusieurs des différences remarquées entre les RPR.

Table Of Contents

List of Tables

List of Figures

I Introduction

Recently, an intercomparison of radiative transfer models used to process data from channel 12 (6.7μm water vapour band) of the High resolution Infrared Radiation Sounder (HIRS) on board the National Oceanic and Atmospheric Administration's (NOAA) polar orbiting satellites was carried out under GVaP (GEWEX Global Water Vapor Project, Soden et al, 2000). At the Tenth International TOVS Study Conference (ITSC-10, 27 Jan.- 2 Feb. 1999) meeting in Boulder USA, the working group on radiative transfer proposed to extend this intercomparison to several HIRS and AMSU (Advanced Microwave Sounding Unit) channels. The following article is a report on one element of the subsequent intercomparison (Garand et al, 2001); namely, the intercomparison of line-by-line radiative transfer models as applied to the HIRS instrument.

Day-to-day global observations from the HIRS instrument are widely used for obtaining global distributions of temperature, water vapour and ozone for use by the numerical weather prediction (NWP) and climatological communities. These observations constitute a very large volume of data that must be processed quickly and efficiently on an ongoing basis.

The most accurate radiative transfer model is the line-by-line radiative transfer model (LBL). An LBL model simulates high resolution spectra for an optical path from first principle physics. The term line-by-line (LBL) derives from the method by which the absorption coefficient at a specified frequency is explicitly evaluated; that is—, the sum of all contributions from neighbouring spectral lines where each contribution is explicitly determined from the spectral line's theoretical shape, line-strength, spectral position, halfwidth, etc...

Some NWP centres use data assimilation to directly incorporate satellite observations into the prediction model. In this case, both a forward model and a gradient model are required. The forward model is one that simulates the observed brightness temperature from a given atmospheric state. The gradient model, or Jacobian, is the derivative of brightness temperature with respect to the model state variables influencing the radiative transfer equation. It is similar to the so-called weighting function which is the derivative of total

transmittance with pressure, but is more specific since it separately expresses the sensitivity to state variables. In a data assimilation scheme the Jacobian plays a critical role in convergence towards the solution.

Unfortunately LBL's are very computationally intensive. Instead, fast accurate parameterized models designed to simulate the results of an LBL using considerably less computational power than an LBL, and their analytical Jacobians are used in an NWP. Fast models are constructed from LBL simulations and then are analytically differentiated to obtain a fast gradient model. Consequently it is important that rival LBLs produce similar simulations, otherwise the confidence in one's fast model could be undermined.

The purpose of the LBL intercomparison is two-fold. First, to evaluate the level of agreement between the LBLs; this level of agreement provides the LBL modeller a measure of confidence in their model and to provide an opportunity for pinpointing subtle model errors which would otherwise go unnoticed, and to update and improve one's model based on the results of the intercomparison. Second, the LBL intercomparison aids in the interpretation of the observed differences between fast forward models and to access the validity of their gradient models.

Five centres contributed a variety of LBLs to the intercomparison; the European Centre for Medium-Range Weather Forecasts (ECMWF), the Meteorological Office (MO), the Centre National de Recherche Scientifique (CNRS), the Meterological Service of Canada (MSC), and the Cooperative Institute for Meterological Satellite Studies (CIMSS). The LBL models used by each group are; GENLN2 (Edwards, 1992) and LBLRTM (Clough and Iacono, 1995), 4A (Scott et al, 1981), FLBL (Turner, 1995) and SYNSATRAD (Tjemkes and Schmetz, 1997) respectively. The first two are traditional LBLs which derive optical depths directly from spectral line parameters. The second two are faster LBLS which derive optical depths using pre-computed tables (ie, work indirectly from line data). SYNSATRAD is not a full LBL, but its approach as well as its accuracy makes it close to an LBL. More detailed model descriptions follow later.

Each group supplied brightness temperatures for 42 diverse atmospheric states, and for a subset of five atmospheric states; the total (all absorber), water

vapour and ozone transmittance profiles; and the brightness temperature jacobians with respect to the temperature profile, specific humidity profile and ozone specific mass profiles, and with respect to the surface pressure and temperature.

This article is broken into six sections, the introduction, a brief description of line-by-line models, the intercomparison definition, results presented in tabular and graphical form, and finally some discussion and suggestions.

II Brief Description of Line-By-Line Modelling

A line-by-line layer-by-layer radiative transfer model is one that divides an optical path into a series of homogenous cells and determines the total monochromatic optical depth due to all the radiatively active absorbers in each cell. A monochromatic path transmittance or radiance is then evaluated by integrating along the optical path. For example, the top of the atmosphere (TOA) monochromatic radiance, R, from a non-reflecting surface in a non-scattering atmosphere is the sum of the attenuated surface emission plus the attenuated atmospheric emissions; ie,

$$R(\tilde{\nu}) = \Im(\tilde{\nu}, p_s, \vec{u}(p))\, B(\tilde{\nu}, T_s) + \int_{p_s}^{o} B(\tilde{\nu}, T(p))\, \frac{d\Im(\tilde{\nu}, p, \vec{u}(p))}{dp}\, dp \qquad (1)$$

where $\tilde{\nu}$ is the wavenumber, $\Im(\tilde{\nu},p,\vec{u}(p))$ is the total transmittance from a pressure p to space, and $B(\tilde{\nu},T(p))$ is the Planck function[1] evaluated at temperature T. The subscript s refers to the surface, and $\vec{u}$ is a vector whose elements are the absorber amounts of the radiatively active absorbers being considered.

The total transmittance is related to the incremental optical depth, χ, along the optical path, by

$$\Im(\tilde{\nu}, p, \vec{u}) = e^{-\int_{p}^{o} \chi(\tilde{\nu}, p, \vec{u})\, dp} \qquad (2)$$

---

[1] This work assumes the entire atmosphere is in local thermal equilibrium (LTE). Otherwise a function other than B would have to be specified.

A spectra results when Eq.1 is evaluated on a grid of closely spaced wavenumbers, typically on the order of .001(cm^{-1}). When a mean transmittance or radiance is required, the spectra is convolved with a response function, $\phi(\tilde{\nu})$, and integrated across wavenumber space; ie,

$$\overline{R} = \int_{\Delta\tilde{\nu}} \phi(\tilde{\nu})\, R(\tilde{\nu})\, d\tilde{\nu} \quad \text{or} \quad \overline{\Im}(p) = \int_{\Delta\tilde{\nu}} \phi(\tilde{\nu})\, \Im(\tilde{\nu}, p, \vec{u})\, d\tilde{\nu} \tag{3}$$

The method of breaking an optical path into a string of cells is not unique to LBLs; hence the various methods will not be discussed here. Rather the method of obtaining high resolution spectra or mean radiances/transmittances that defines an LBL is discussed.

The total monochromatic optical depth of a cell, $\chi(\tilde{\nu})$, is the sum of the product of a cell's monochromatic absorption coefficient, $k(\tilde{\nu})$ and absorber amount, u, for each radiatively active absorber. A cell's optical depth is defined as the sum of the contributions due to spectral lines, continua, cross-sections and line mixing; ie,

$$\begin{aligned}\chi_i(\tilde{\nu}) = & \sum_{j=1}^{N_{gas}} \sum_{\ell=1}^{N_{line}} S(\tilde{\nu}_{o\ell j}, T_{ij})\, f(\tilde{\nu}-\tilde{\nu}_{o\ell j}, p_{ij}, T_{ij}, u_{ij})\, u_{ij} + \\ & \sum_{j=1}^{N_{con}} k_{ij}^{con}(\tilde{\nu}, p_{ij}, T_{ij}, u_{ij})\, u_{ij} + \sum_{j=1}^{N_{x\text{-}sec}} k_{ij}^{x\text{-}sec}(\tilde{\nu}, p_j, T_{ij}, u_{ij})\, u_{ij} + \\ & \sum_{j=1}^{N_{gas}} k_{ij}^{LM}(\tilde{\nu}, p_{ij}, T_{ij}, u_{ij})\, u_{ij}\end{aligned} \tag{4}$$

where S is the strength of a line, $f(\tilde{\nu}-\tilde{\nu}_{oj})$ is the shape function, $\tilde{\nu}_o$ is the position of line ℓ and absorber j, k^{con} is the absorption coefficient due to a continuum, $k^{x\text{-}sec}$ to a cross section and k^{LM} to line-mixing.

Although relatively innocuous in appearance, this equation is computationally intensive and is the fundamental reason why parameterized models are currently preferred over LBLs for general applications.

The first term of Eq.4 is the contribution to the absorption coefficient at a specific wavenumber due to neighbouring spectral lines; hence the term LBL. Neighbouring lines are defined by a radius of influence, which defines the region

where a line's contribution is non-negligible. The radius of influence is determined from the strong lines in a region as their influence can be perceived from a greater distance than weak lines. Typically tens of thousands of lines contribute to k at $\tilde{\nu}$.

The shape function is generally a Voigt function, although there are a few other functions it can follow (Doppler, Lorentz, etc...). The Voigt function is a non-analytic integral; consequently it must be evaluated for every single line contributing to $\tilde{\nu}$. Considering the number of summations required to evaluate the contribution to k at just one wavenumber for one cell, it is easy to see why an LBL consumes vast amounts of computational resources when it simulates a spectrum for a heterogenous path.

The second term covers two types of continua, ones where the physics is not very well known and ones where the physics is known. Occasionally, when an LBL simulation assuming a basic shape function is compared to laboratory observations, very conspicuous discrepancies[2] appear. Sometimes this discrepancy can be reduced to a tolerable level by modifying the shape function with a chi-factor, C; ie, $f(\tilde{\nu}-\tilde{\nu}_0)C(|\tilde{\nu}-\tilde{\nu}_0|)$. The effect of the chi-factor is to make the line wings more absorbing (super-Lorentzian) or less absorbing (sub-Lorentzian).

More frequently a parameterization that is slowly varying with respect to wavenumber is fitted to the discrepancies. Water vapour, a particularly glaring example, is an example of correcting for what appears to be super-Lorentzian behaviour using a continuum-like parameterization. Most LBLs employ a version of the Clough-Kneizys-Davies (CKD) water vapour continuum parameterization (Clough et al, 1989). CKD-like parameterizations can also be used to parameterize other absorbers' discrepancies, ie CO_2 and N_2.

There are absorbers, such as N_2 and O_2, which have true continuums in the infrared that are induced by collisional processes. Traditionally, the N_2 continuum has been handled by a CKD-like parameterization, but recently the

---

[2] In the case of CO_2, the discrepancies can be largely attributed to line-mixing which is difficult to implement; eg, P-R branch mixing (Strow, private communication).

continuum has been measured and parameterized[3] (Lafferty et al, 1996).

The most commonly used parameterization for the observed O_2 continuum was introduced many years ago by Timofeyev and Tonkov (1978). However this continuum has been recently re-evaluated and a new parameterized model has been made available[3] (Thibault et al, 1997).

The third term covers absorption due to cross-sections. For many heavy molecules the spectral lines are so dense that they can not be resolved by current spectroscopy. The absorption coefficients for such spectra are available as absorption cross-sections which are treated in a manner similar to continua.

The final term listed is for molecules which exhibit line-mixing (also known as line-coupling). Line-mixing occurs when the spectral transitions can no longer be considered independent of each other. This most commonly occurs in Q-branches and is pressure-dependent. The evaluation of the absorption coefficient due to line-mixing is very complex, involving the manipulation of matrices comprising all the spectral line data for a given band. Line-mixing in CO_2 has been identified as a factor to be considered for high resolution instruments (Strow and Reuter, 1988). There are two models available for Q-branch mixing, J-M Hartman[3], or L.L. Strow[4].

The spectral line parameters (line position, half-widths, etc...) as a function of absorber are generally provided from one of two sources, HITRAN (Rothman et al, 1998) and/or GEISA (Jacquinet-Hussen et al, 1999). Cross-section absorption spectra are also available from these sources. These compilations represent the work of many researchers, both theoretical and experimental. Both compilations are constantly updated and contain similar data. The main difference between the two are the criteria that must be met in order to be incorporated into the database.

The pressure and temperature dependencies in Eq.4 are generally the mass weighted pressure and temperature of a cell. An LBL may use a simple or more

---

[3] Interested parties can contact J-M Hartmann, Laboratoire de PhotoPhysique Moleculaire, University Paris-Sud, France (jean-micheal.hartmann@ppm.u-psud.fr)

[4] Interested parties can contact L. Strow, Physics Dept, University of Maryland Baltimore County, MD, USA (strow@umbc.edu).

complex method for estimating these values. The cell's absorber amounts are determined from the pressure, temperature, volume mixing ratios and the physical path length of a cell[5]. If radiances are being determined, then the Planck emission temperature is the value used for evaluating the absorption coefficient.

Finally it should be pointed out that LBLs are not very well calibrated against reality in a grand sense; that is— against a well calibrated spectrometer viewing a well defined path[6]. However much laboratory work has been done to validate LBLs against measurements in the laboratories for various homogenous paths, albeit short ones. Sufficient laboratory work has been done that one generally has a high level of confidence in an LBL when it is used to predict the observed radiance from a chain of heterogenous mixed path cells (ie, a true atmospheric path).

IIa Brief Description of the Contributing LBL Models

GENLN2 and LBLRTM are traditional LBLs that determine the optical depths directly from spectral databases whereas 4A, FLBL and SYNSATRAD do not. In order to reduce the computational time, FLBL, SYNSATRAD and 4A simply replace the time consuming summations of Eq.4 with pre-computed lookup tables. The lookup tables are constructed on a high resolution grid utilizing an LBL that calculates absorption coefficients directly from the spectral databases. The tables for FLBL, 4A and SYNSATRAD are pre-computed using GENASIS (Turner et al, 1996), STRANSAC (Scott, 1974) and LBLRTM (Clough and Iacono, 1995) respectively.

The FLBL uses high resolution lookup tables of absorption coefficients to replace the summations over lines for a particular absorber. By assuming that k is independent of u, then Eq.4 simplifies to:

---

[5] Note that there are other sets of variables from which the absorber amount can be determined, eg: density, pressure and specific mass.

[6] Ideally it would be gratifying to have a very long white cell (a km or so) partitioned off into individual well controlled cells to mimic a long heterogenous path that varies in pressure, temperature and absorbers.

$$\chi_i(\tilde{\nu}) = \sum_{j=1}^{N_{gas}} k_{ij}(\tilde{\nu}, p_{ij}, T_{ij})\, u_{ij} \quad , \quad \text{where} \quad k_{ij} = k_{ij}^{line} + k_{ij}^{con} + k_{ij}^{x\text{-}sec} + k_{ij}^{LM}$$

k cannot always be assumed independent of u, however there are methods of getting around the problem (Turner, 1995). The tables are functions of wavenumber, pressure and temperature. The assumption of a k independent of u and the bi-cubic interpolation within the table to the desired p and T are the only differences between the FLBL and a tradition LBL.

SYNSATRAD is very similar to the FLBL in that it also uses absorption coefficient lookup tables to replace the explicit absorption coefficient calculation. SYNSATRAD differs from the other LBLs in that its products are a mean radiance or transmittance for a specific instrument channel; that is —, it cannot recreate a high resolution spectrum. This restriction is due to SYNSATRAD operating on a much sparser wavenumber grid; usually two or three orders of magnitude less than that of a traditional LBL.

The vastly reduced wavenumber set is chosen by utilizing the radiance sampling method (Tjemkes and Schmetz, 1997). This procedure can be simply visualized by considering the numerical wavenumber integration of a traditional high resolution LBL; ie,

$$\overline{R} = \sum R(\tilde{\nu}_i)\, \Delta\tilde{\nu}_i$$

SYNSATRAD's reduced grid is basically found by locating and discarding the negligible terms of $\overline{R}$ until an acceptable error relative to the correct answer is met. Once a reduced wavenumber set has been found the absorption coefficient lookup tables are created containing only those wavenumbers left in the summation. As with the FLBL there is a table for each absorber.

4A relies on tables of high resolution optical depths for a set of twelve nominal atmospheres on a fixed pressure grid for each absorber. The optical depths for the atmosphere of interest are determined by linearly interpolating for temperature between atmospheres at each pressure level and re-scaling the

optical depth for each absorber. Once the high resolution optical depths have been created, 4A proceeds like a traditional LBL. As with the FLBL there is a table for each absorber. It should be noted that unlike the other models, 4A has the capability to calculate Jacobians by analytical means.

The five LBL-class models that participated in the intercomparison are summarized in Table 1. Tabulated with each model are; the researcher who submitted results, any special considerations taken for H_2O, CO_2, O_2 and N_2; the spectral line data compilations used; and a reference. Henceforth, the models will be referred to by the abbreviated name in parentheses found in the first column beside the model's full name.

Model	Contributor	Continuum H2O	O2	N2	CO2	Spectral Database	Reference
GENLN2 4.0 (GEN2)	Rayer	2.1	TT	N	b	HITRAN 96	Edwards (1992)
4A_00 LBL (4A)	Scott	2.1	TT	L	c	GEISA 97	Scott et al. (1981)
FLBL_00 (FLBL)	Turner	2.1	T	L	b	HITRAN 96	Turner (1995)
LBLRTM (RTM)	van Delst	2.2	T	L	a	HITRAN 96	Clough and Iacono(1995)
SYNSATRAD (SYNS)	Chevallier	2.2	T	L	a	LBLRTM	Tjemkes and Schmetz (1997)

Table 1: List of contributing models to the intercomparison and some of their characteristics. The first two columns name the model and contributor. Under the heading Continuum are listed the parameterizations used for each of the four continuums. The number under H2O indicates the version of the Clough-Kneizys-Davies (CKD, Clough et al, 1989) used. Under O2, a T or TT indicates the O_2 continuum parameterization used, Thibault et al (1997) or Timofeyev and Tonkov (1978). Under N2, an N or L indicates the N_2 parameterization used; a parameterization similar to CKD, or Lafferty et al (1996). Under CO2, an a, b or c indicates the parameterization used to account for anomalous behaviour in CO_2; a) use of an anomalous continuum similar to CKD (Ridgeway et al, 1981); b) for lines $\leq$ 1000 (cm^{-1}) contributions are truncated at 385 Lorentz halfwidths from line centre and for lines $\geq$ 2000 (cm^{-1}) the shape functions are modified by Cousin's chi-factors (Cousin et al, 1985); and c) for the CO_2 15μm band, the Rodrigues line coupling formulation is used (Rodrigues et al, 1999,) and for lines $\geq$ 2000(cm^{-1}), the shape functions are modified by Perrin's chi-factors (Perrin et al, 1989). In the column labelled Spectral Database, the name of the spectral database used, HITRAN or GESIA. The two digits refer to the year the database was released. The last column furnishes a reference for each model.

III INTERCOMPARISON DEFINITION

The definition of the intercomparison is primarily driven by the fast model community's requirements to assess their role in numerical weather prediction models.

Unfortunately LBLs are not suitable at this time for real-time processing due to the large number of spectral lines and their possible overlaps which requires unacceptable amounts of computational resources, especially when computing Jacobians. Consequently, processing requires a fast and accurate radiative transfer model to simulate the satellite observations.

In general, a fast forward model consists of a fast transmittance model and an algorithm to evaluate the radiative transfer integral of Eq.1, which would include a Planck function. The fast transmittance model is typically constructed from a database of suitable atmospheric states and their LBL simulated transmittances. The gradient or K-model is then by analytical differentiation of the fast forward model. In some cases, (eg; MSC or ECMWF NWP models) the gradient model may be more easily constructed from the adjoint of the forward model if it is readily available.

The common quantities required from an LBL to construct a fast model are transmittance profiles and brightness temperatures. As a fast gradient model is not directly derived from an LBL, it is useful to have LBL simulations of brightness temperature Jacobians available to compare with. With this in mind, the radiative transfer quantities selected for the intercomparison are; brightness temperature, water vapour transmittance, ozone transmittance and total transmittance profiles; and brightness temperature jacobians with respect to surface temperature, surface pressure, atmospheric temperature, atmospheric water vapour and atmospheric ozone.

The water vapour and ozone components have been included since they are treated separately by most fast models. Other absorbers, which are considered non-varying are generally lumped together and treated as a single entity.

IIIa) Channel Selection

In order to reduce the computational work load, it was decided that only seven HIRS channels from NOAA-14 would be considered. These channels were chosen as the most representative to study the impact on the quality of radiative transfer models with respect to temperature, humidity and ozone. The chosen

seven are; HIRS-2, HIRS-5, HIRS-9, HIRS-10, HIRS-11, HIRS-12 and HIRS-15. The significant absorbers for these channels, a brief description of the channel's intended purpose and the channels typical pre-launch noise equivalent temperatures (Saunders et al, 1999) are listed in Table 2. A plot of the seven response functions can be found in figure 1.

HIRS	NEΔT K	Band Correction Coef's $\tilde{\nu}_c$	b	c	Major Absorbers	Purpose
2	.44	679.36	.99997	.000	CO2 H2O O3	stratospheric temperature sounding
5	.09	714.50	.99997	-.014	CO2 H2O O3	mid-tropospheric temperature sounding
9	.03	1028.30	.99980	.050	O3 H2O CO2	total O3 sounding
10	.07	796.04	.99990	.021	H2O CO2 O3	lower tropospheric H2O sounding
11	.11	1361.00	.99971	.073	H2O CH4 CO2	mid-tropospheric H2O sounding
12	.30	1481.00	.99931	.284	H2O O2 CH4	upper tropospheric H2O sounding
15	.06	2236.40	.99998	.024	CO2 N2O N2 H2O CO	mid-tropospheric temperature sounding

Table 2: Features of the HIRS channels. Listed are typical pre-launch noise equivalent temperature, NEΔT, for a typical target temperature, the central wavenumber of the response function, $\tilde{\nu}_c$, the major absorbers, and the intended purpose of the channel. $\tilde{\nu}_c$, b and c are the band correction coefficients (Planet, 1988) used to convert radiance to brightness temperature and vice versa.

IIIb) Selection of Atmospheric States

As mentioned earlier, the fast transmittance model is typically constructed from a database of representative atmospheric states. A widely diverse set of forty-two atmospheric states was selected from a working set of 189 states which was developed at MSC (Turner, 1997). Each atmospheric state consists of an altitude profile, a common pressure profile (Table 3), temperature profile and volume mixing ratio profiles for each of H_2O, CO_3, O_3, N_2O, CO, CH_4, O_2 and N_2.

0.10	0.29	0.69	1.42	2.61	4.41	6.95	10.37
14.81	20.40	27.26	35.51	45.29	56.73	69.97	85.18
102.05	122.04	143.84	167.95	194.36	222.94	253.71	286.60
321.50	358.28	396.81	436.95	478.54	521.46	565.54	610.60
656.43	702.73	749.12	795.09	839.95	882.80	922.46	957.44
985.88	1005.43	1013.25					

Table 3: Set of pressure levels that all profiles are defined on.

The scatter plots of figures 2 and 3 illustrate the range of temperatures and volume mixing ratios within the 42 states. A more detailed description of how

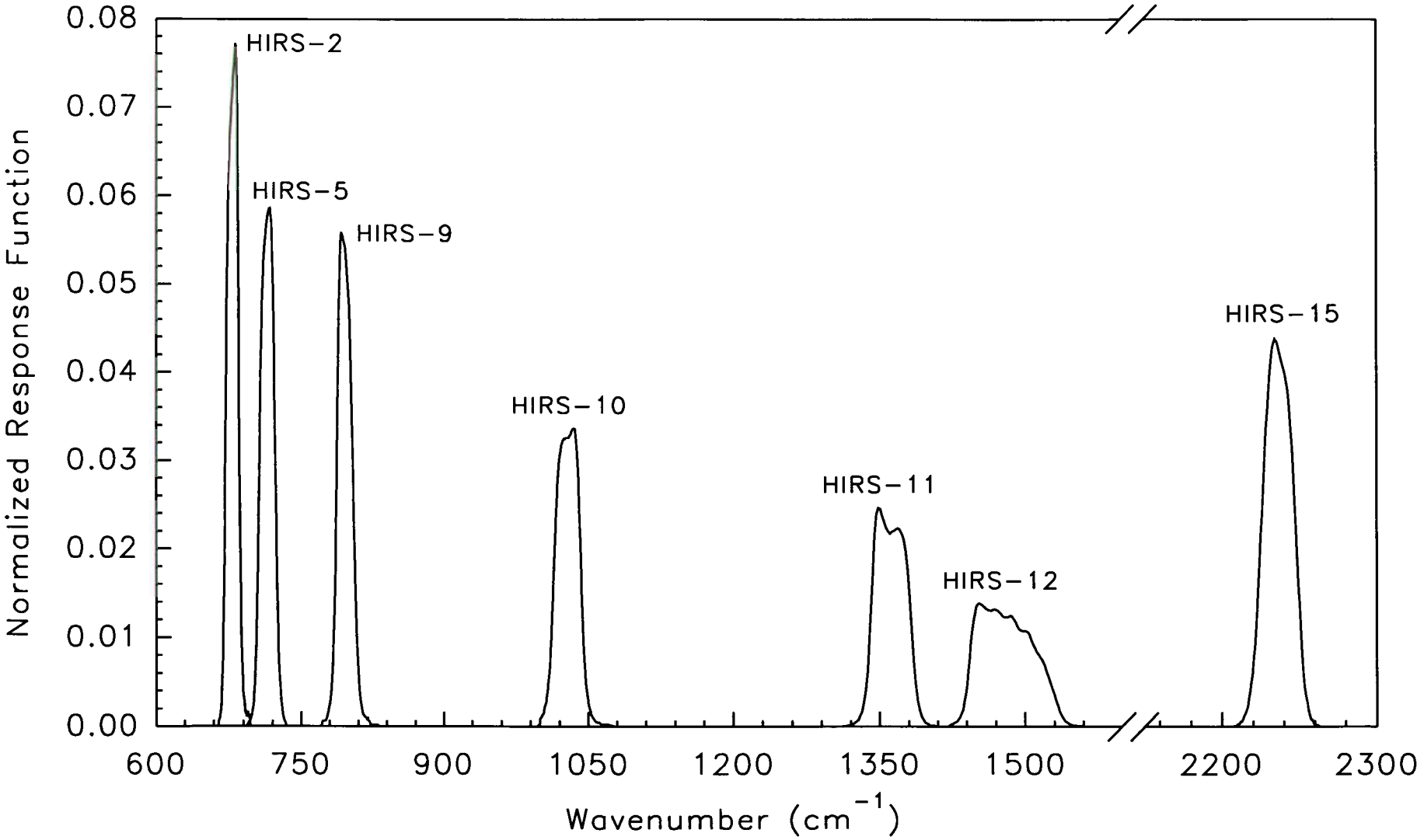

Fig 1: NOAA-14 response functions used in the LBL intercomparison

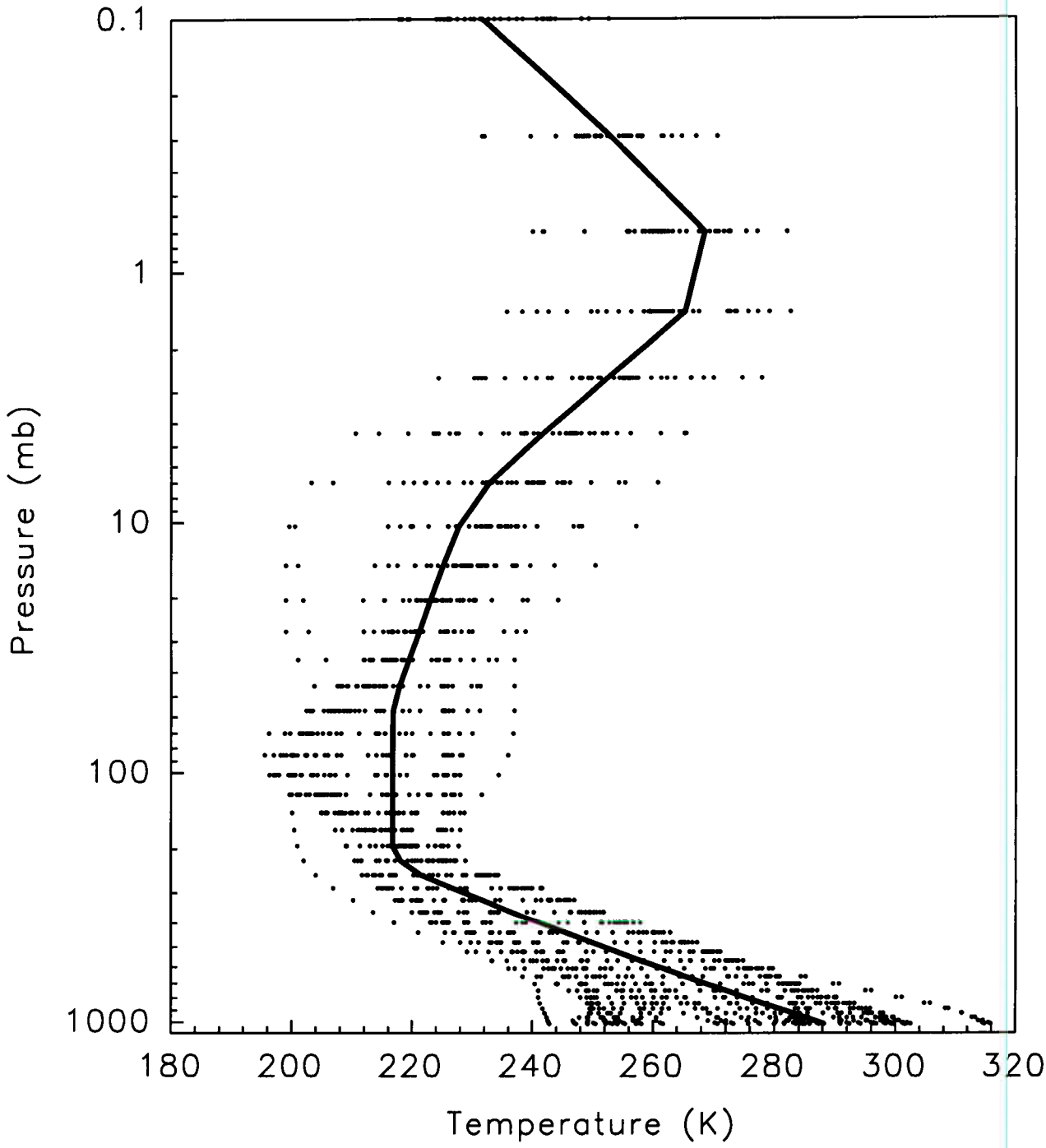

Fig 2: Scatter plot of the 42 atmosphere's temperature profiles as a function of pressure. The solid line is the US standard atmosphere.

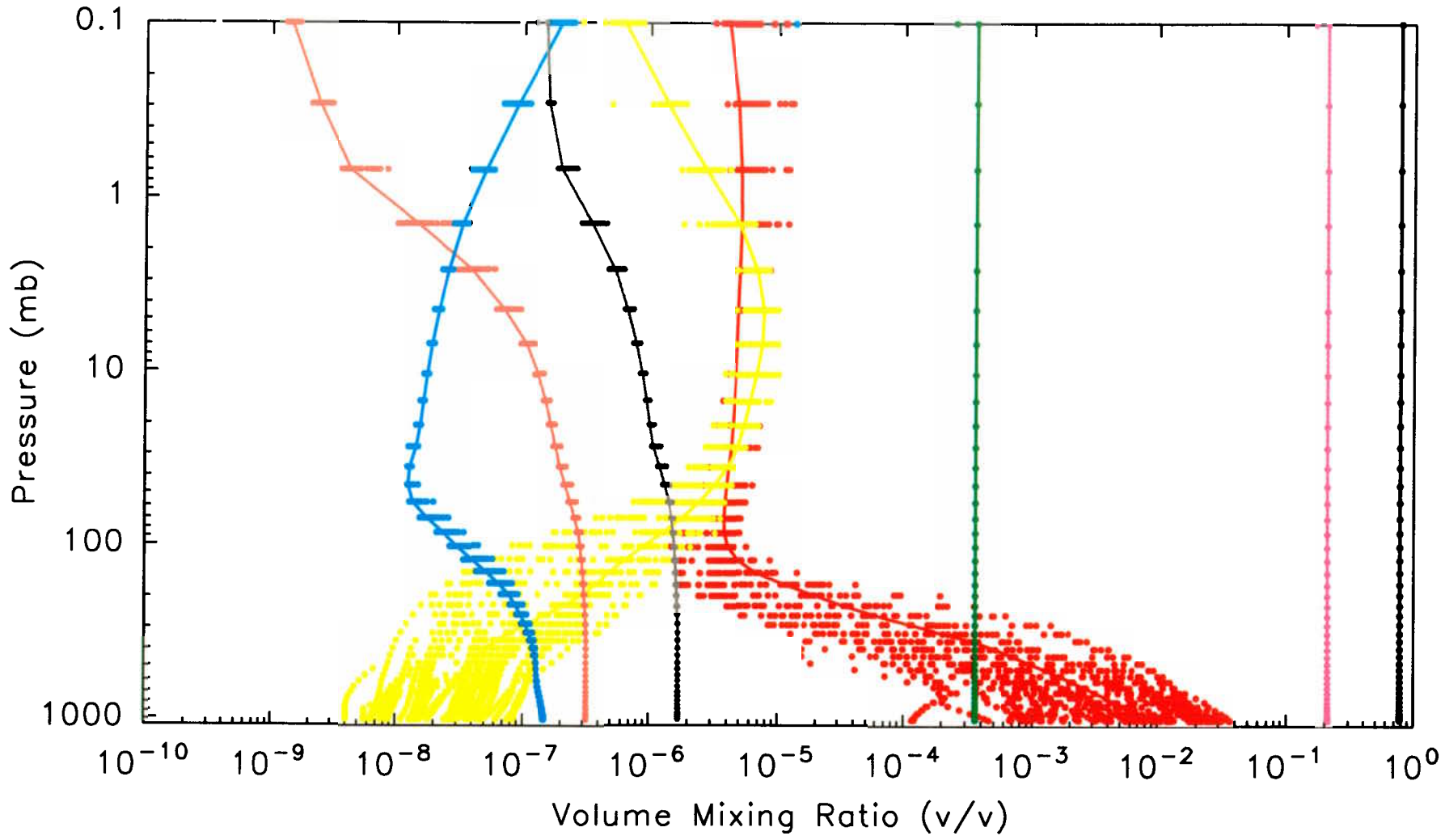

Fig 3: Scatter plot of the 42 atmosphere's volume mixing ratio profiles as a function of pressure. Solid lines belong to the US Standard Atmosphere (Profile 6)

H_2O · CO_2 O_3 N_2O · CO · CH_4 O_2 · N_2

the states for this study were selected can be found in Appendix I. The surface temperature and column amounts (defined in appendix I) for each state is tabulated in table 4.

State	Tsurf K	H2O amt kg/m**2	O3 amt DU	MW temp K	State	Tsurf K	H2O amt kg/m**2	O3 amt DU	MW temp K
1	299.71	40.73	276.35	258.34	22	314.81	19.63	268.59	264.46
2	294.21	29.06	330.47	258.07	23	299.50	22.01	231.13	259.92
3	272.07	8.33	373.74	244.55	24	281.69	33.88	230.69	255.56
4	287.35	21.04	343.48	253.97	25	292.38	37.26	270.62	255.71
5	257.24	4.07	371.23	237.60	26	296.87	44.95	255.76	258.17
6	**288.20**	**14.12**	**340.24**	**250.35**	27	301.43	52.20	270.68	259.84
7	247.28	3.11	205.76	227.52	28	301.84	59.90	255.72	260.41
8	242.85	.62	483.99	232.16	29	298.42	61.46	217.91	259.17
9	258.09	8.25	334.23	236.83	**30**	**301.63**	**70.93**	**239.05**	**260.72**
10	258.08	3.00	320.58	238.16	**31**	**250.50**	**1.74**	**222.45**	**232.41**
11	275.78	6.95	355.72	242.46	32	299.35	26.60	255.23	259.91
12	277.65	9.73	343.72	243.14	33	296.28	37.28	276.41	257.55
13	280.02	9.93	272.36	246.14	34	283.58	11.98	286.54	247.04
14	284.25	15.22	364.09	251.57	35	273.30	7.73	316.99	244.92
15	284.71	25.98	262.72	254.00	36	254.19	3.73	338.43	238.02
16	285.85	16.57	242.27	256.46	37	261.64	5.21	371.26	241.14
17	302.54	51.08	235.93	259.79	38	270.65	3.83	384.34	237.04
18	**315.91**	**33.11**	**271.29**	**263.94**	39	254.14	2.29	417.85	234.80
19	**252.19**	**2.35**	**492.78**	**234.45**	40	249.20	.80	449.24	236.19
20	290.94	10.19	235.02	258.06	41	253.27	1.98	470.76	236.98
21	285.11	12.91	331.06	248.73	42	255.37	.66	494.79	235.29

Table 4: Tabulation of the surface temperature, column amount of water vapour, column amount of ozone and the column mass weighted temperature for each of the 42 atmospheres used in this study. The members of the five state subset are highlighted in bold.

The simulation of Jacobians with an LBL requires considerably more computational resources than the forward calculation. In order to maintain a reasonable computational workload, a smaller subset of five states was chosen for simulating Jacobians. The subset was chosen to represent an average state and extreme cases in H_2O and O_3 column amount. These atmospheres (6, 18, 19, 30 and 31) are illustrated in figure 4 and highlighted in table 4.

IIIc) Brightness Temperature

For this study the atmosphere is assumed to be cloudless, non-refracting, non-scattering and the planetary surface is assumed to have an emissivity of 1. The unit emissivity implies that all reflected solar and atmospheric downwellings are neglected. Only nadir views are simulated. The mean radiance, $\overline{R}$, is evaluated by integrating Eq.1 across an instrument response function, ϕ; ie,

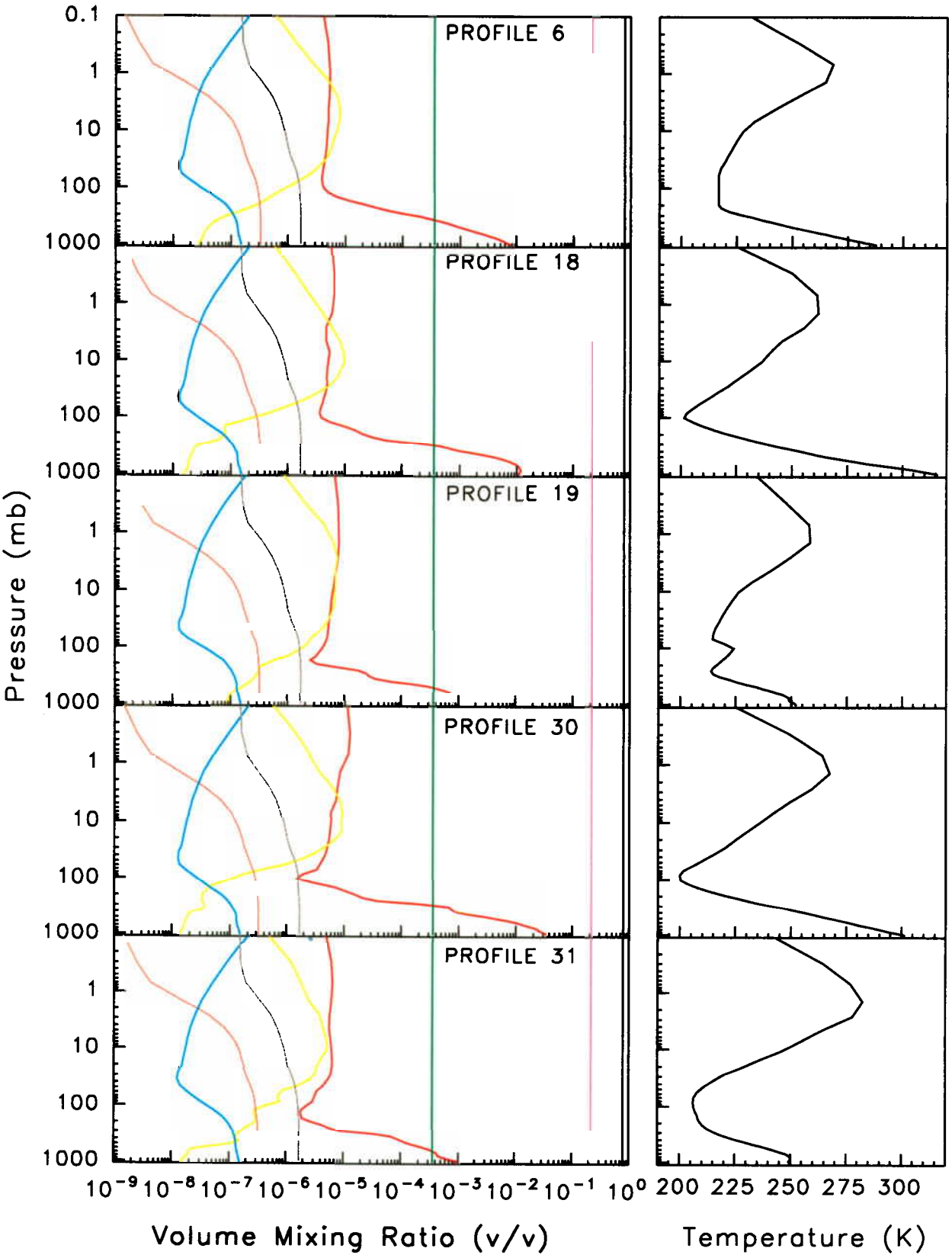

Fig 4: The subset of 5 volume mixing ratio and temperature profiles. (see fig 3 & 2)

$$\overline{R} = \int_{\Delta\tilde{\nu}} \phi(\tilde{\nu})\, B_s(\tilde{\nu}, T(p_s))\, \Im(\tilde{\nu}, p_s, \vec{u})\, d\tilde{\nu} + \int_{\Delta\tilde{\nu}} \phi(\tilde{\nu}) \int_{p_s}^{\infty} B(\tilde{\nu}, T(p))\, d\Im(\tilde{\nu}, p, \vec{u})\, d\tilde{\nu}$$

where $\Delta\tilde{\nu}$ denotes the region of spectral integration; ie, the width of the response function.

The spectra of the various radiatively active absorbers do not necessarily exist in all of the regions defined by the chosen response functions, hence they do not have to be considered by the LBL. The absorbers chosen to represent each channel varies slightly from LBL to LBL and are listed in Table 5.

An LBL simulates radiances; however for comparisons it is more convenient to compare equivalent brightness temperatures, since it behaves more linearly than radiances[7]. The equivalent brightness temperature, T_b, is defined indirectly through the equation,

$$\overline{R} = \int \phi(\tilde{\nu})\, B(\tilde{\nu}, T_b)\, d\tilde{\nu}$$

where the Planck function evaluated at the brightness temperature.

	GENLN2								4A								FLBL								RTM								SYNS							
HIRS	1	2	3	4	5	6	7	8	1	2	3	4	5	6	7	8	1	2	3	4	5	6	7	8	1	2	3	4	5	6	7	8	1	2	3	4	5	6	7	8
2	y	y	y						y	y	y	y		y			y	y	y	y		y			y	y	y	y		y				y						
5	y	y	y						y	y	y	y		y			y	y	y	y		y			y	y	y	y		y			y	y	y					
9	y	y	y						y	y	y						y	y	y						y	y	y						y		y					
10	y	y	y						y	y	y	y		y			y	y	y	y		y			y	y	y	y		y			y	y						
11	y	y			y	y			y	y	y	y		y	y		y	y	y	y		y	y		y	y	y	y		y	y		y						y
12	y	y			y	y			y	y				y	y		y					y	y		y	y				y	y		y						
15	y	y		y				y	y	y	y	y	y	y		y	y	y	y	y	y	y		y	y	y	y	y	y	y		y								

Table 5: Table of absorbers used by the models by channel.
1-H_2O 2-CO_2 3-O_3 4-N_2O 5-CO 6-CH_4 7-O_2 8-N_2

Transforming between a mean radiance and brightness temperature is slow and cumbersome. An alternate method which does not require wavenumber integration is described in Planet (1988). This method is defined by the equations:

---

[7] This convenience extends to the bias correction schemes within a data assimilation system.

$$\overline{R} = \frac{c_1 \tilde{\nu}_c^3}{\exp\left[\frac{c_2 \tilde{\nu}_c}{T_b}\right] - 1}, \quad \textit{and} \quad T_b = \frac{1}{c} \frac{c_2 \tilde{\nu}_c}{ln\left[1 + \frac{c_1 \tilde{\nu}_c^3}{\overline{R}}\right]} - b$$

where c_1 and c_2 are constants[8]. $\tilde{\nu}_c$, b and c, are the band correction coefficients and are specific to a response function. The coefficients for the HIRS channels are tabulated in Table 2.

IIId) Transmittance Profiles

The mean total transmittance profile is simply the wavenumber integration of Eq.2; ie,

$$\overline{\Im}(p, \vec{u}) = \int_{\Delta\tilde{\nu}} \phi(\tilde{\nu})\, \Im(\tilde{\nu}, p, \vec{u})\, d\tilde{\nu}$$

In addition to the mean total transmittance profile, contributors were asked to supply mean water vapour and mean ozone transmittance profiles. These transmittances are evaluated exclusive of the other absorbers; ie,

$$\overline{\Im}(p, u_{H_2O}) = \int_{\Delta\tilde{\nu}} \phi(\tilde{\nu})\, \Im(\tilde{\nu}, p, u_{H_2O})\, d\tilde{\nu} \quad \text{and} \quad \overline{\Im}(p, u_{O_3}) = \int_{\Delta\tilde{\nu}} \phi(\tilde{\nu})\, \Im(\tilde{\nu}, p, u_{O_3})\, d\tilde{\nu} \ .$$

Appraising a plot of the difference between two or more models' transmittance profiles is difficult if the transmittance profiles are very similar, as is the case for many of the plots presented here, and in the asymptotic regions where large relative differences may have no impact. For example: Although the relative difference between 10^{-3} and 10^{-4} is large, there is little impact on the brightness temperature. A plot of the difference between a model's effective optical depth profile, $\overline{\chi}$, and that of the reference model has no asymptotes, thus the behaviour between models can be examined more effectively in these regions.

Effective optical depth differences are defined as;

$$\Delta\overline{\chi}_X = -\ln(\overline{\Im}_X) + \ln(\overline{\Im}_{GENLN2}) \qquad X = SYNS,\ 4A,\ FLBL,\ RTM$$

[8] $c_1 = 1.1910439 \times 10^{-8}$ W/m^2/(cm^{-1})^4 and $c_2 = 4.387691$ (cm^{-1})K

IIIe) Sensitivity (Jacobians)

With the exception of the 4A model, the LBL's do not directly calculate Jacobians. The Jacobian is evaluated by numerical differentiation; ie,

$$\frac{\partial T_b}{\partial x_j} = \frac{T_b(x_j+\delta x_j) - T_b(x_j-\delta x_j)}{2\,\delta x_j}$$

where $T_b(x_j+\delta x_j)$ and $T_b(x_j-\delta x_j)$ are LBL simulations of an atmosphere where the parameter x has been perturbed by $\pm\delta x$. The subscript j can represent a surface parameter or a level in the atmosphere.

The values of δx employed in this study are; δT_s=.5K, δp_s=.5mb and δT_j=.5K. The specific mass profiles are perturbed by 5%, ie, δq=.05q. The profiles were perturbed at every pressure level thereby creating a Jacobian profile.

Comparing the magnitude of various Jacobians is difficult since the units are different, thus it is more convenient to examine sensitivities. The sensitivity is a re-scaling of the Jacobian into comparable units and is defined as the change in brightness temperature due to a change in x.

The sensitivities of the surface temperature, surface pressure, temperature profile, specific humidity profile and the ozone specific mass profile are defined as;

$$S_{T_s} = \Delta T_s \frac{\partial T_b}{\partial T_s}, \quad S_{p_s} = \Delta p_s \frac{\partial T_b}{\partial p_s}, \quad S_T = \Delta T \frac{\partial T_b}{\partial T_j}, \quad S_{H_2O} = a\,q_j^{H_2O} \frac{\partial T_b}{\partial q_j^{H_2O}}, \quad S_{O_3} = a\,q_j^{O_3} \frac{\partial T_b}{\partial q_j^{O_3}}$$

where q_j^{H2O} is the specific humidity and q_j^{O3} is the specific mass of ozone. a, ΔT, Δp_s and ΔT_s are constants set to .1 (10%), 1K, 1mb and 1K, respectively.

IIIf) Summary of Submissions

HIRS brightness temperatures for all 42 atmospheres, total, H_2O and O_3 transmittance profiles, and brightness temperature Jacobians with respect to surface temperature, surface pressure, temperature, H_2O and O_3 for five atmospheres were submitted by contributors where possible. No O_3 data were requested for HIRS-10, HIRS-11, HIRS-12 and HIRS-15, since O_3 doesn't play a significant role in these channels.

Table 6 summarizes the results that were supplied by each contributor. Some elements were not submitted as some models were not set up to simulate all the requested radiative quantities. For example, SYNSATRAD doesn't exist for HIRS-15.

HIRS		Total Transmittance 6 18 19 30 31	Water Vapour Transmittance 6 18 19 30 31	Ozone Transmittance 6 18 19 30 31	Temperature Jacobian 6 18 19 30 31	Water Vapour Jacobian 6 18 19 30 31	Ozone Jacobian 6 18 19 30 31
2	GEN2	y y y y y	y y y y y	y y y y y	y y y y y		y y y y y
	4A	y y y y y	y y y y y	y y y y y	y y y y y		y y y y y
	AES	y y y y y	y y y y y	y y y y y	y y y y y		y y y y y
	RTM	y y y y y			y y y y y		y y y y y
	SYNS	y y y y y			y y y y y		
5	GEN2	y y y y y	y y y y y	y y y y y	y y y y y	y y y y y	y y y y y
	4A	y y y y y	y y y y y	y y y y y	y y y y y	y y y y y	y y y y y
	AES	y y y y y	y y y y y	y y y y y	y y y y y	y y y y y	y y y y y
	RTM	y y y y y			y y y y y	y y y y y	y y y y y
	SYNS	y y y y y	y y y y y	y y y y y	y y y y y	y y y y y	y y y y y
9	GEN2	y y y y y	y y y y y	y y y y y	y y y y y	y y y y y	y y y y y
	4A	y y y y y	y y y y y	y y y y y	y y y y y	y y y y y	y y y y y
	AES	y y y y y	y y y y y	y y y y y	y y y y y	y y y y y	y y y y y
	RTM	y y y y y			y y y y y	y y y y y	y y y y y
	SYNS	y y y y y	y y y y y	y y y y y	y y y y y	y y y y y	y y y y y
10	GEN2	y y y y y	y y y y y		y y y y y	y y y y y	
	4A	y y y y y	y y y y y	y y y y y	y y y y y	y y y y y	
	AES	y y y y y	y y y y y	y y y y y	y y y y y	y y y y y	
	RTM	y y y y y			y y y y y	y y y y y	
	SYNS	y y y y y	y y y y y		y y y y y	y y y y y	
11	GEN2	y y y y y	y y y y y		y y y y y	y y y y y	
	4A	y y y y y	y y y y y	y y y y y	y y y y y	y y y y y	
	AES	y y y y y	y y y y y	y y y y y	y y y y y	y y y y y	
	RTM	y y y y y			y y y y y	y y y y y	
	SYNS	y y y y y	y y y y y		y y y y y	y y y y y	
12	GEN2	y y y y y	y y y y y		y y y y y	y y y y y	
	4A	y y y y y	y y y y y		y y y y y	y y y y y	
	AES	y y y y y	y y y y y		y y y y y	y y y y y	
	RTM	y y y y y			y y y y y	y y y y y	
	SYNS	y y y y y	y y y y y		y y y y y	y y y y y	
15	GEN2	y y y y y	y y y y y		y y y y y	y y y y y	
	4A	y y y y y	y y y y y		y y y y y	y y y y y	
	AES	y y y y y	y y y y y		y y y y y	y y y y y	
	RTM	y y y y y			y y y y y	y y y y y	
	SYNS						

Table 6: Summary of LBL transmittance and Jacobian profile data submitted by the LBL groups.

IV RESULTS

The preliminary graphs and tables of results were posted on a website[9] for all contributors to examine. Three groups, SYNS, FLBL and 4A, utilized the information to reexamine their models. SYNS and FLBL found a couple of subtle errors in their codes which may never have been noticed if not for the intercomparison. The 4A model was already in the process of upgrades based on other recent intercomparisons (eg; Soden et al, 2000) and this intercomparison supplied further incentive to upgrade. These three groups submitted a new set of results based on the upgraded models. The results shown here are from the most upgraded models.

In some graphical presentations of the data, the difference between two or more models is too small to discern. In these circumstances it is more useful to consider the relative differences between the models and a reference model. Small systematic differences indicative of potential problems in a model are easier to recognize in such graphs. For this work the relative difference of a quantity X is defined as:

$$\Delta X = X(model) - X(GENLN2)$$

GENLN2 was chosen to be reference model for no other reason than it is commonly used as a reference. This in no way implies that it is a better model. In fact it is difficult to establish which model best represents reality since at least one of the models would have to be compared with observations, and it is difficult to obtain a large set of atmospheric observations of high resolution with very well defined optical paths.

IVa) Brightness Temperature, T_b

The standard deviation of T_b across the atmospheres is indicative of the variation of the 42 atmospheres. The lower sounding channels tend to have larger deviations than the higher sounding channels. Table 7 tabulates the mean T_b and its standard deviations within the 42 atmospheres for each channel. The spread

[9] www.cmc.ec.gc.ca/rpn/arma/intercomparison

of the mean across the models of any channel does not exceed .85K and the spread in deviations is less than .6K. Agreement between models is best for HIRS-10, whereas it is worst for HIRS-5 and HIRS-9.

Table 8 summarizes the mean of ΔT_b, or bias, for each channel and model and their corresponding standard deviation. As was seen in table 7, HIRS-5 has the largest spread, followed by HIRS-9. If SYNS is excluded, then the spread across the HIRS-9 models is much lower. The difference between models is more easily recognizable in figure 5. Figure 5 is a plot of ΔT_b as a function of GENLN2's T_b for each channel. Data from all 42 atmospheres are plotted but are not identified. It is easy to identify the channels in which there is favourable agreement amongst the models.

HIRS	GENLN2		4A		FLBL		RTM		SYNS	
	mean	std	mean	std	mean	std	mean	std	mean	std
2	223.058	6.719	222.995	6.705	222.906	6.680	223.012	6.683	222.808	6.677
5	239.308	6.633	239.224	6.641	238.814	6.546	239.671	6.706	239.103	6.626
9	259.189	15.981	259.213	15.955	259.177	15.961	259.307	15.989	259.675	16.522
10	274.016	16.320	274.029	16.369	274.036	16.338	274.057	16.355	274.055	16.321
11	253.880	7.850	253.633	7.832	253.804	7.838	253.802	7.825	253.934	7.758
12	240.487	5.408	240.349	5.454	240.343	5.374	240.328	5.356	240.331	5.317
15	246.113	10.900	246.161	10.896	246.220	10.957	246.296	10.980		

Table 7: Mean brightness temperature of the 42 profiles and its standard deviation as a function of channel and model.

Neither tables 7 and 8 nor figure 5 give much information pertaining to localized ΔT_bs. Figure 6 improves on figure 5 by plotting ΔT_b against the atmospheric state index (see table 4). For interested readers, the values plotted in figures 5 and 6 are compiled in appendix II.

HIRS	4A		FLBL		RTM		SYNS	
	bias	std	bias	std	bias	std	bias	std
2	-.063	.037	-.152	.123	-.046	.050	-.249	.157
5	-.084	.025	-.493	.139	.363	.104	-.205	.141
9	.024	.055	-.012	.055	.117	.050	.486	.585
10	.013	.093	.020	.038	.041	.060	.039	.031
11	-.246	.064	-.076	.035	-.078	.057	.054	.134
12	-.138	.132	-.144	.147	-.159	.189	-.156	.205
15	.047	.015	.107	.061	.182	.086		

Table 8: TOA brightness temperature bias of the 42 profiles with respect to GENLN2 and its standard deviation as a function of channel and model.

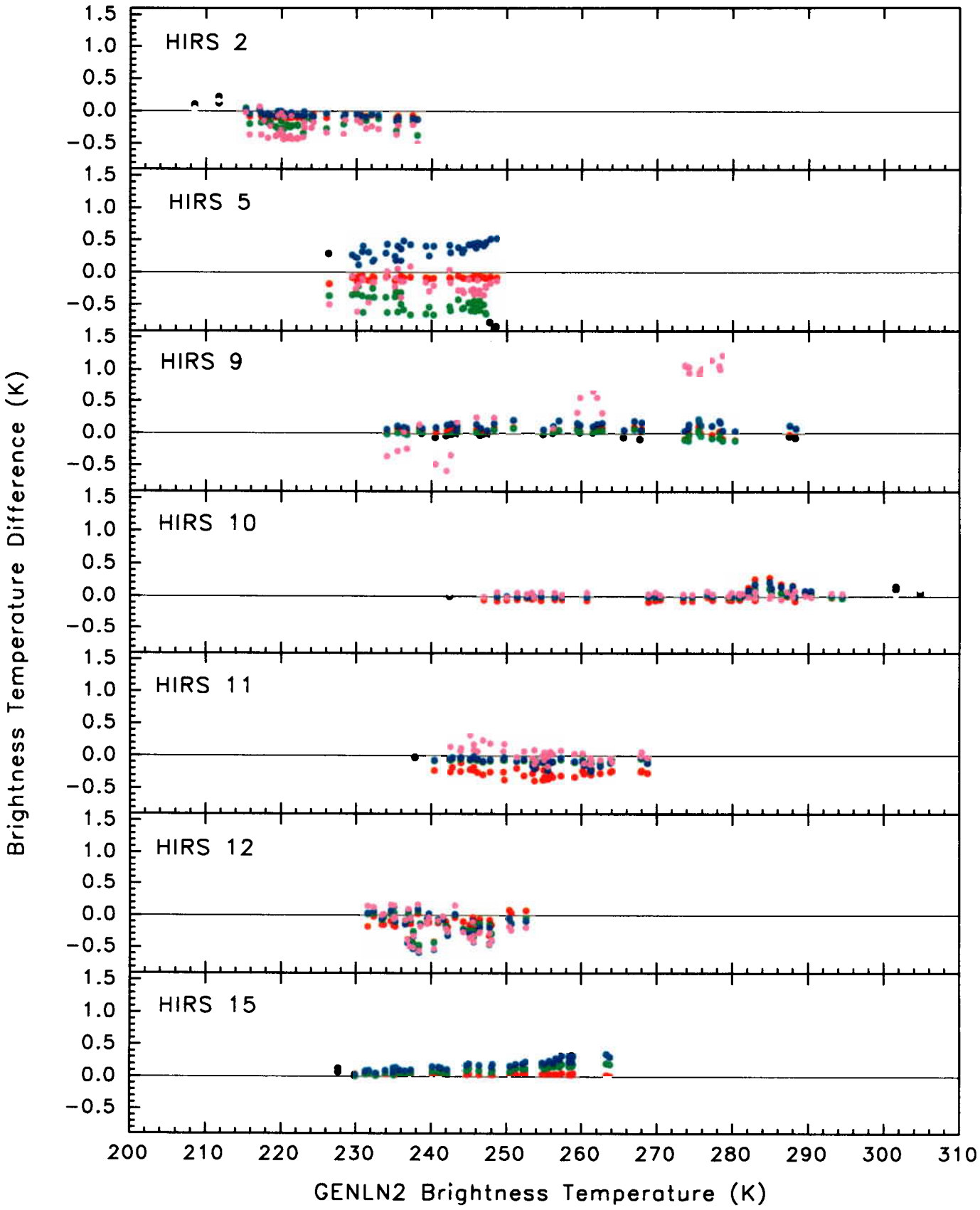

Fig. 5: Comparison of the TOA T_b with respect to GENLN2 plotted as a function of GENLN2's T_b for the 42 atmospheric states. The LBL models are 4A, • FLBL, • RTM and SYNS.

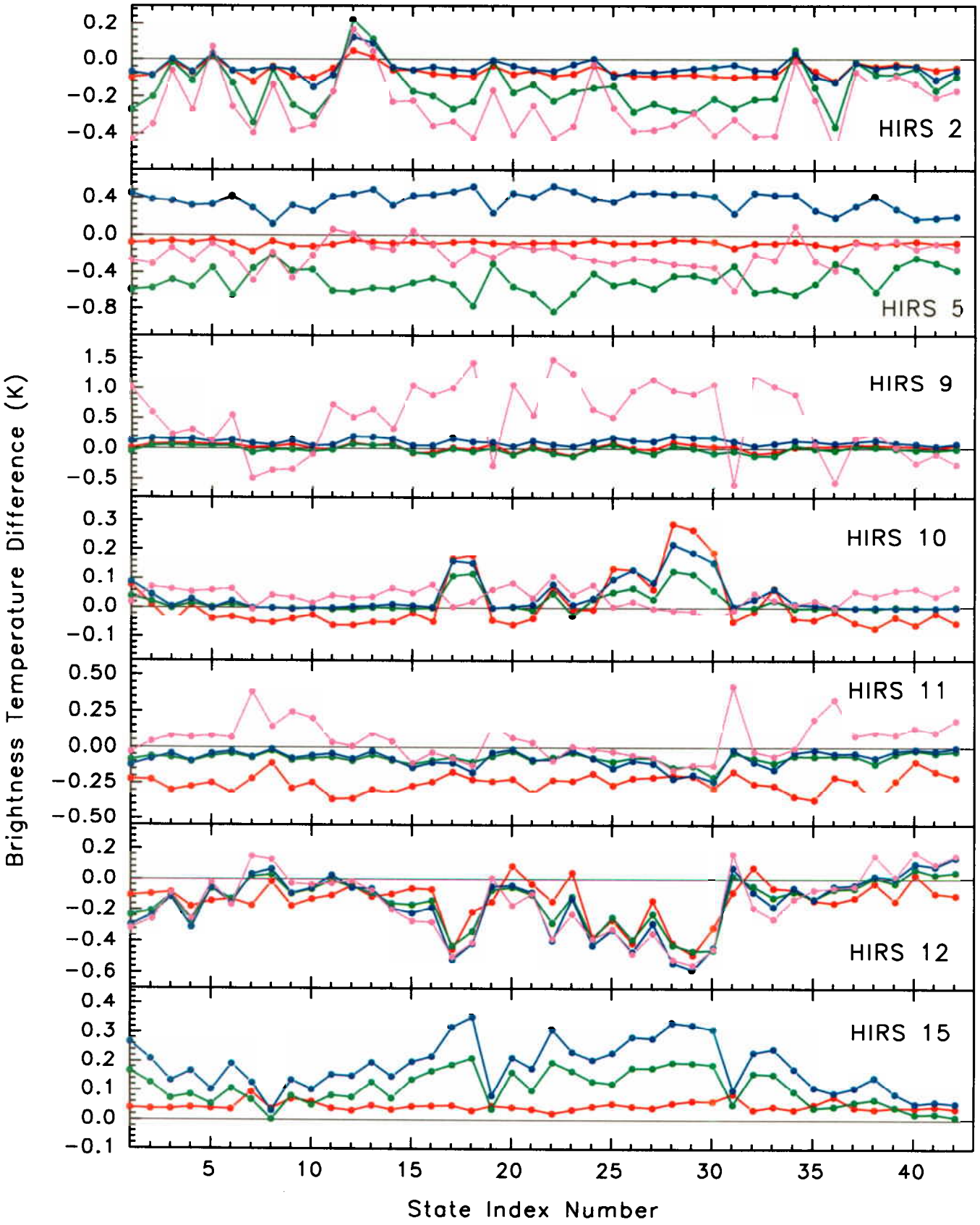

Fig. 6: Comparison of the T_b differences with respect to GENLN2 as a function of the states. The LBL models are 4A, • FLBL, • RTM and SYNS.

In general the models tend to behave in a similar manner with the exception of SYNSATRAD in HIRS-9. In HIRS-9, SYNS fluctuates strongly from atmosphere to atmosphere, whereas the other models tightly follow each other. SYNSATRAD was originally developed for another instrument and as a side effort it was prepared (ad hoc) for HIRS. It is possible that the method can be further optimized for HIRS-9. At the time of this writing HIRS-9 was being reviewed (S. Tjemkes, pri. comm.).

Referring back to table 4 one will recall that the atmospheres were sorted into four groups, the six AFGL standard atmospheres, followed by twelve atmospheres with increasing column temperature, twelve with increasing H_2O amount and finally by twelve with increasing O_3 amounts. In HIRS-10, HIRS-12 and HIRS-15, the magnitude of the difference increases from atmospheres 19 to 30. Atmospheres 19 to 30 also represent an increase in H_2O amount from 2 to 70kg/m^2. A bump is also observed from atmospheres 16 to 18 which also have a high H_2O content. In HIRS-12, the four models follow each other closely, implying that there is something dissimilar between them and GENLN2. As most of the HIRS-12 signal is due to H_2O absorption, the discrepancy is most likely related to water vapour. As GENLN2, 4A and FLBL use CKD2.1, and LBLRTM and SYNSATRAD use CKD2.2, this difference is unlikely due to the water vapour continuum parameterization.

The differences in HIRS-15 appear to correlate with increasing column temperature (atmospheres 7 to 18) and also appear to decrease with column O_3 from atmosphere 31 onward, although there appears an additional effect due to H_2O. The temperature dependency is probably due, in part, to the manner in which CO_2 is handled in the 4.5μm region (see table 1).

There are no other obvious correlations. It is unclear why FLBL and LBLRTM have such relatively large and opposite differences in HIRS-5. Some of the other small scale differences may be in part due to; the different absorbers used (table 5), (eg; on average the FLBL tends to use more absorbers), differences in the procedures used to obtain the values of pressure, temperature and absorber amount used to evaluate the optical depths, or differences in numerical procedures.

IVb) Transmittances/Optical Depth

The water vapour transmittance profiles for each channel are plotted in figures 7 through to 13. Each panel contains a set of transmittance profiles, one for each model, for each member of the atmospheres subset described in section IIIb. In general these graphs are uninteresting in that one cannot differentiate between the models where the transmittance would lead to a significant contribution to T_b (eg; transmittances < .92). SYNS tends to be slightly more absorbing for HIRS-5, HIRS-9 and HIRS-10 in the wetter atmospheres and 4A is slightly more absorbing in the drier atmospheres in HIRS-11.

In figure 6 it was observed that the HIRS-12 T_b models disagreed with GENLN2 as a function of column water. Atmospheres 19 and 30 represent a very dry and a very wet atmosphere and yet no significant difference between the models can be seen in figure 12. As HIRS-12 is strongly dominated by H_2O, one must conclude that this channel is very sensitive to small changes in H_2O, or in part, a numerical sensitivity in the radiative transfer code.

Plots of $\Delta\bar{\chi}_{H2O}$ as a function of GENLN2's $\bar{\chi}_{H2O}$ can be found in figures 14 and 15. For most channels, the relative difference in χ increases somewhat linearly with χ_{GENLN2}, indicating that the difference is systematic with increasing pressure. It is unclear what the source of these discrepancies are. The 4A model exhibits a greater variability of $\Delta\chi$ in the more significant region of $\chi < 5$; presumably this is due to the more interpolative nature of the 4A code.

The ozone transmittance profiles for each channel are plotted in figures 16 through to 20. Each panel contains a set of transmittance profiles, one for each model, for each member of the atmospheres subset described in section IIIb. Except for HIRS-9 the transmittance does not fall below .92. As mentioned earlier, the SYNSATRAD values for HIRS-9 are thought to be in error. Excluding SYNSATRAD, and considering the scale of the high transmittance plots, the agreement between the plots is good.

Figure 21 is a plot of $\Delta\bar{\chi}_{O3}$ as a function of GENLN2's $\bar{\chi}_{O3}$ for HIRS-2, HIRS-5 and HIRS-9. In these channels, 4A and FLBL both tend to agree with GENLN2 to within a couple of percent. The deviations in HIRS-9 are relatively strong, but

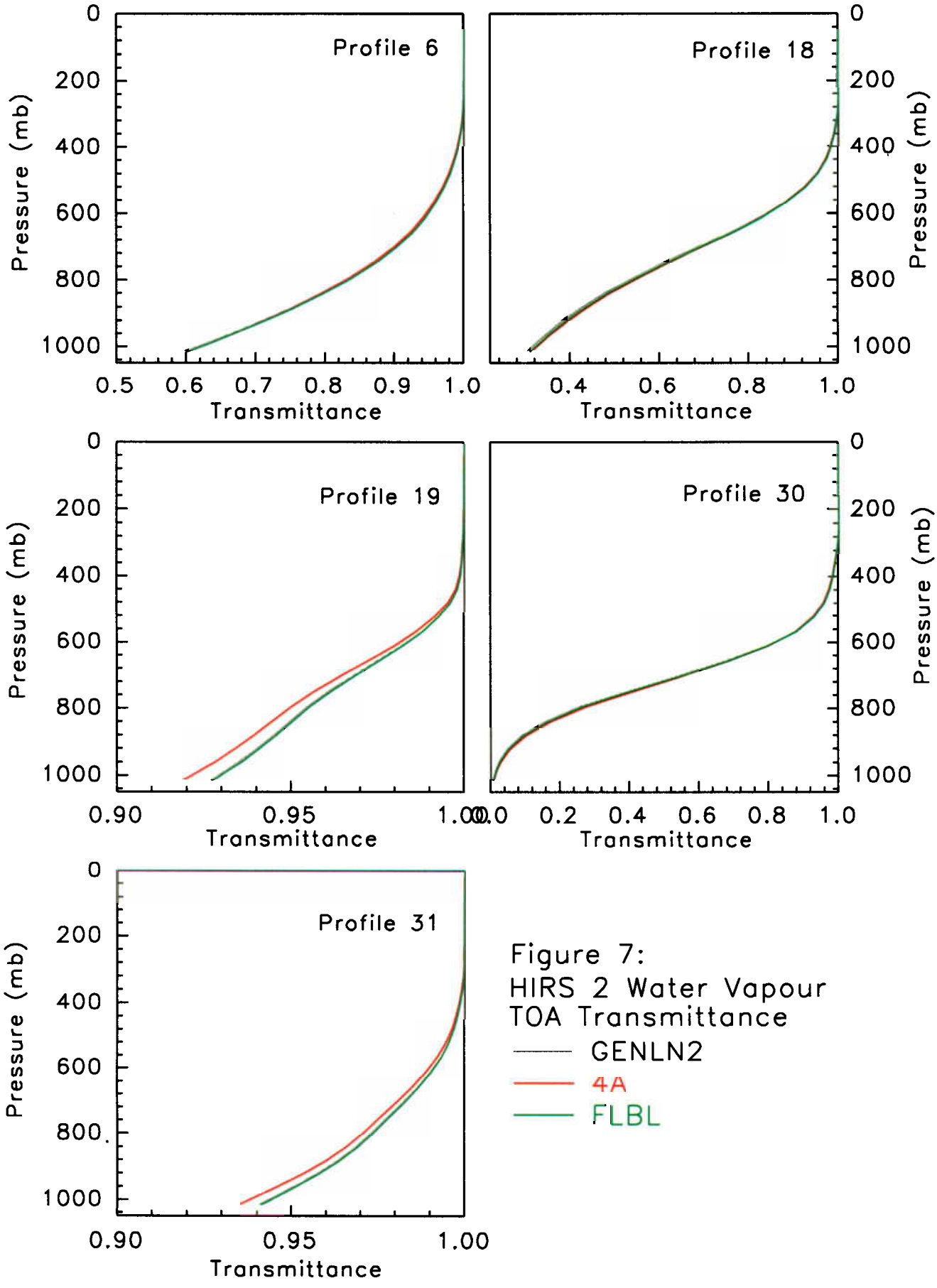

Figure 7:
HIRS 2 Water Vapour
TOA Transmittance

GENLN2
4A
FLBL

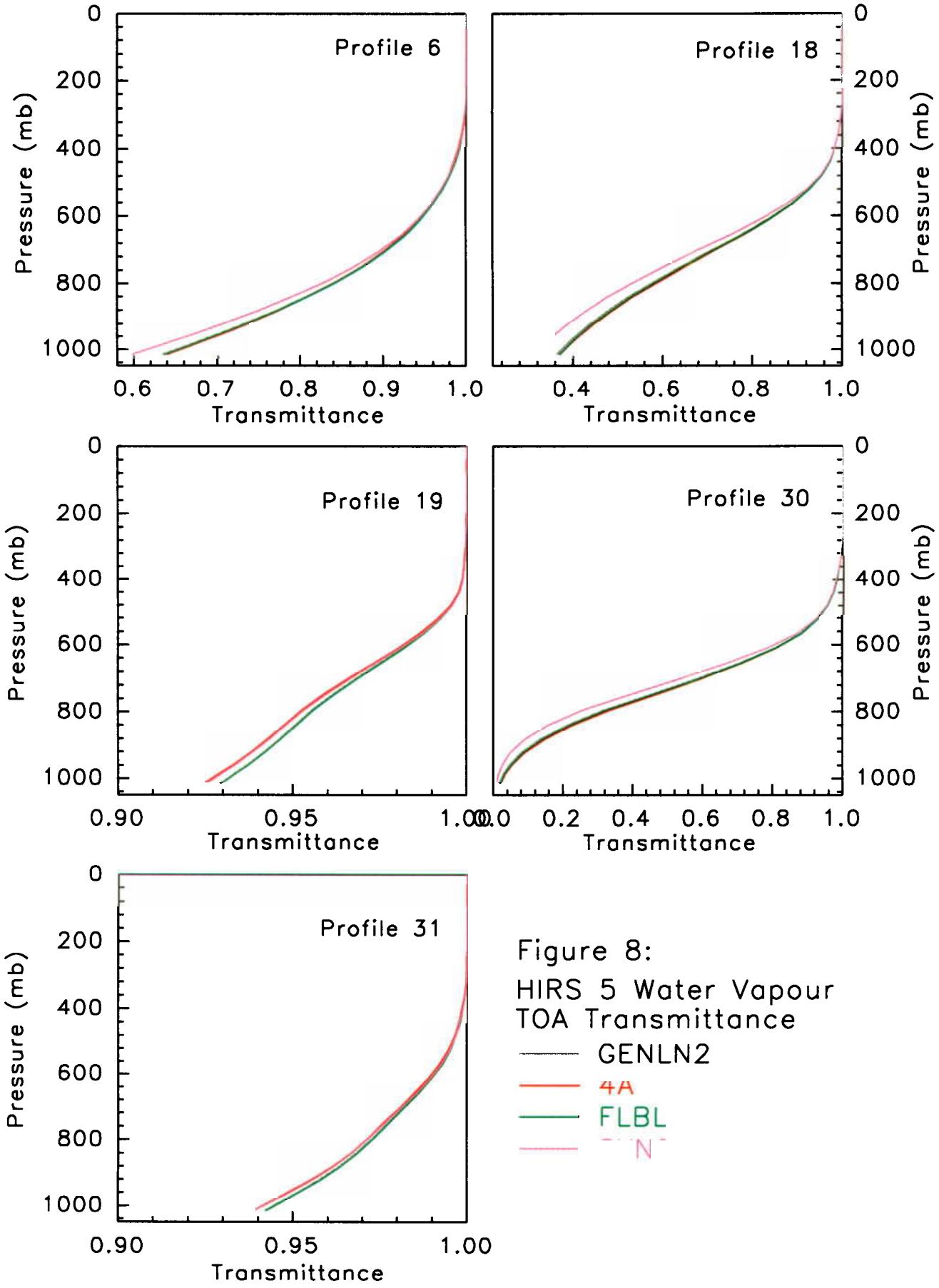

Figure 8:
HIRS 5 Water Vapour
TOA Transmittance

GENLN2
4A
FLBL
LN

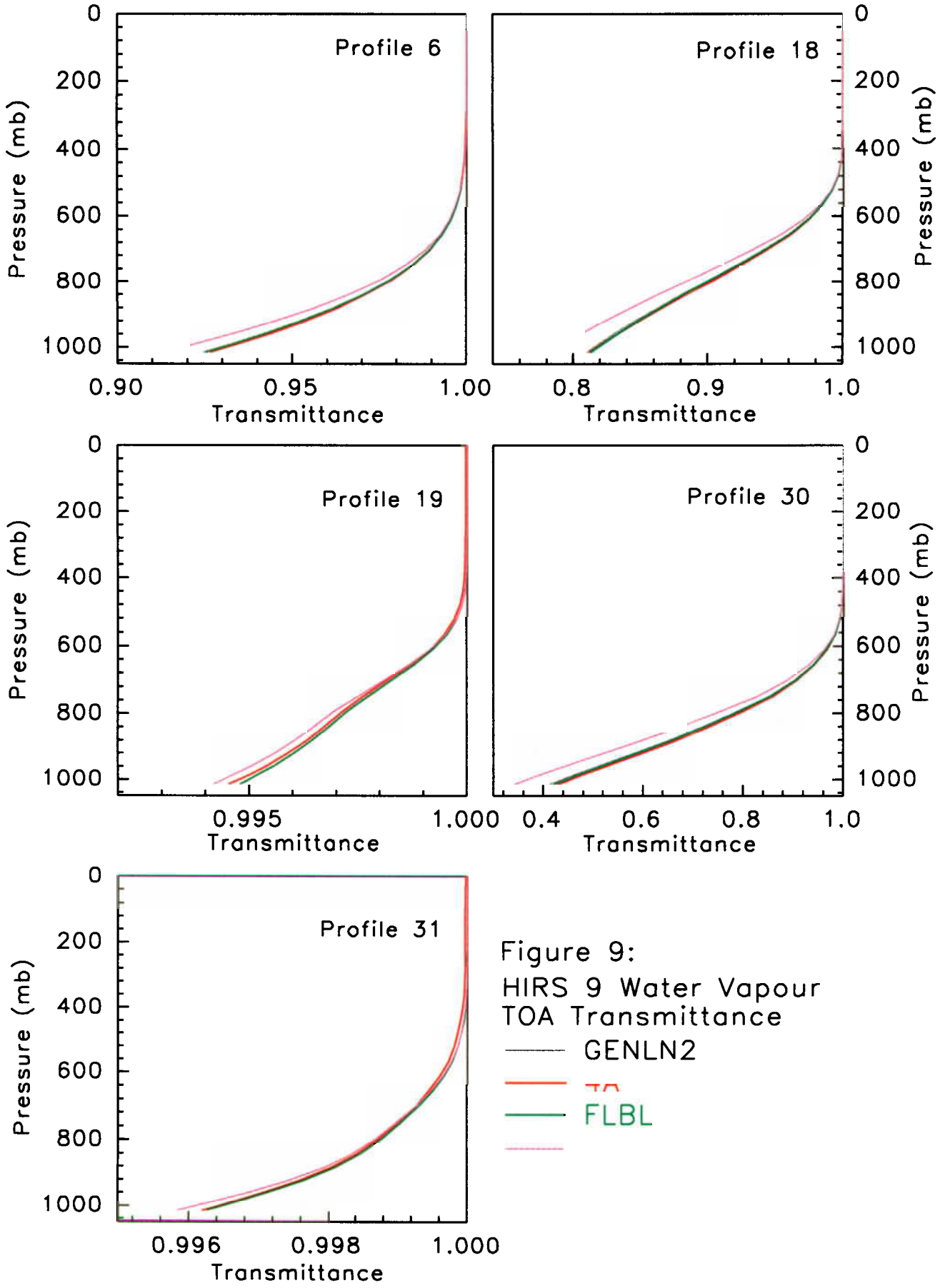

Figure 9:
HIRS 9 Water Vapour
TOA Transmittance

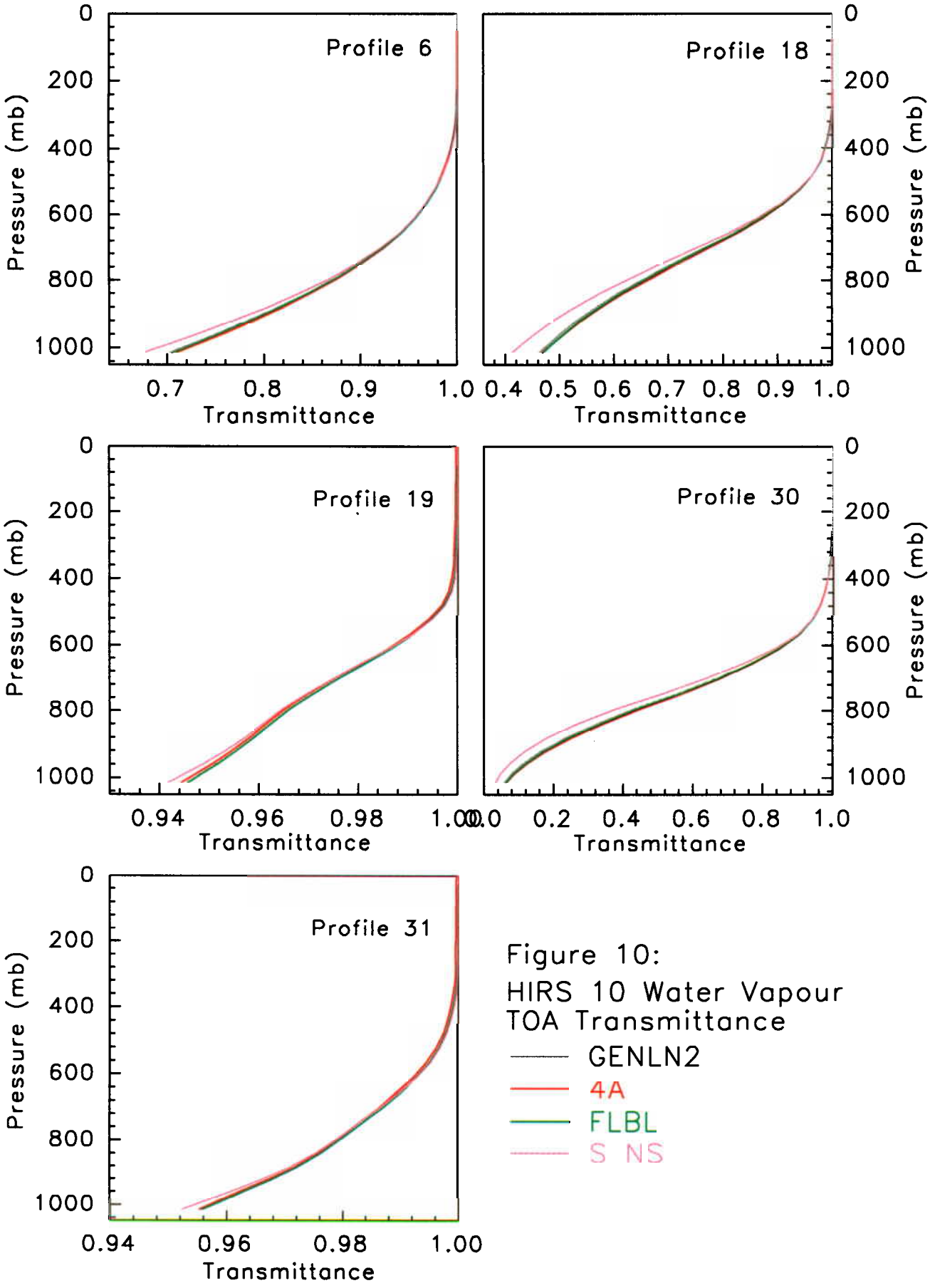

Figure 10:
HIRS 10 Water Vapour
TOA Transmittance

GENLN2
4A
FLBL
S NS

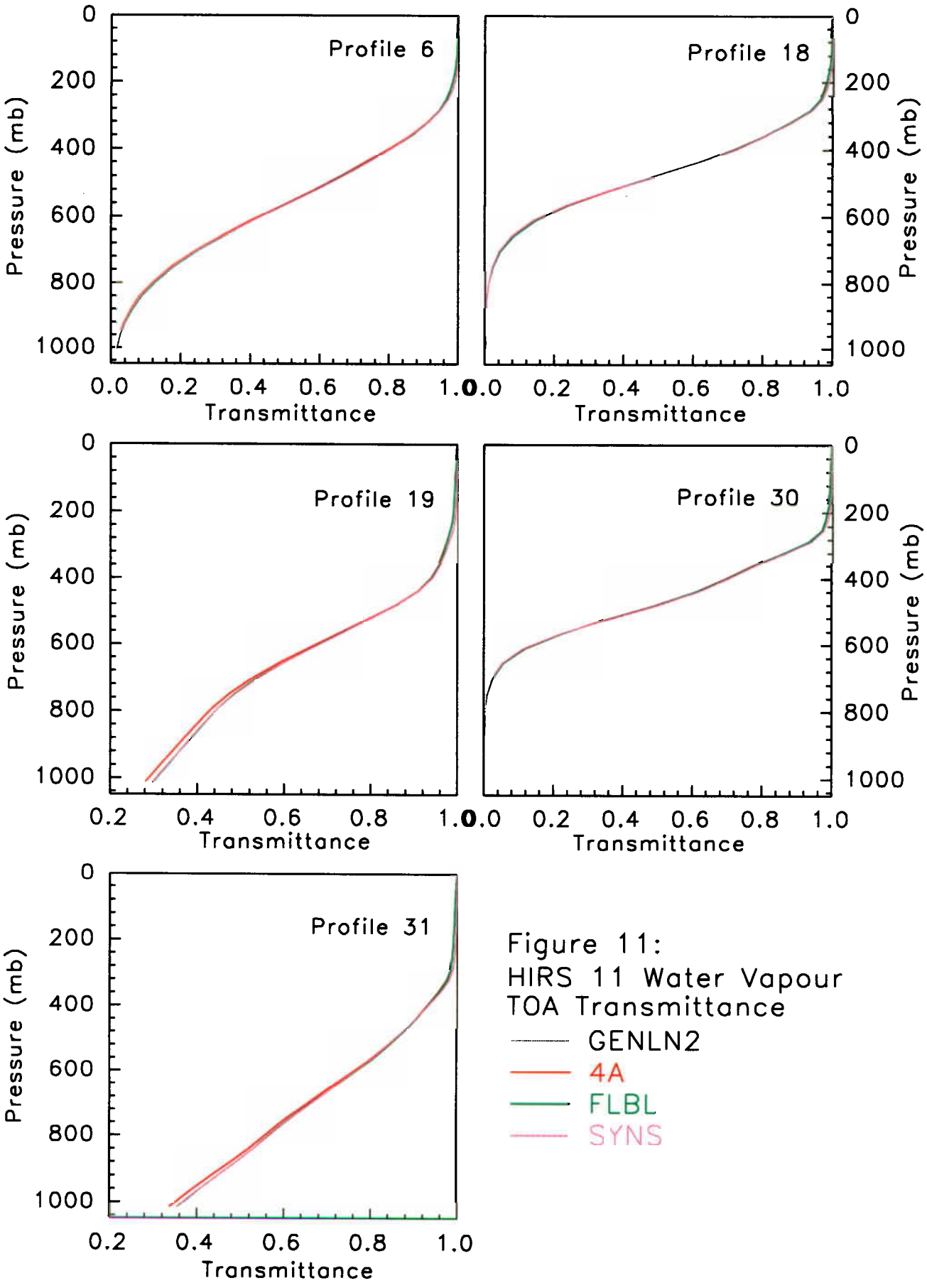

Figure 11:
HIRS 11 Water Vapour
TOA Transmittance

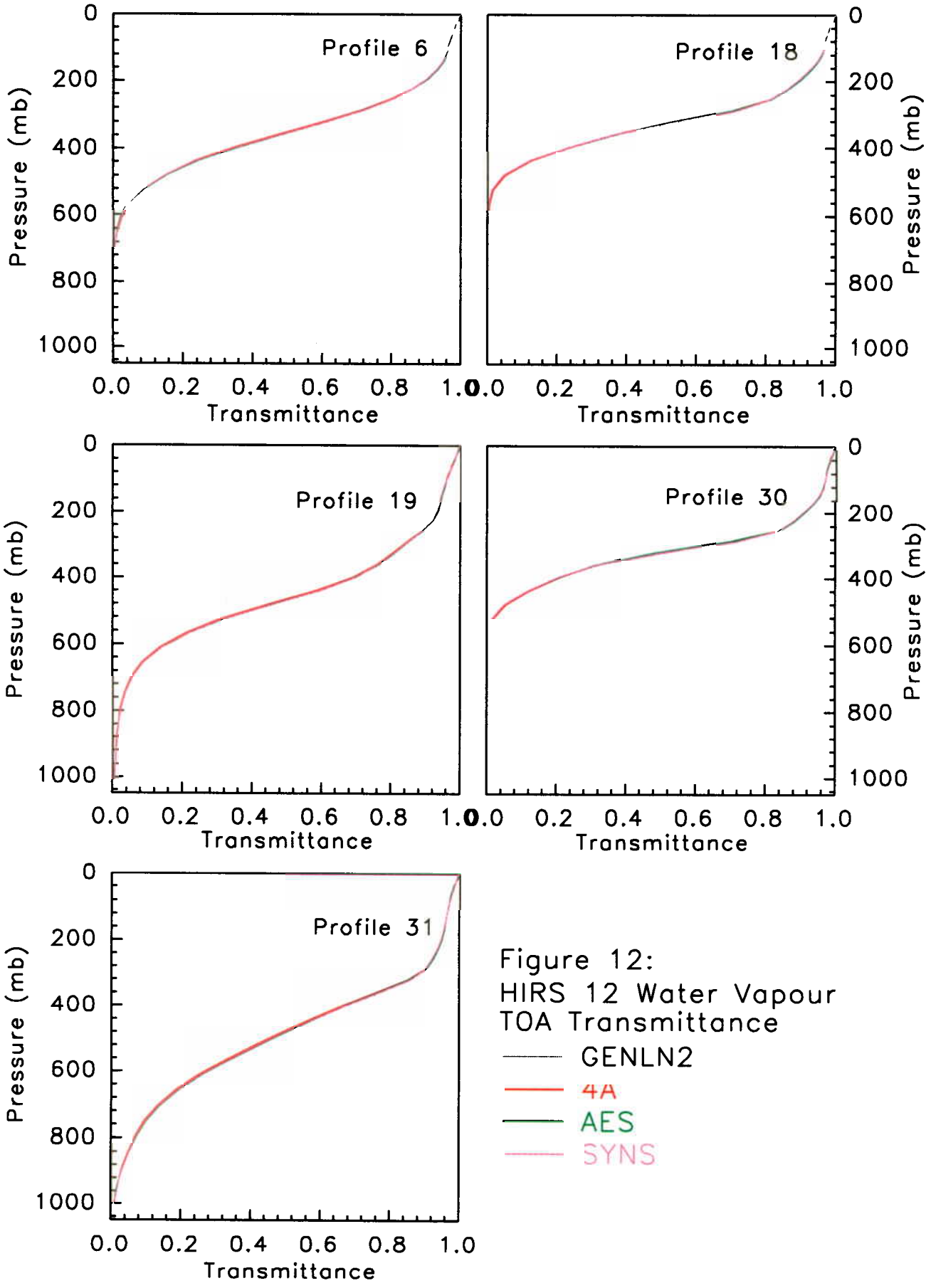

Figure 12:
HIRS 12 Water Vapour
TOA Transmittance

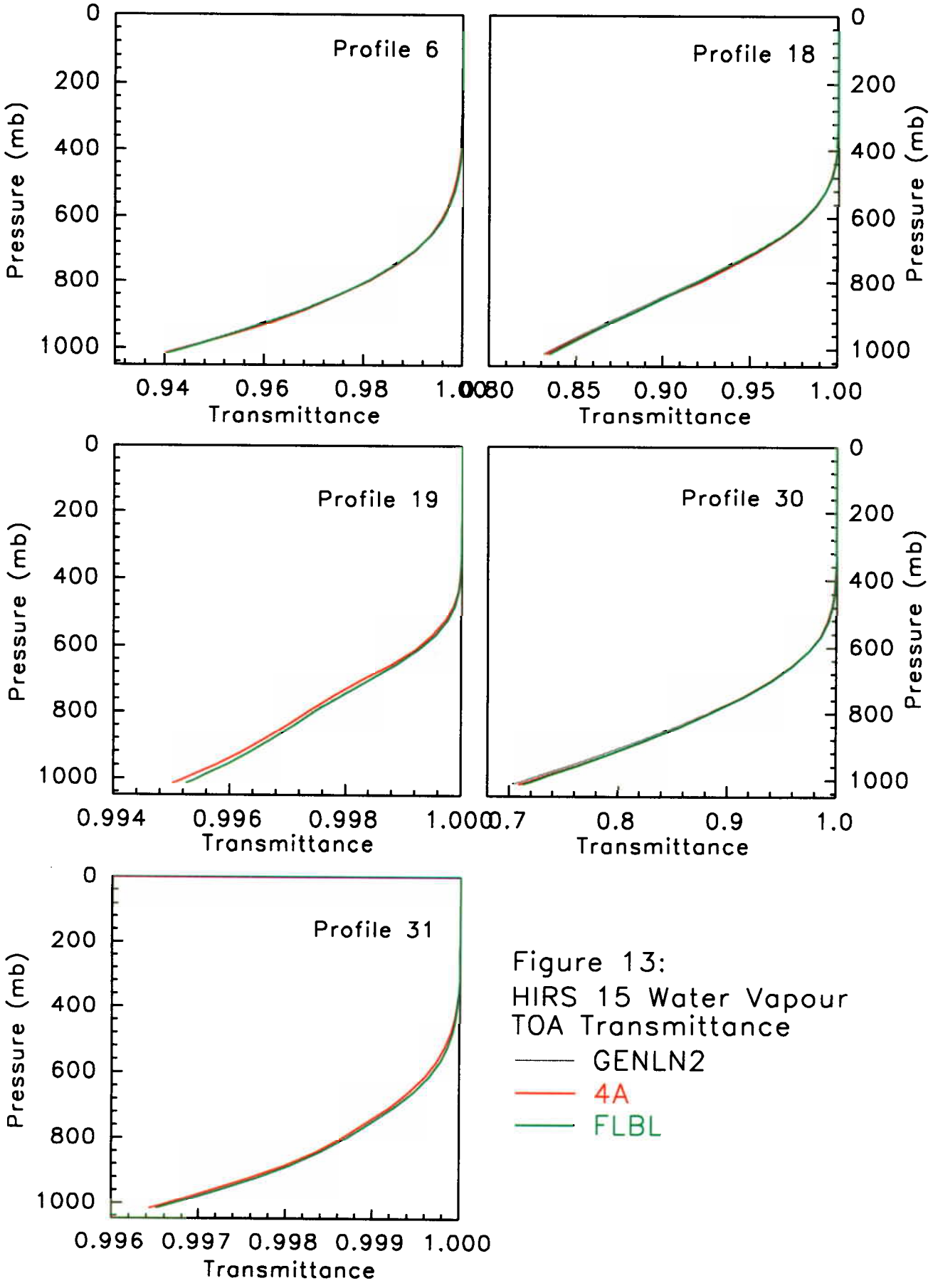

Figure 13:
HIRS 15 Water Vapour
TOA Transmittance

GENLN2
4A
FLBL

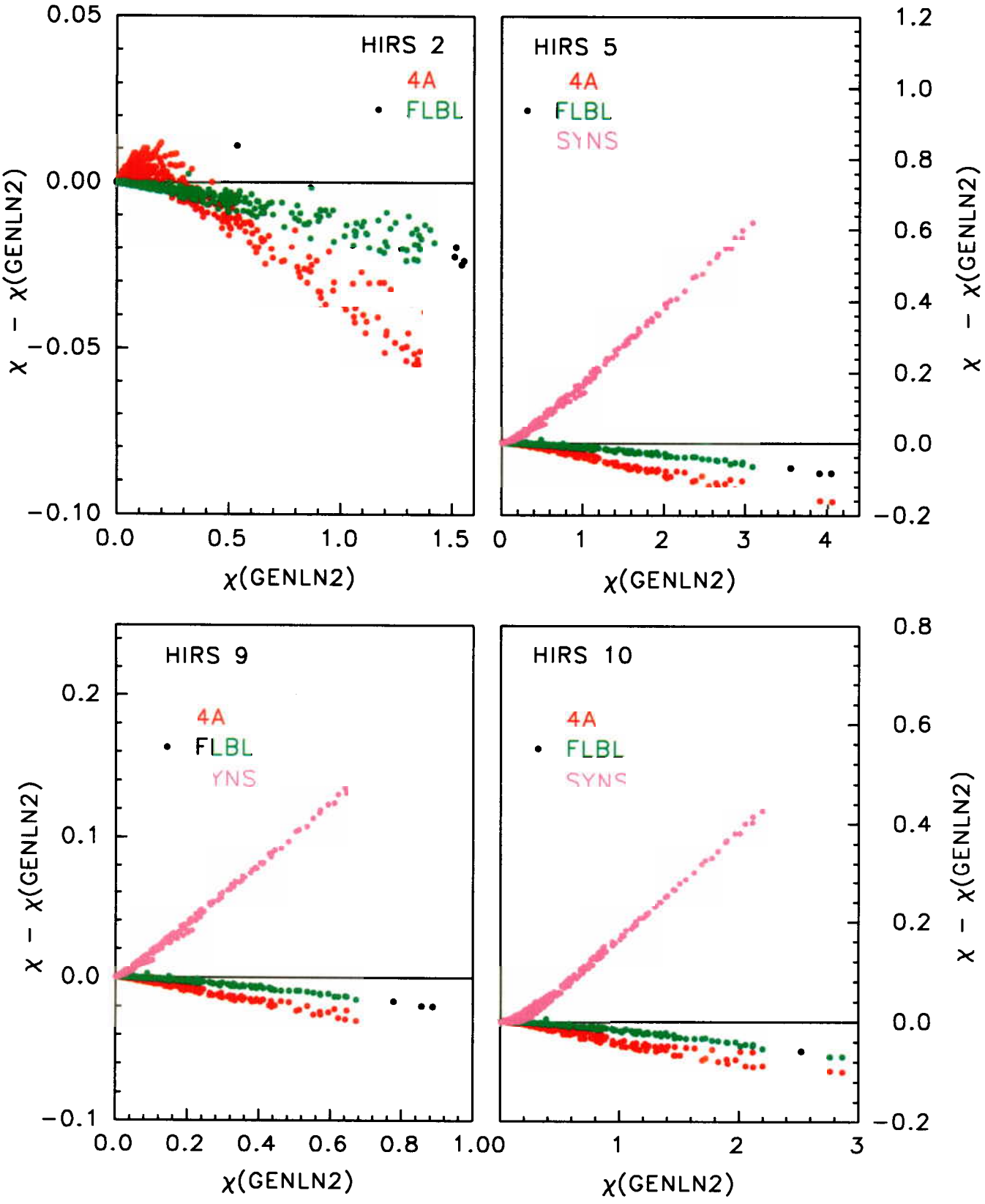

Figure 14: H_2O Effective Optical Depths

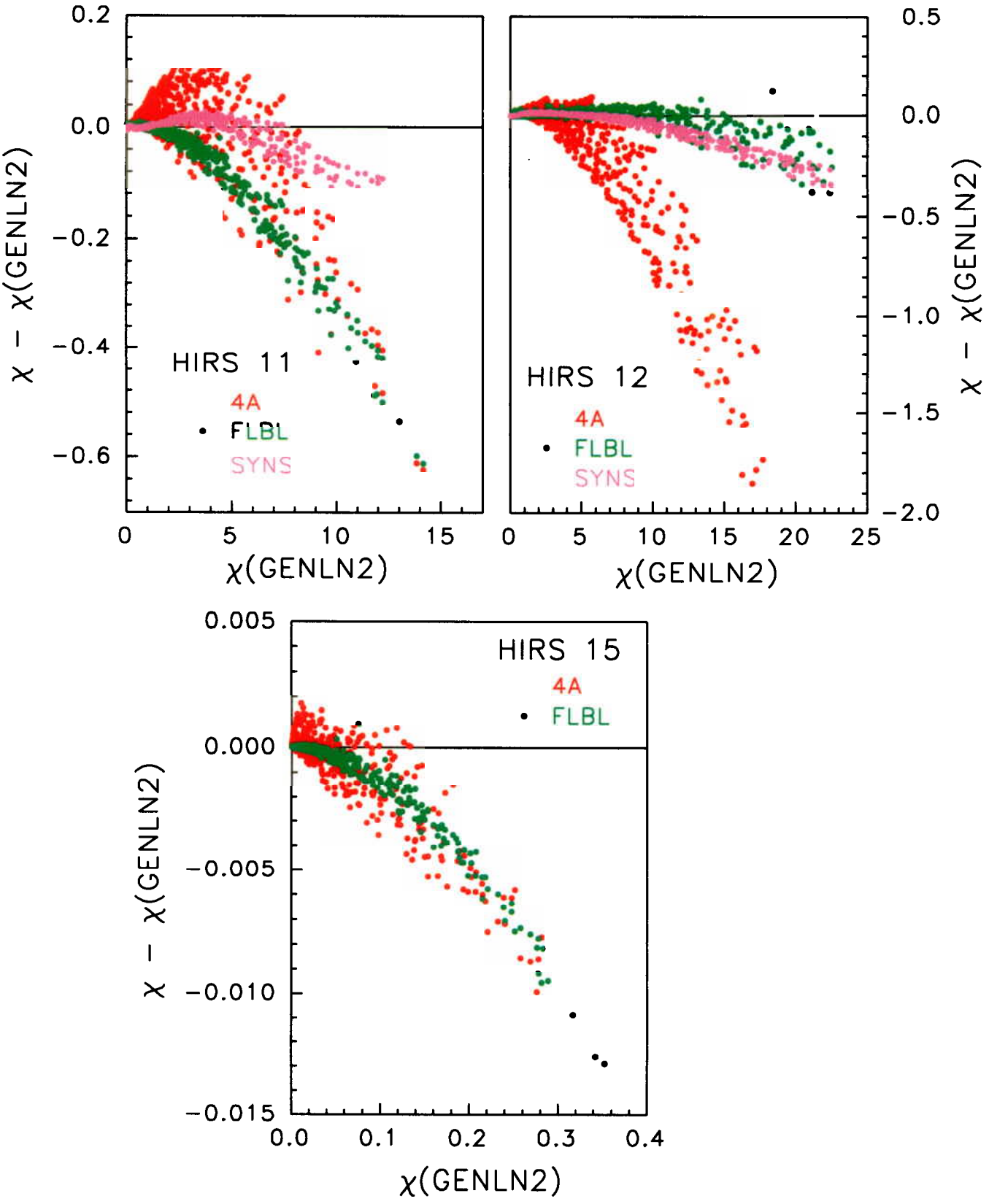

Figure 15: H_2O Effective Optical Depths

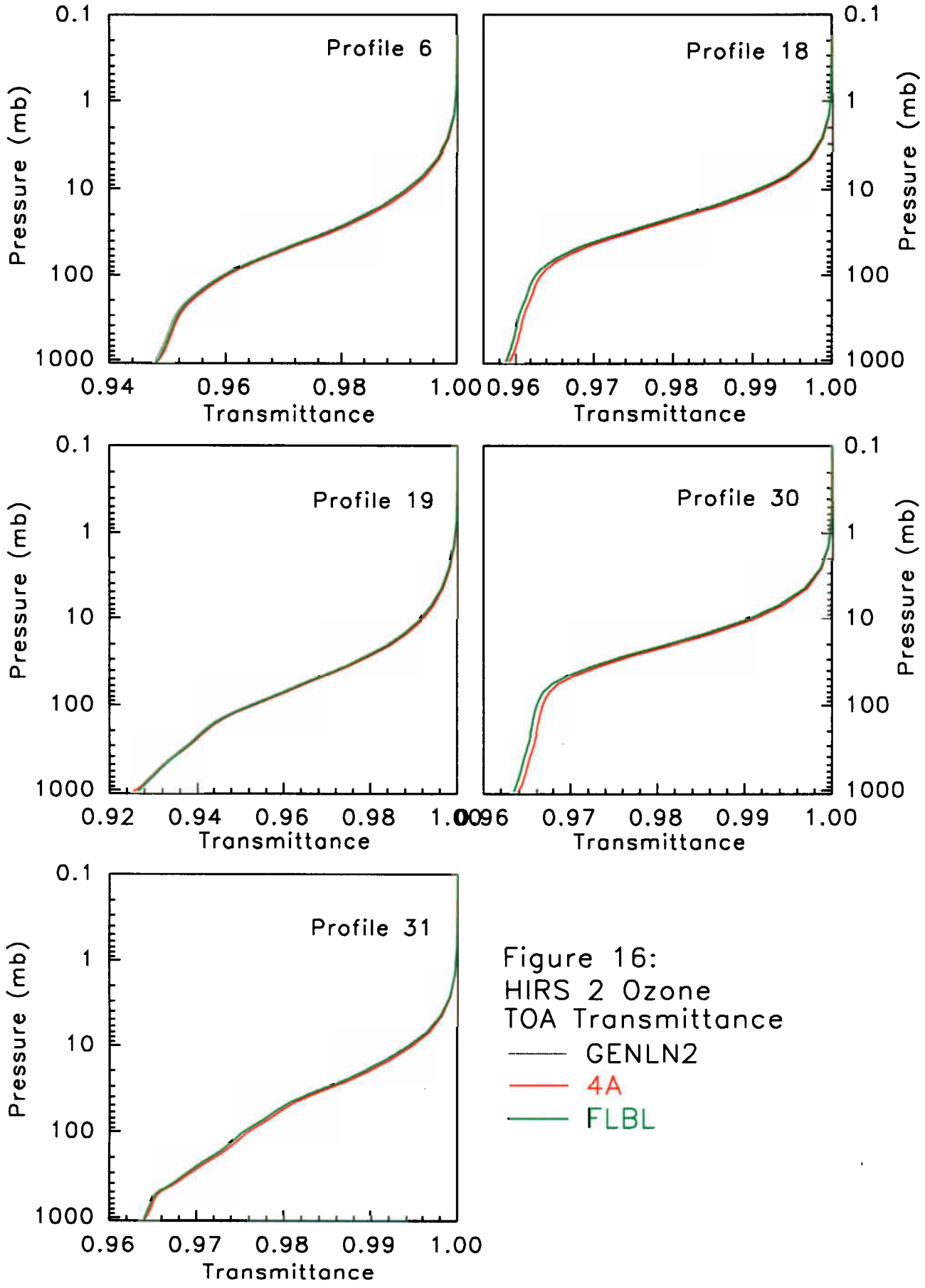

Figure 16:
HIRS 2 Ozone
TOA Transmittance

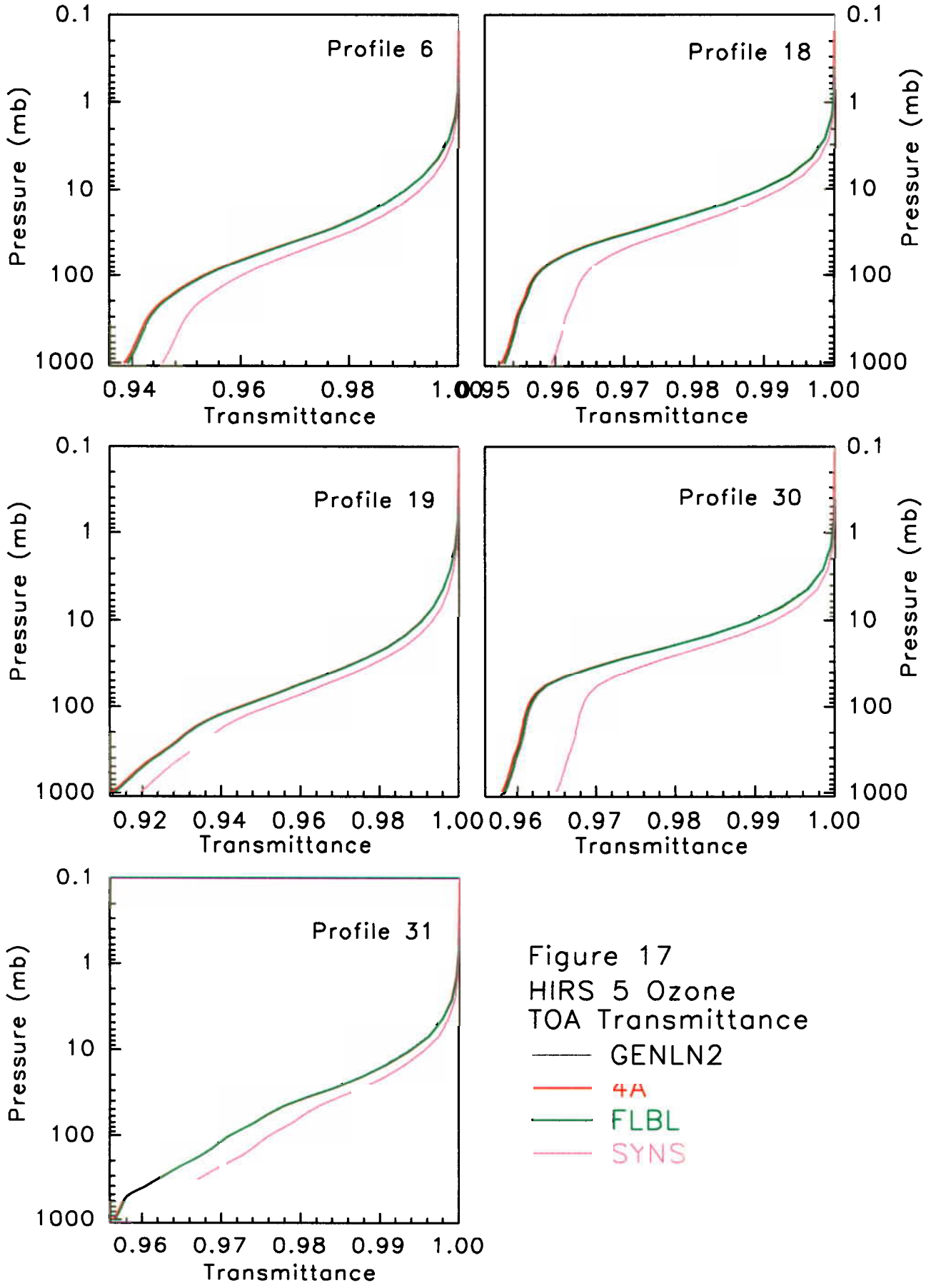

Figure 17
HIRS 5 Ozone
TOA Transmittance

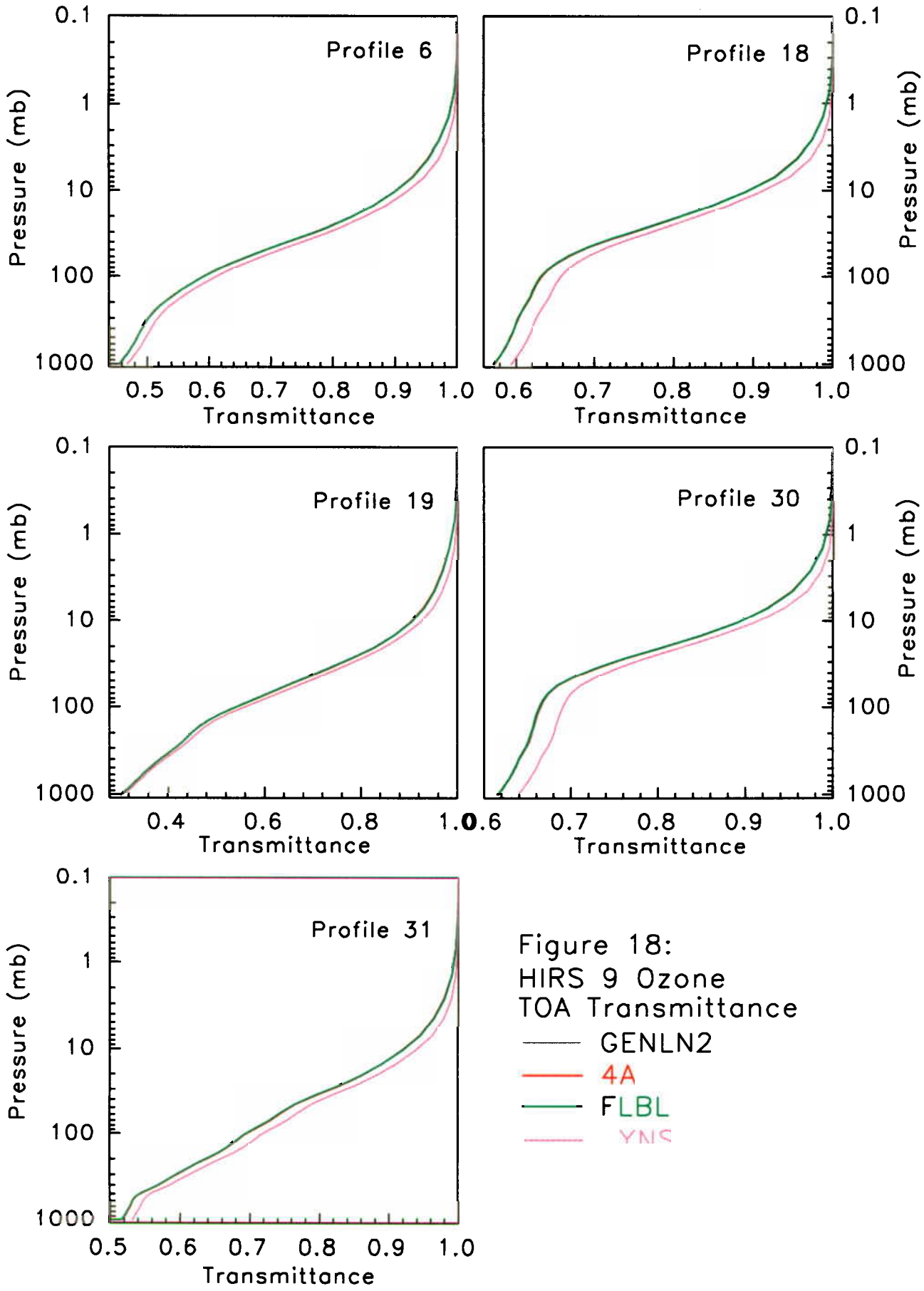

Figure 18:
HIRS 9 Ozone
TOA Transmittance

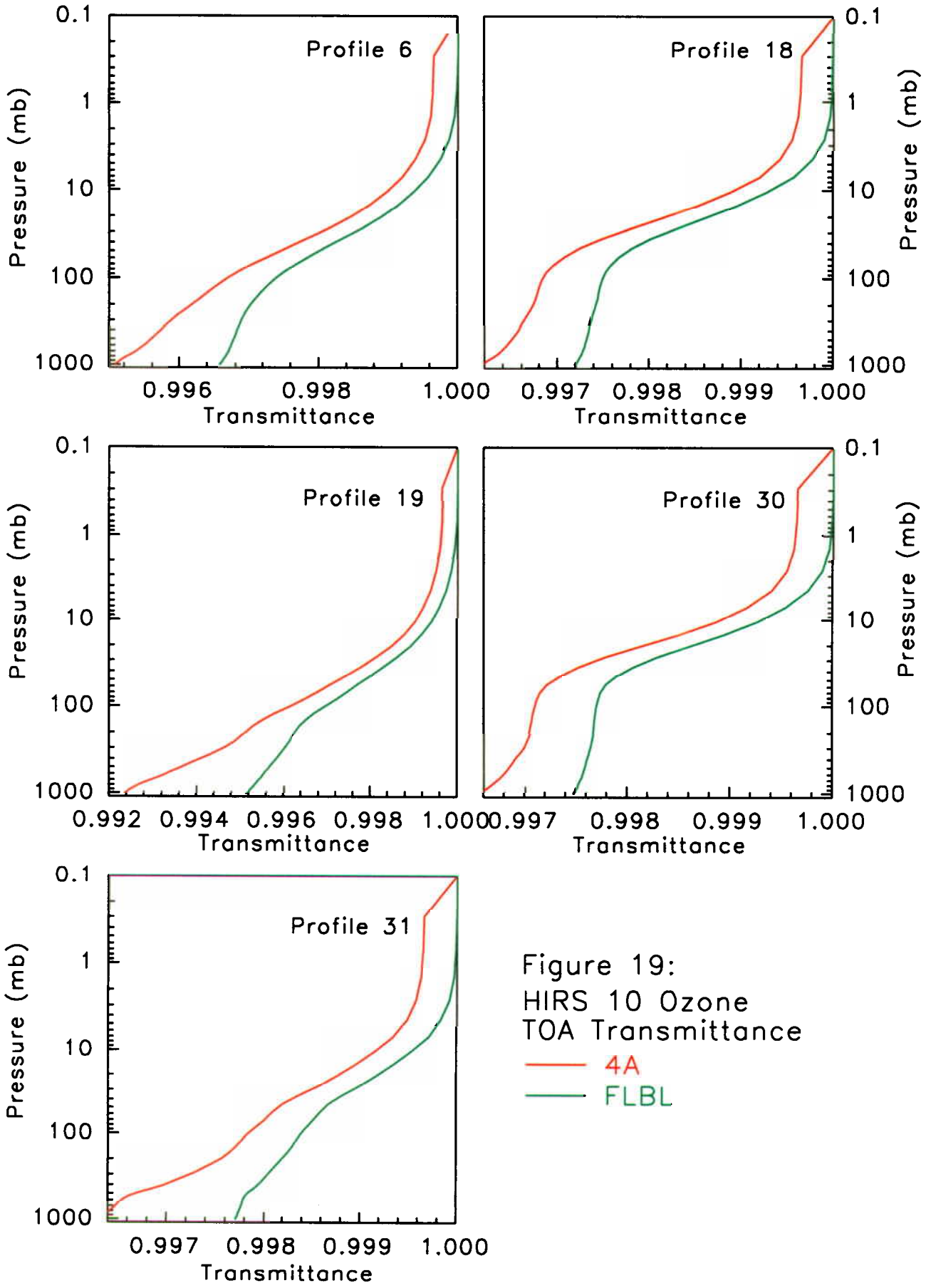

Figure 19:
HIRS 10 Ozone
TOA Transmittance

4A

FLBL

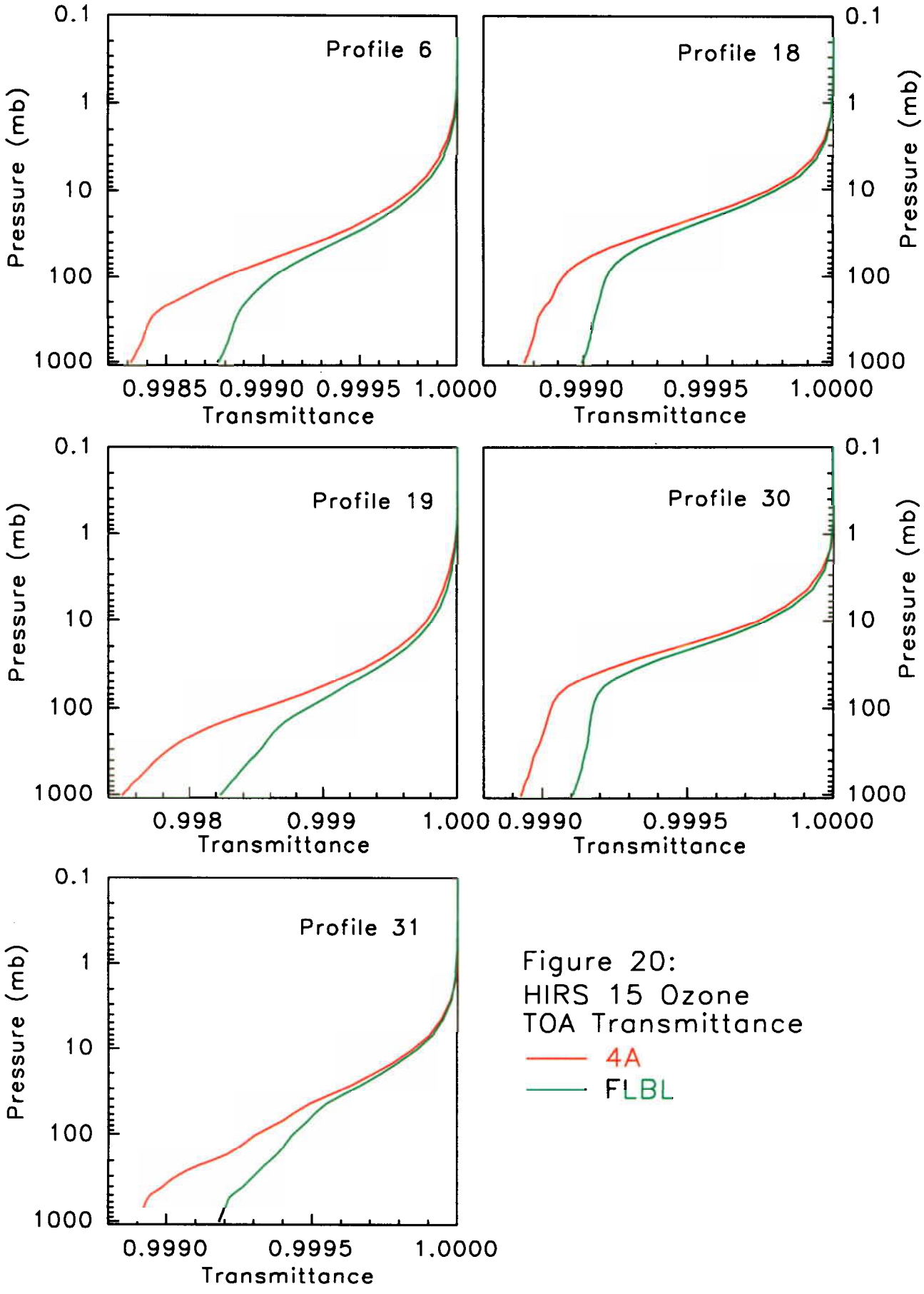

Figure 20:
HIRS 15 Ozone
TOA Transmittance

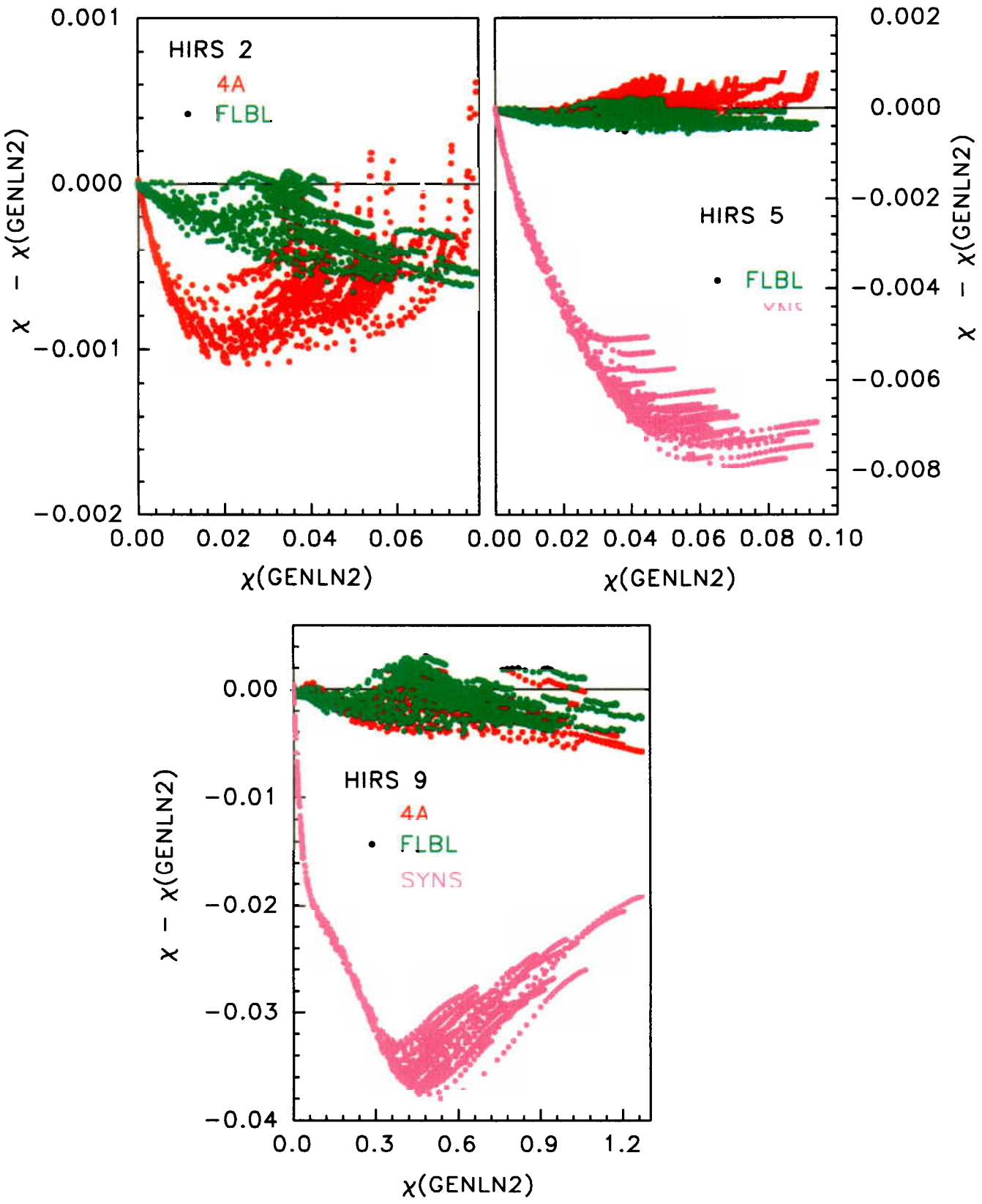

Figure 21: O_3 Effective Optical Depths

as noted earlier SYNS's HIRS-9 channel may be in error. In HIRS-5 SYNS strongly deviates from GENLN2 indicating that SYNS requires some further adjustment.

The total transmittance profiles for each channel are plotted in figures 22 through to 28. Each panel contains a set of transmittance profiles, one for each model, for each member of the atmospheres subset described in section IIIb. For the most part the models are indistinguishable. As expected from the previous graphs, SYNS differentiates from the other models in HIRS-9.

Figures 29 and 30 are plots of $\Delta\bar{\chi}_{total}$ as a function of GENLN2's $\bar{\chi}_{total}$. The plots of HIRS-11, HIRS-12 and HIRS-9 appear similar to their counterparts in figures 15 and 21; which is not surprising since those channels are strongly dominated by H_2O or O_3. Without the other component parts of the total transmittance these plots do not provide much additional information.

IVc) Sensitivity (Jacobian)

No results for the surface pressure Jacobian are presented. Values of zero were reported for all submitted models and channels, except for GENLN2 which reported values ≤ .001K.

The surface temperature sensitivities for each model and channel are tabulated in table 9. In addition, a representative value of the total surface to space transmittance is recorded. As one would expect, the more transparent channels are more sensitive to the surface temperature. HIRS-10 is the most transparent and sensitive to surface temperature, followed by HIRS-9 and HIRS-11.

HIRS	GENLN2 mean	GENLN2 std	FLBL mean	FLBL std	LBLRTM mean	LBLRTM std	SYNSATRAD mean	SYNSATRAD std	TOA $\mathcal{T}_s$
2	.000	.000	.000	.000	.000	.000	.000	.000	.000
5	.040	.032	.031	.026	.043	.035	.041	.033	.030
9	.496	.129	.501	.128	.501	.124	.513	.135	.390
10	.606	.361	.608	.360	.611	.357	.602	.362	.590
11	.111	.147	.092	.125	.112	.148	.111	.146	.085
12	.004	.005	.002	.003	.004	.006	.004	.006	.002
15	.118	.025	.119	.025	.121	.026			.032

Table 9: Mean surface temperature sensitivities (K). The last column contains a representative value of TOA total surface transmittance, $\mathcal{T}_s$.

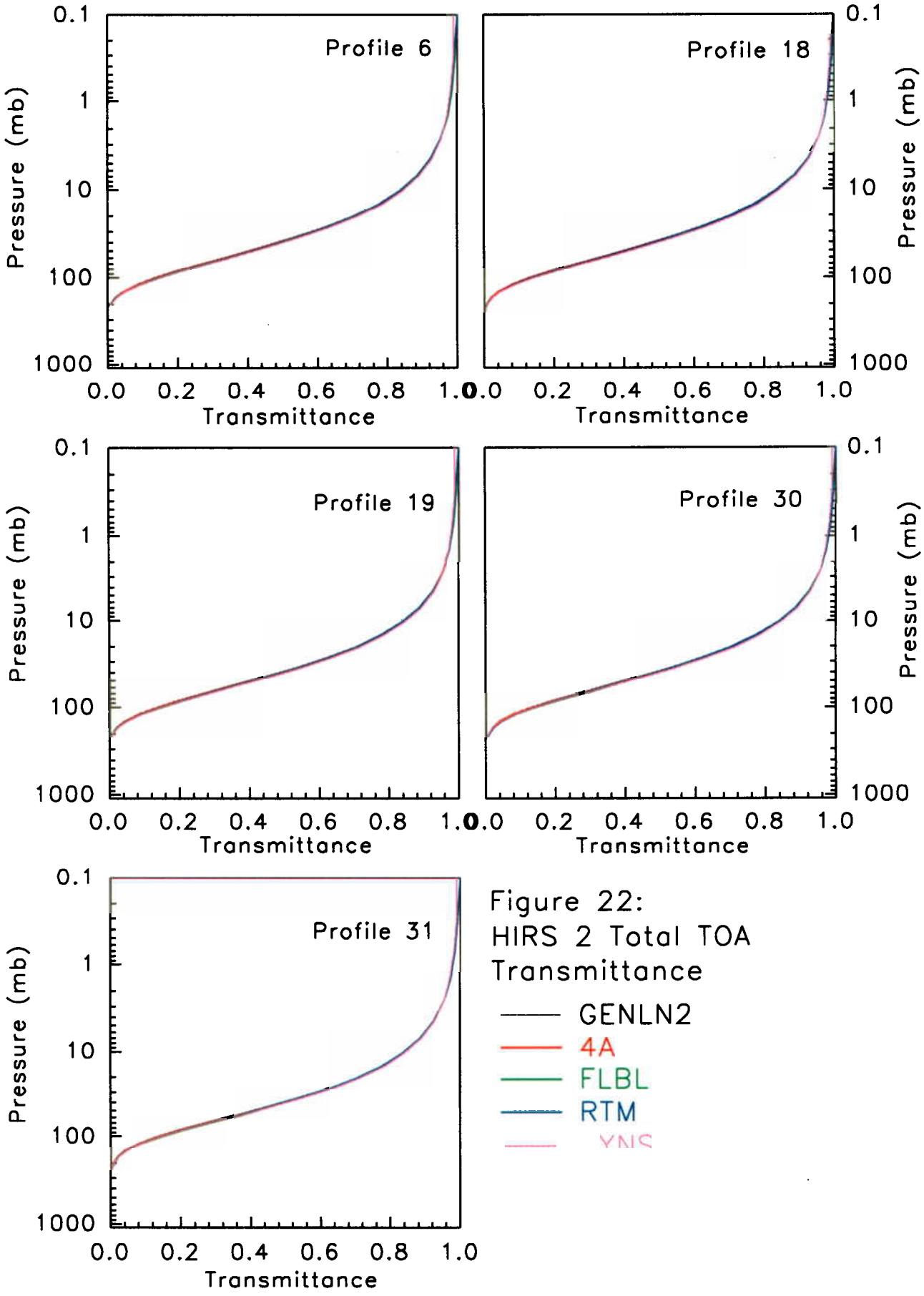

Figure 22:
HIRS 2 Total TOA Transmittance

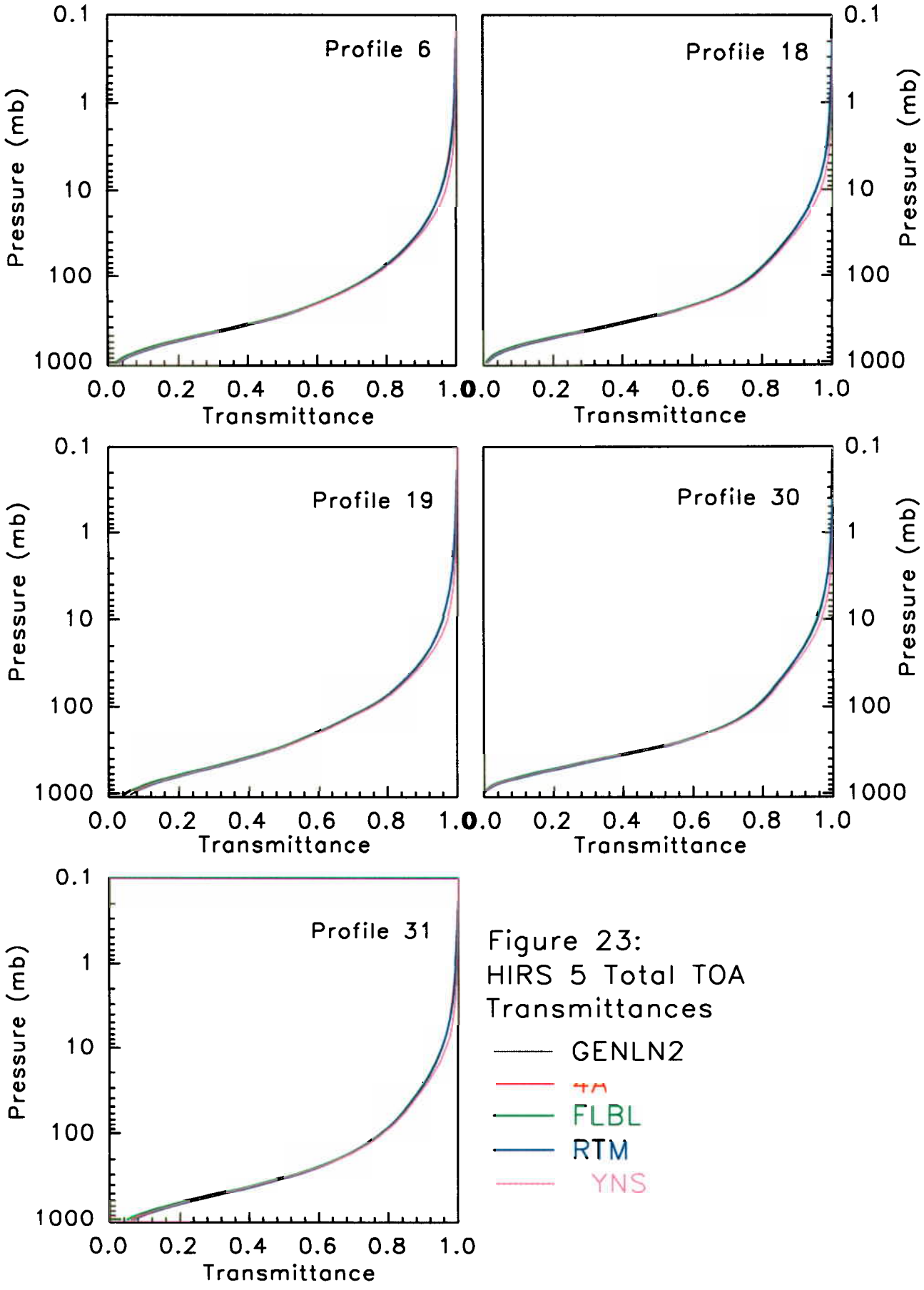

Figure 23:
HIRS 5 Total TOA Transmittances

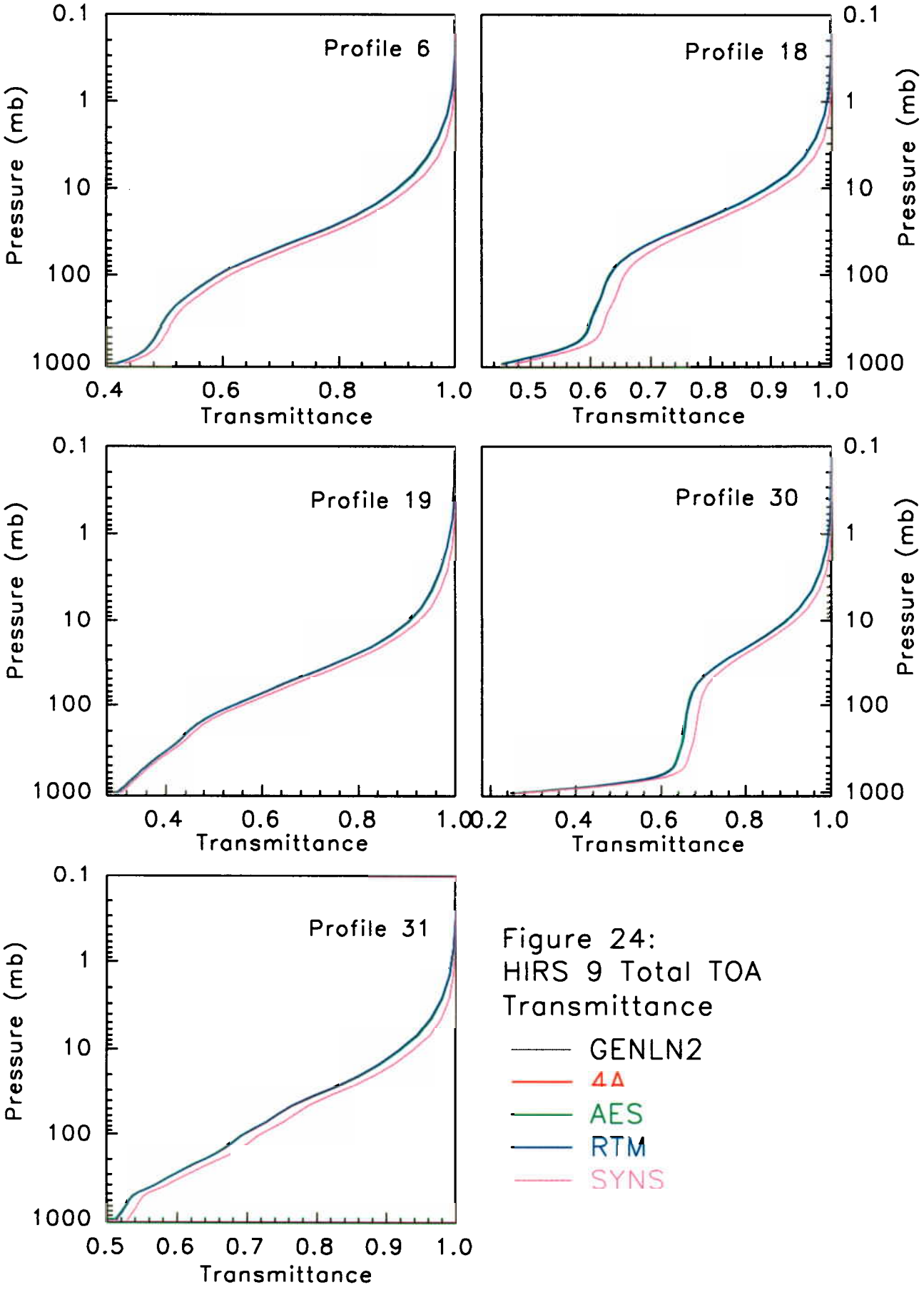

Figure 24:
HIRS 9 Total TOA Transmittance

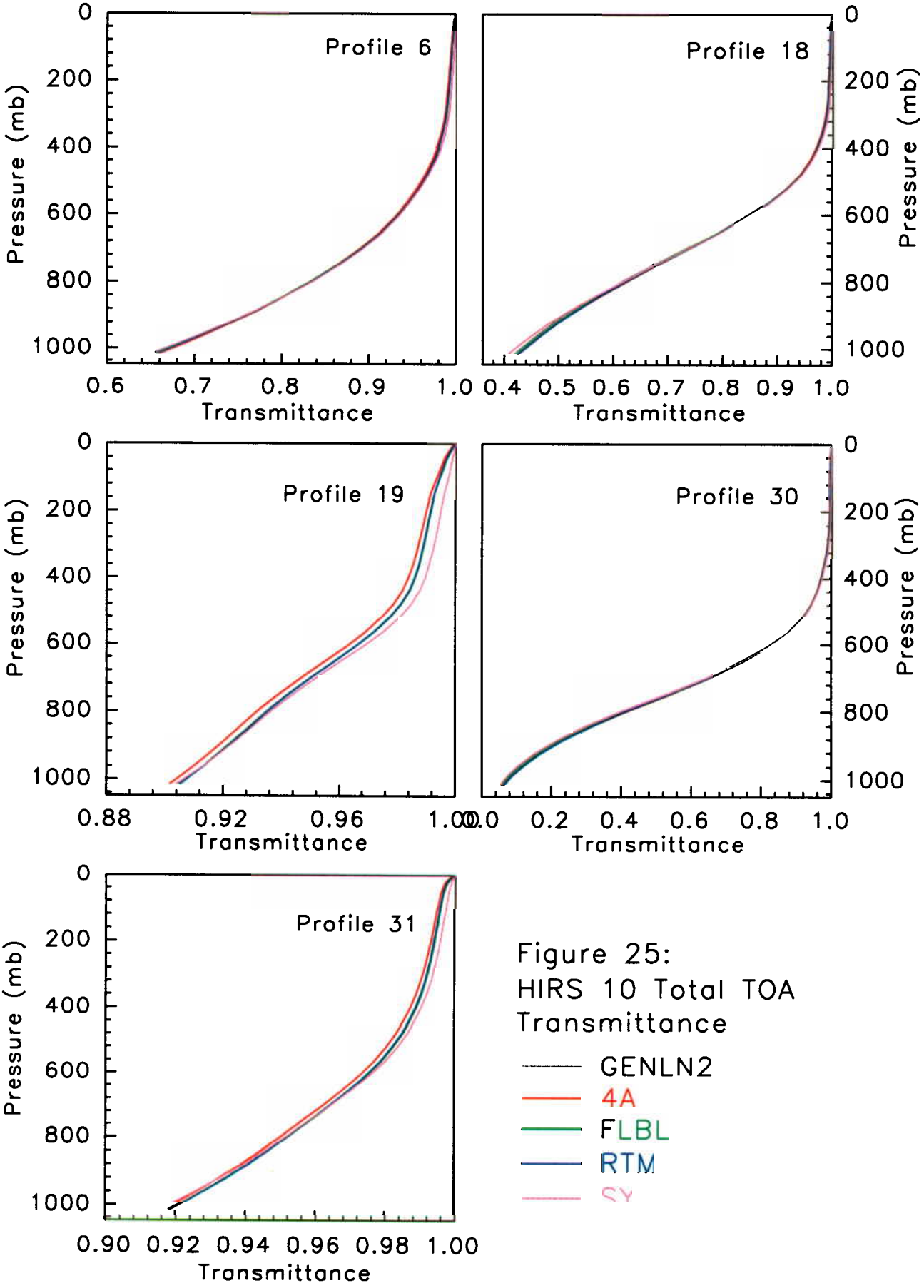

Figure 25:
HIRS 10 Total TOA Transmittance

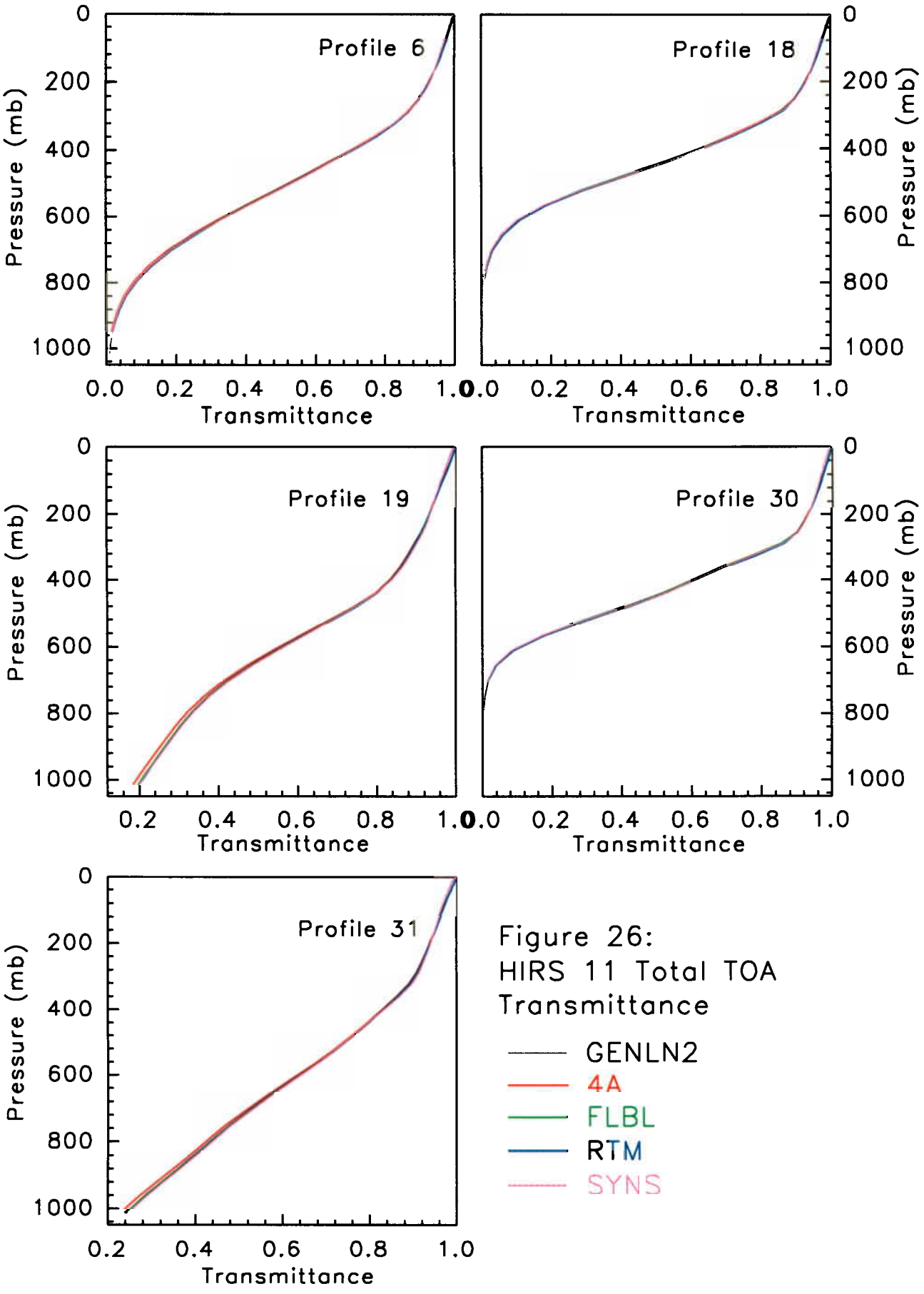

Figure 26:
HIRS 11 Total TOA Transmittance

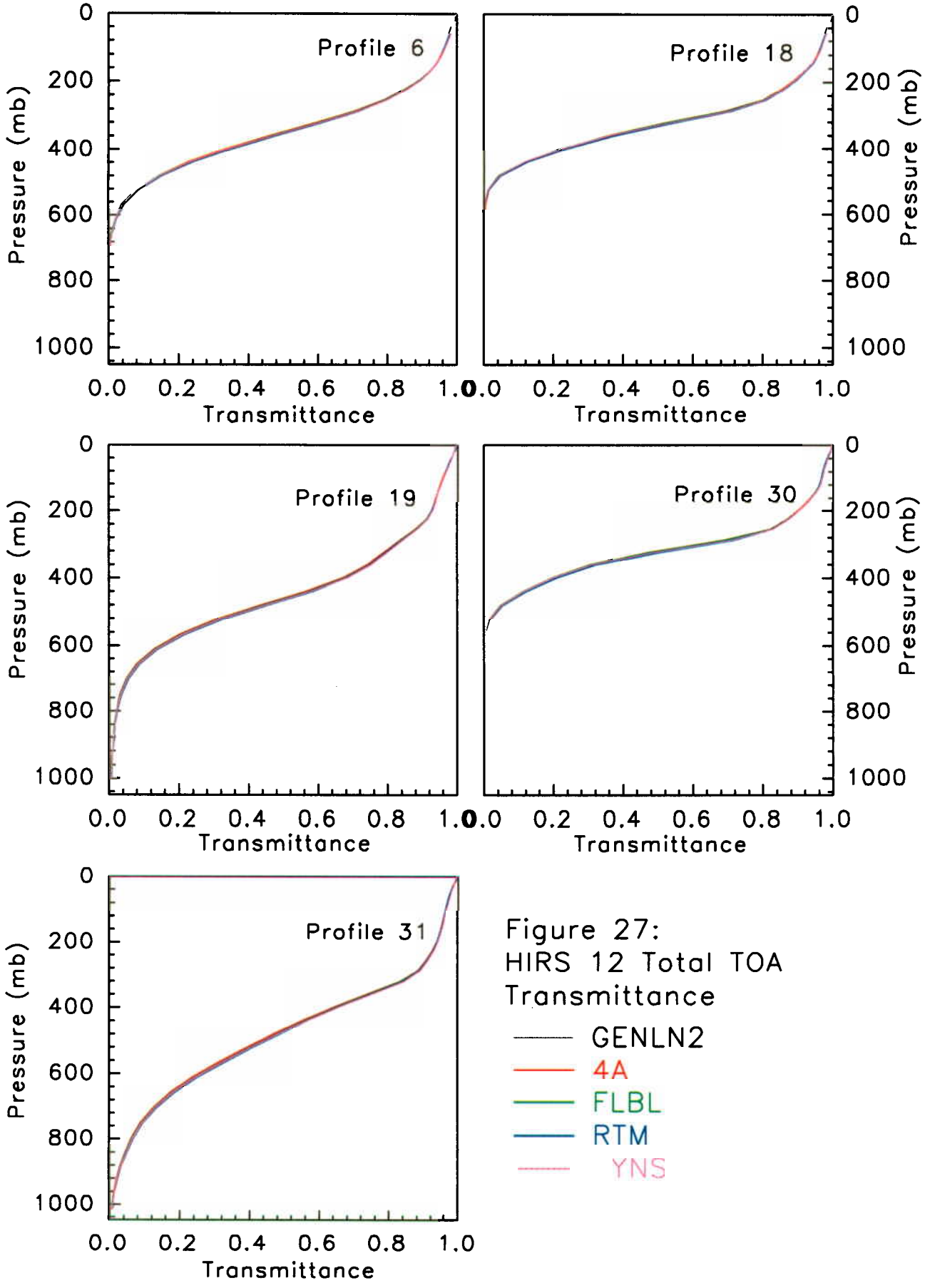

Figure 27:
HIRS 12 Total TOA Transmittance

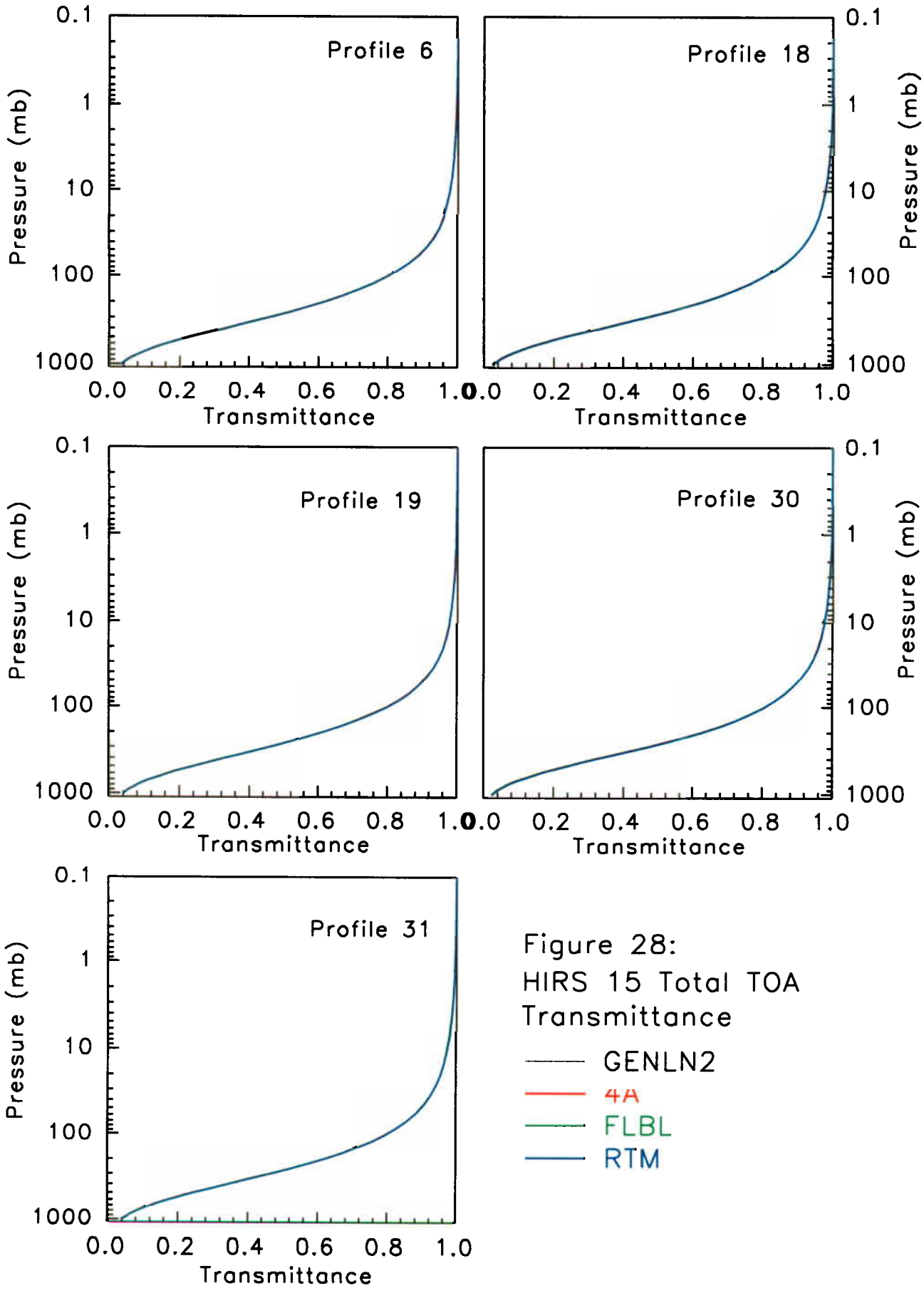

Figure 28:
HIRS 15 Total TOA Transmittance

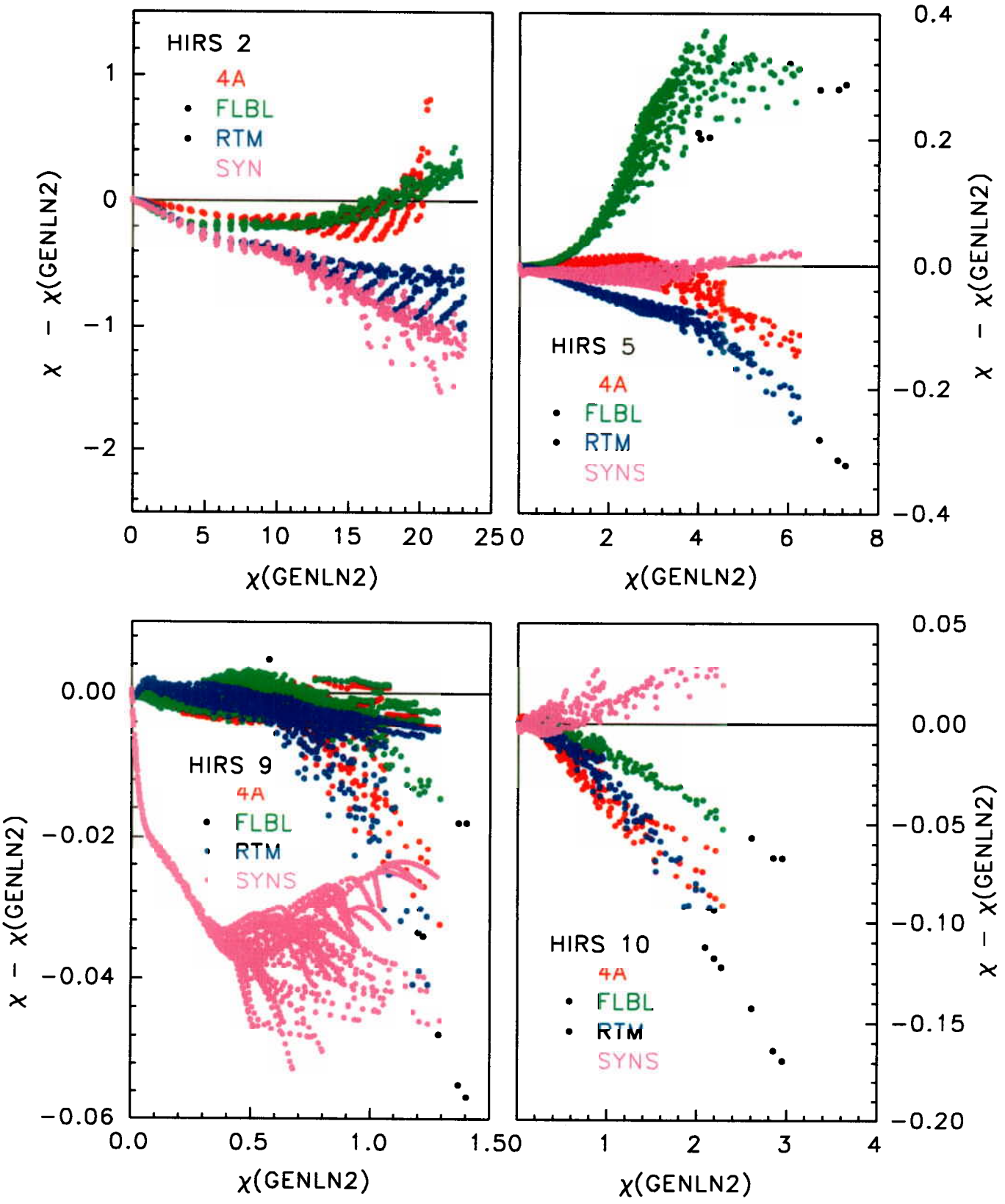

Figure 29: Total Effective Optical Depths

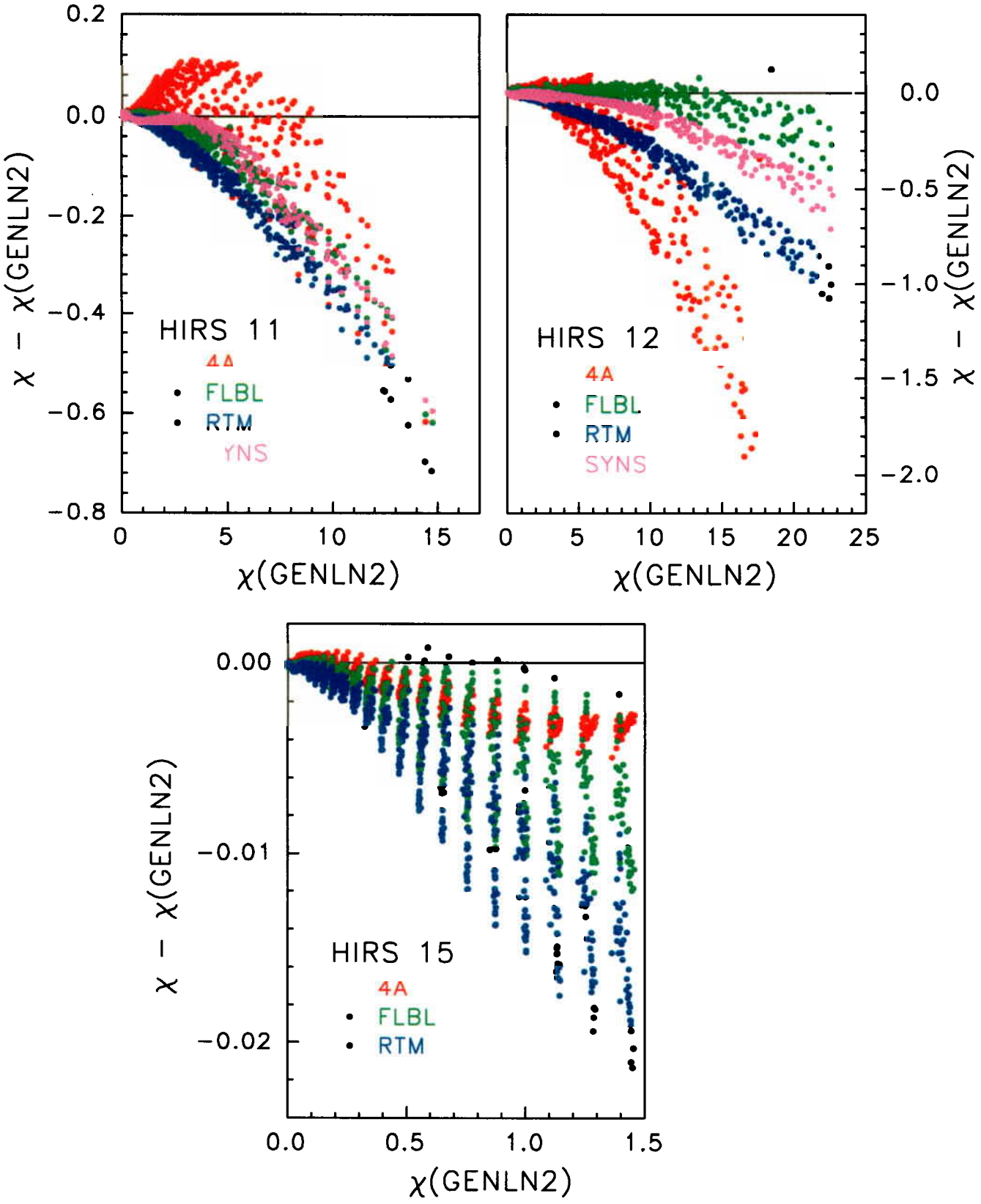

Figure 30: Total Effective Optical Depths

Figures 31 to 37 are plots of the sensitivity of each channel/profile to atmospheric temperature. In general the models tend to follow each other reasonably well and the curves are smooth. SYNSATRAD has slightly noisy curves (ie, small differential spikes) in HIRS-5 and LBLRTM has an anomaly in atmosphere 18 in HIRS-10. On many occasions the 4A curve tends to sit slightly higher (~20mb) in the atmosphere (for example, HIRS-12) which is due to the Jacobians being analytically evaluated in the middle of the layer rather than on the boundary.

Agreement between the models is at its worst in HIRS-9 (figure 33) around the primary peak in the upper atmosphere which tends to be lower than the ozone peak (figure 4). FLBL and RTM tend to agree, but disagree with 4A and SYNS. At first glance, HIRS-9 appears noisy in the troposphere of atmospheres 19 and 31, however the bumps correlate with the ozone profile of these atmospheres (figure 4 and table 4). These atmospheres are dry ones, thereby reducing the masking effect of tropospheric H_2O. The other atmospheres are wetter and exhibit a strong second peak in the troposphere which is clearly related to the tropospheric moisture content (figure 4 and table 4).

Noticeable variation between the models is also seen in HIRS-5, mostly in the primary peak in the lower tropopause. The curves appear to have strong secondary peaks in the stratosphere, however the trough between the peaks is correlated to the tropopause; hence the two peaks are due to the suppression of the sensitivity by a cold tropopause rather than by enhanced sensitivity in the stratosphere. The secondary peaks in HIRS-15 (figure 37) also exhibit characteristics of tropospausal suppression, but there also appears to be enhancement due to strong stratospheric temperatures.

Figures 38 to 43 are plots of the sensitivity of each channel/profile to atmospheric water vapour. In general the models tend to follow each other reasonably well, the curves are generally smooth and there are no double peaks. Again, 4A tends to sit slightly higher in the atmosphere. As one would expect, the magnitude of the peaks is obviously correlated to the column amount of water. Except for HIRS-11 and HIRS-12, the sensitivity to the dry atmospheres (19 and

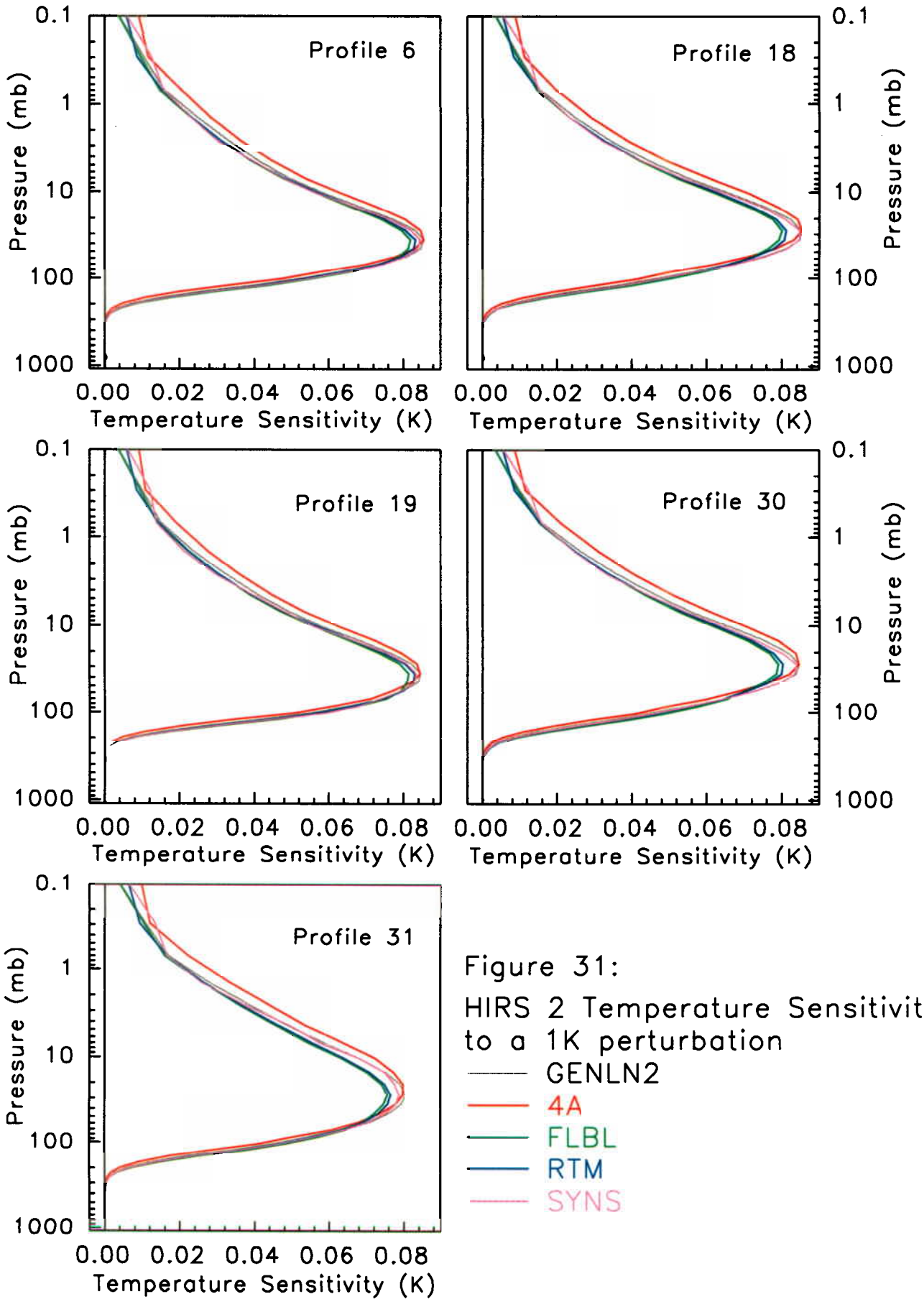

Figure 31:
HIRS 2 Temperature Sensitivity to a 1K perturbation

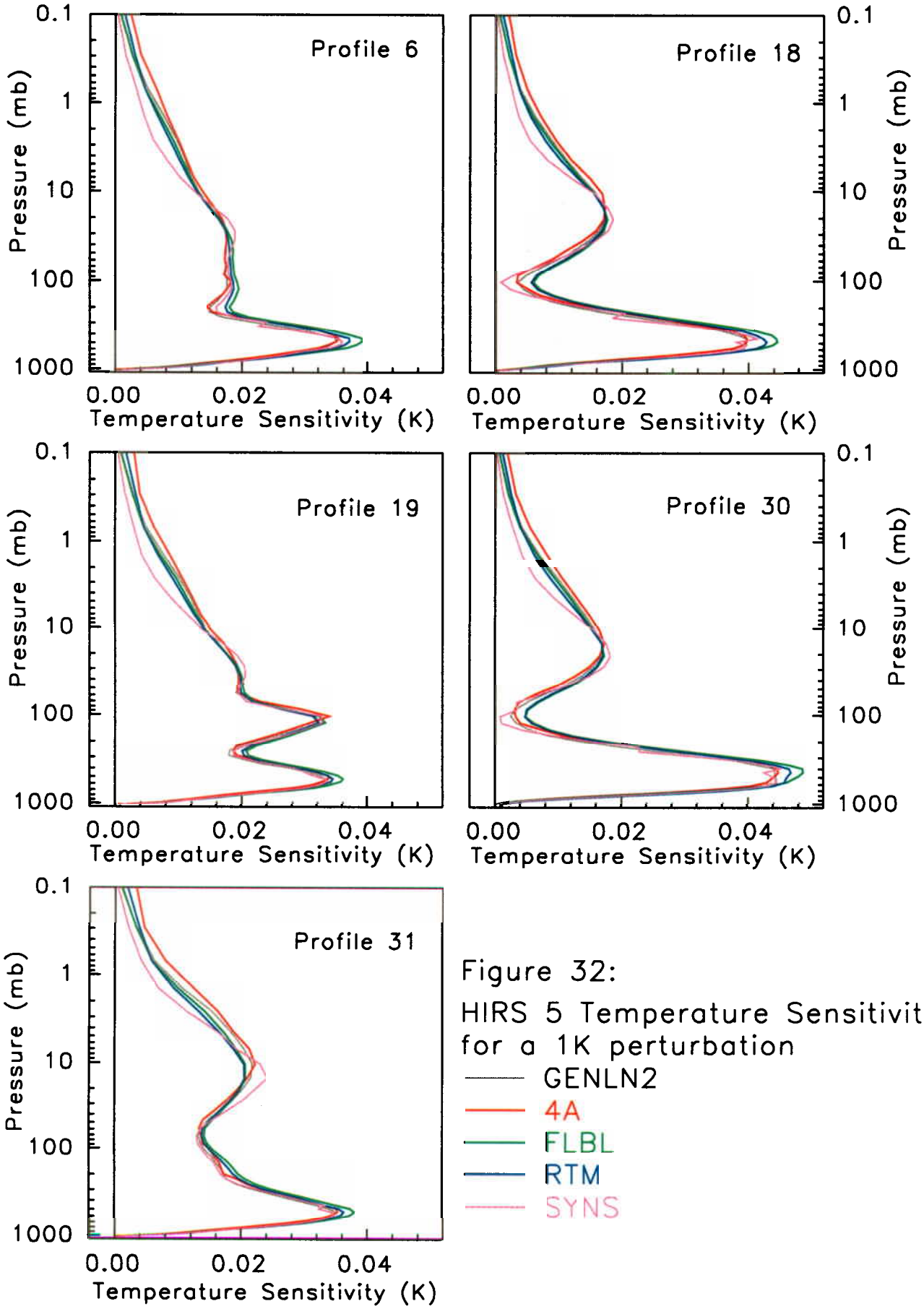

Figure 32:

HIRS 5 Temperature Sensitivity for a 1K perturbation

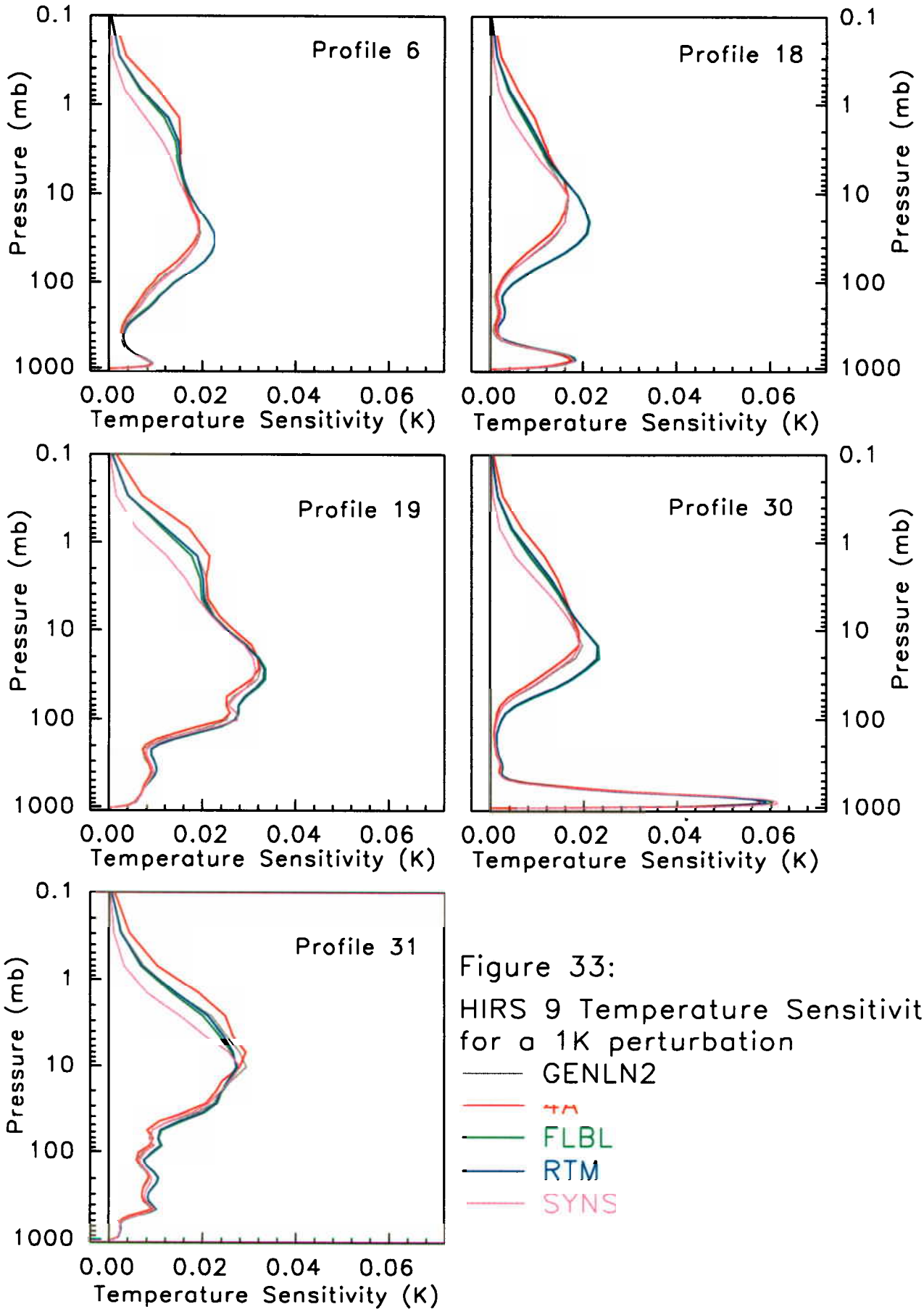

Figure 33:

HIRS 9 Temperature Sensitivity for a 1K perturbation

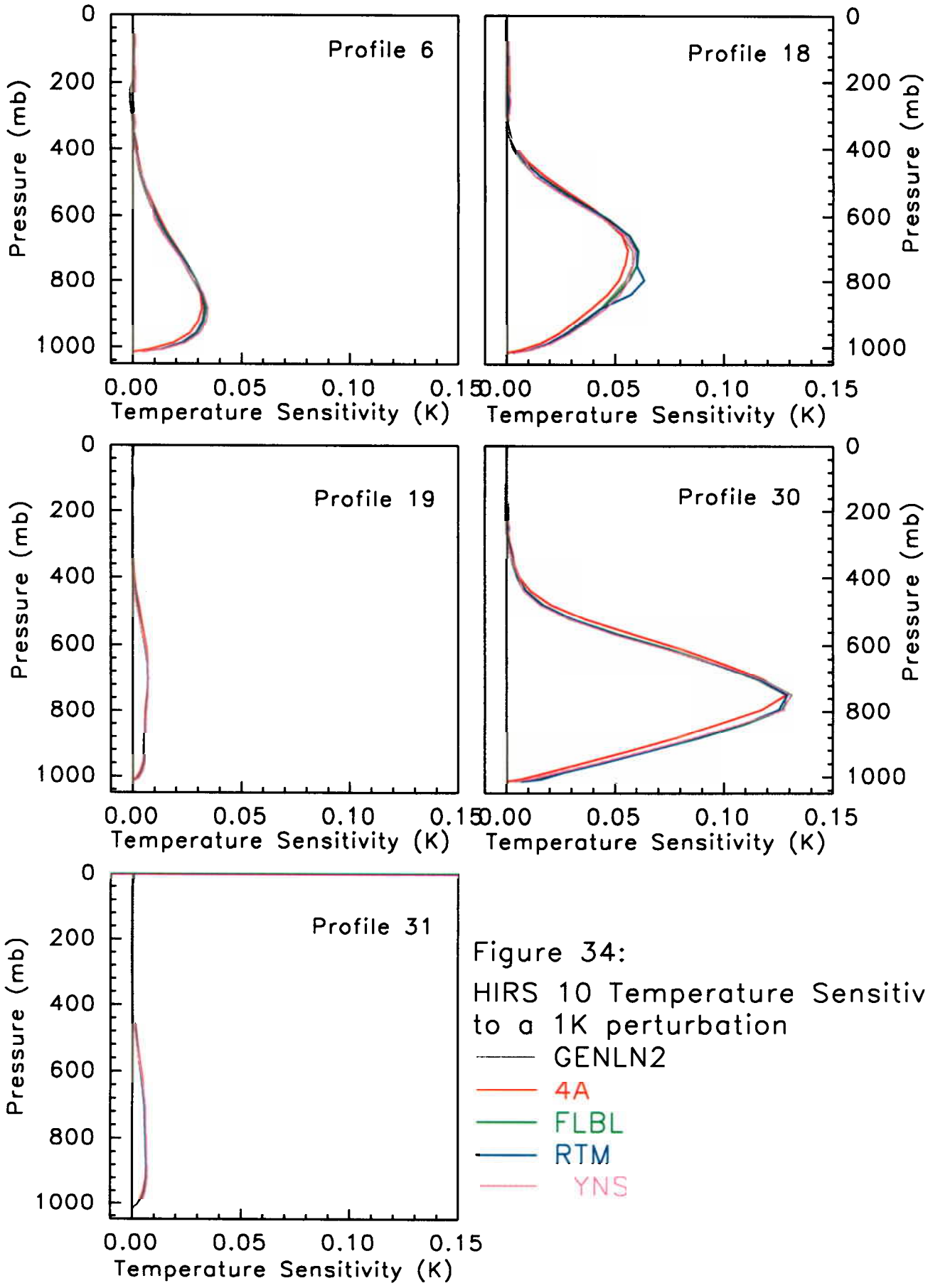

Figure 34:

HIRS 10 Temperature Sensitivity to a 1K perturbation

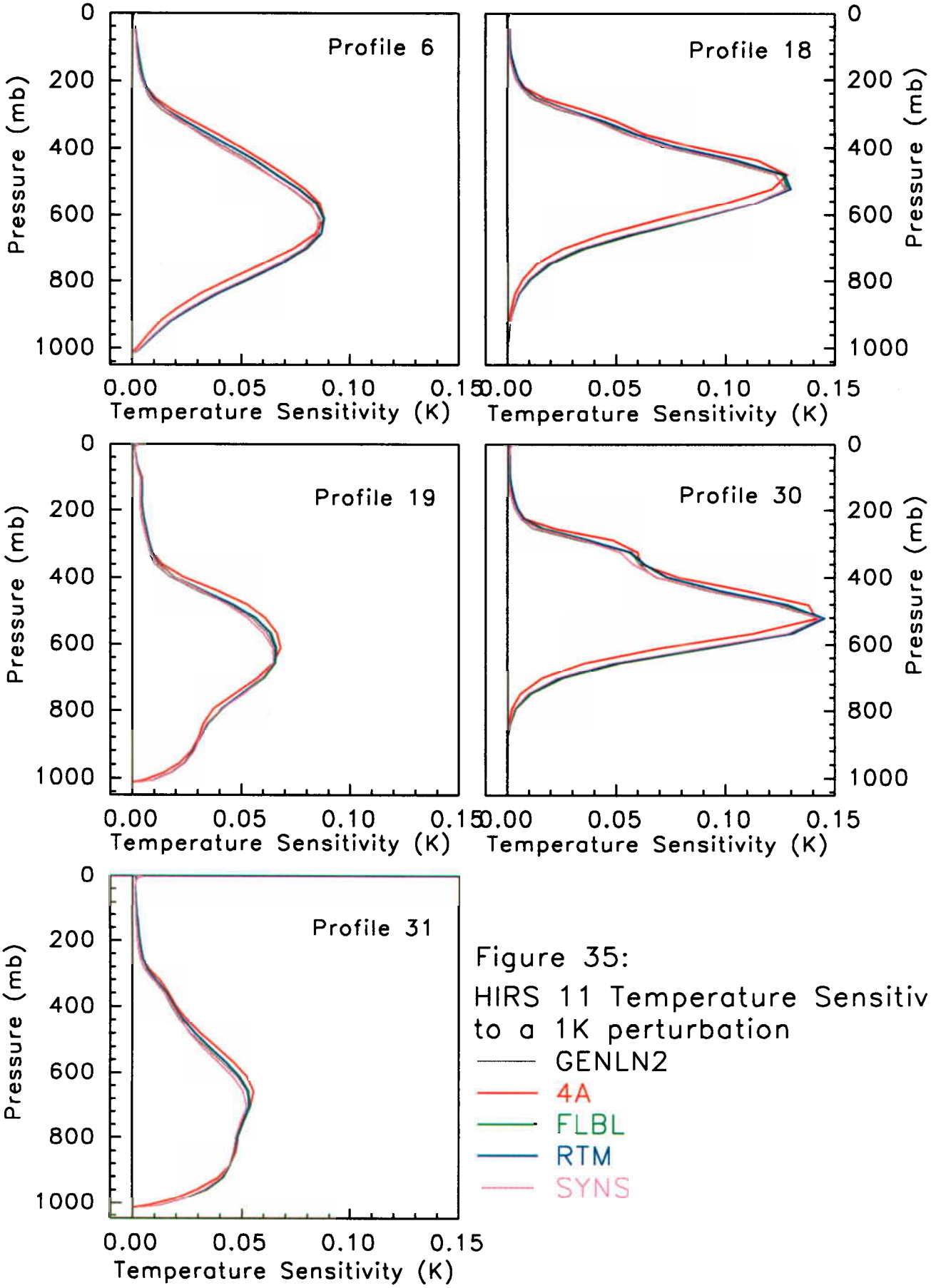

Figure 35:
HIRS 11 Temperature Sensitivity to a 1K perturbation

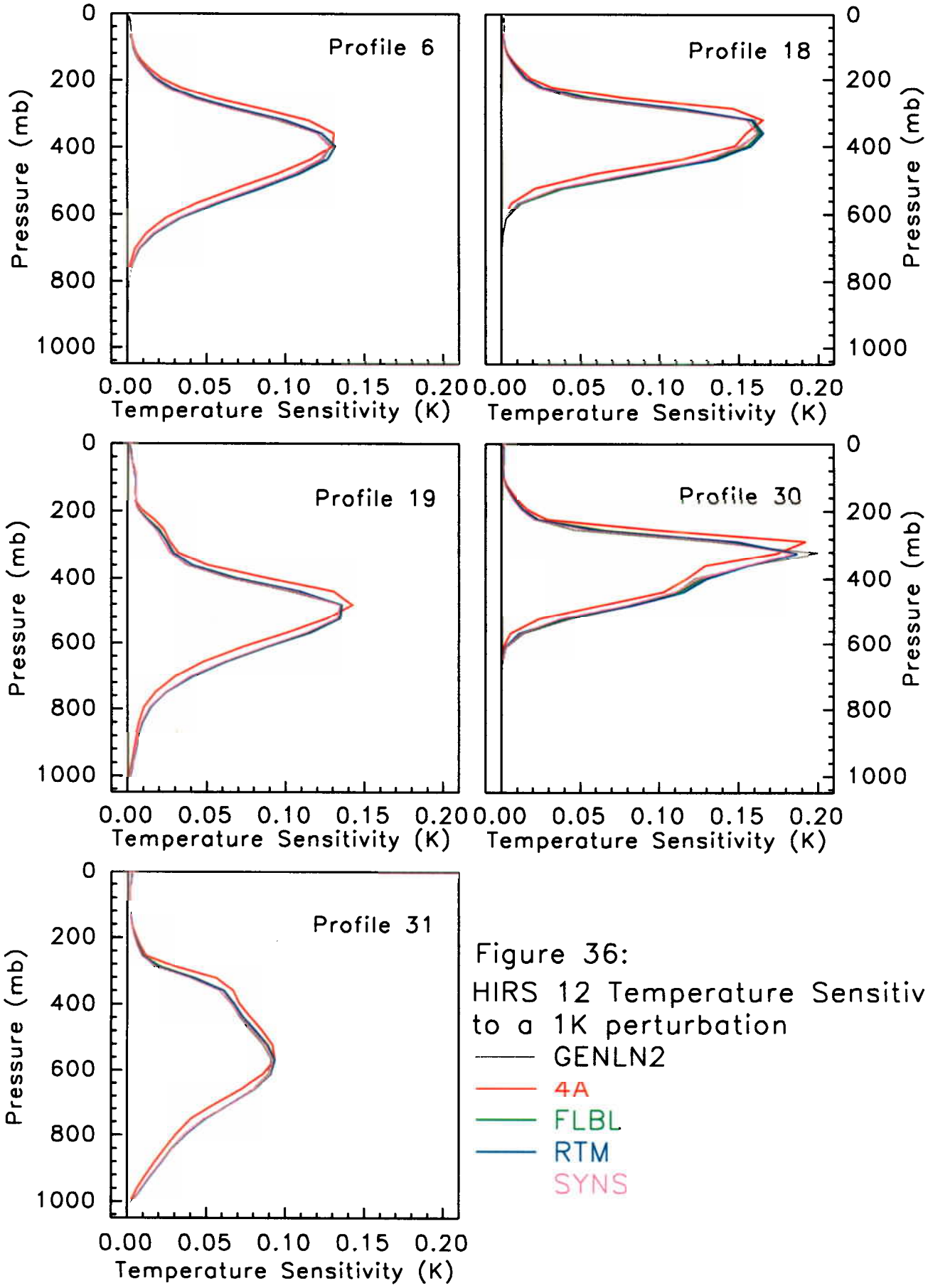

Figure 36:
HIRS 12 Temperature Sensitivity to a 1K perturbation

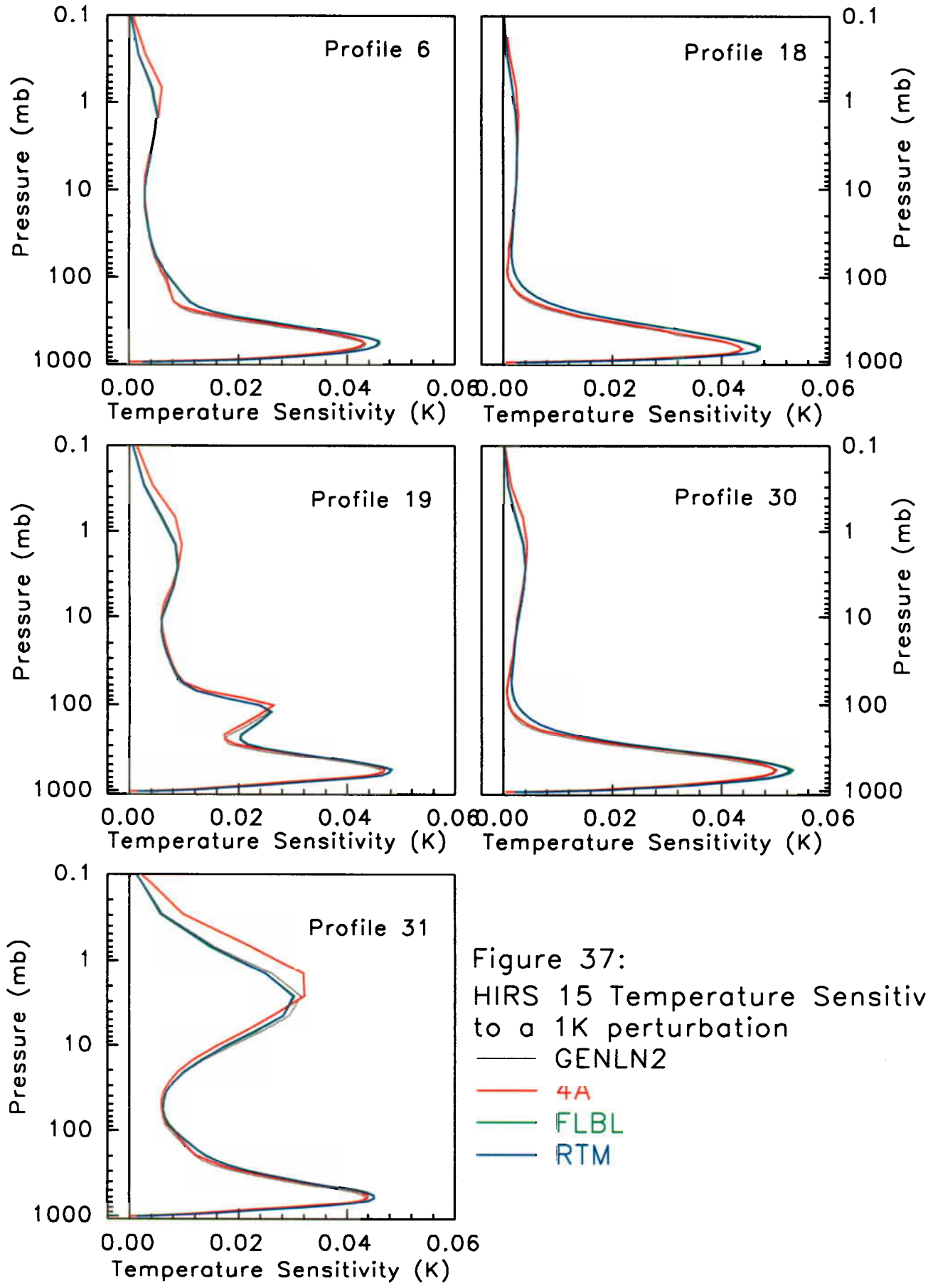

Figure 37:
HIRS 15 Temperature Sensitivity to a 1K perturbation

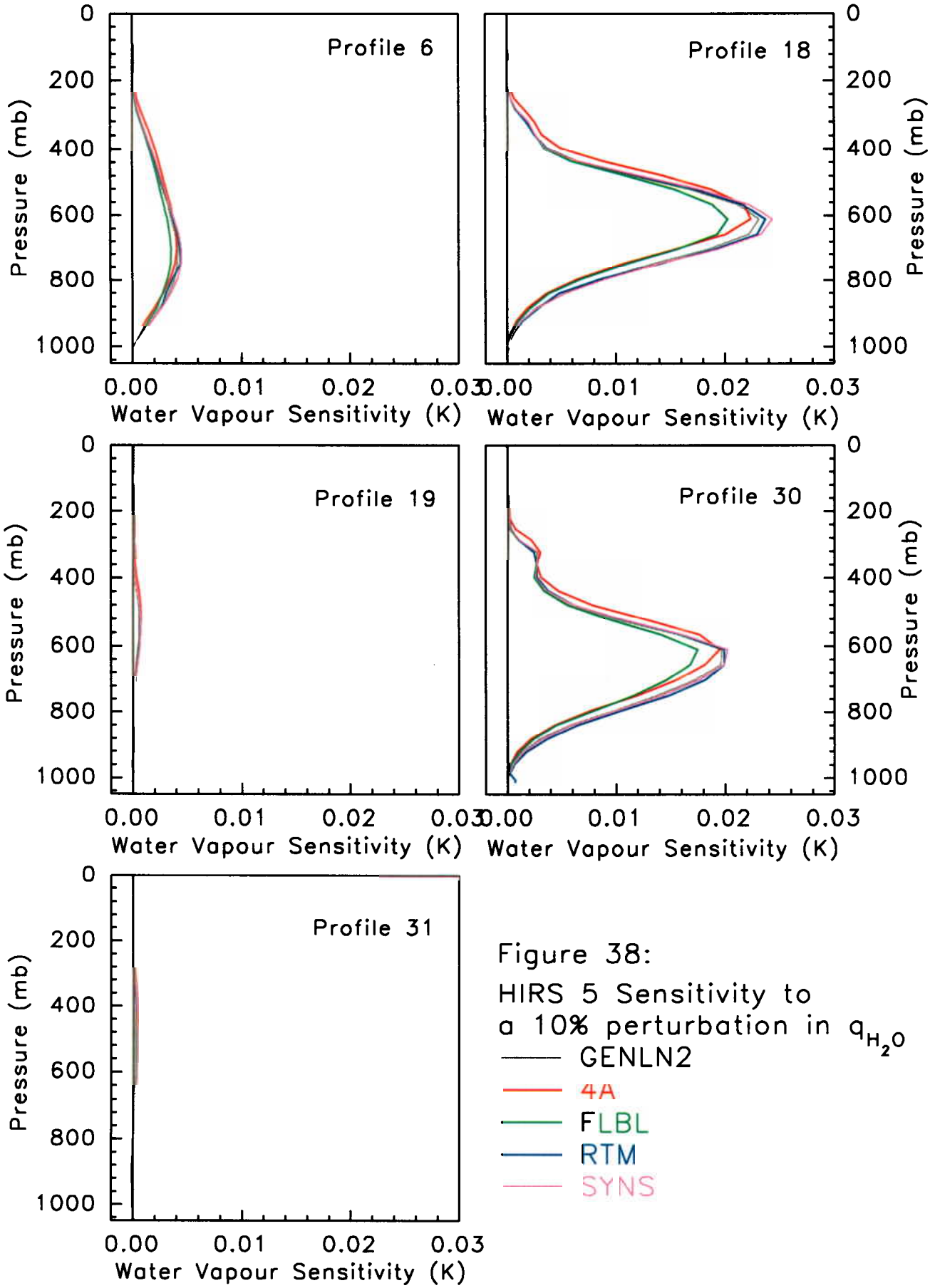

Figure 38:
HIRS 5 Sensitivity to a 10% perturbation in q_{H_2O}

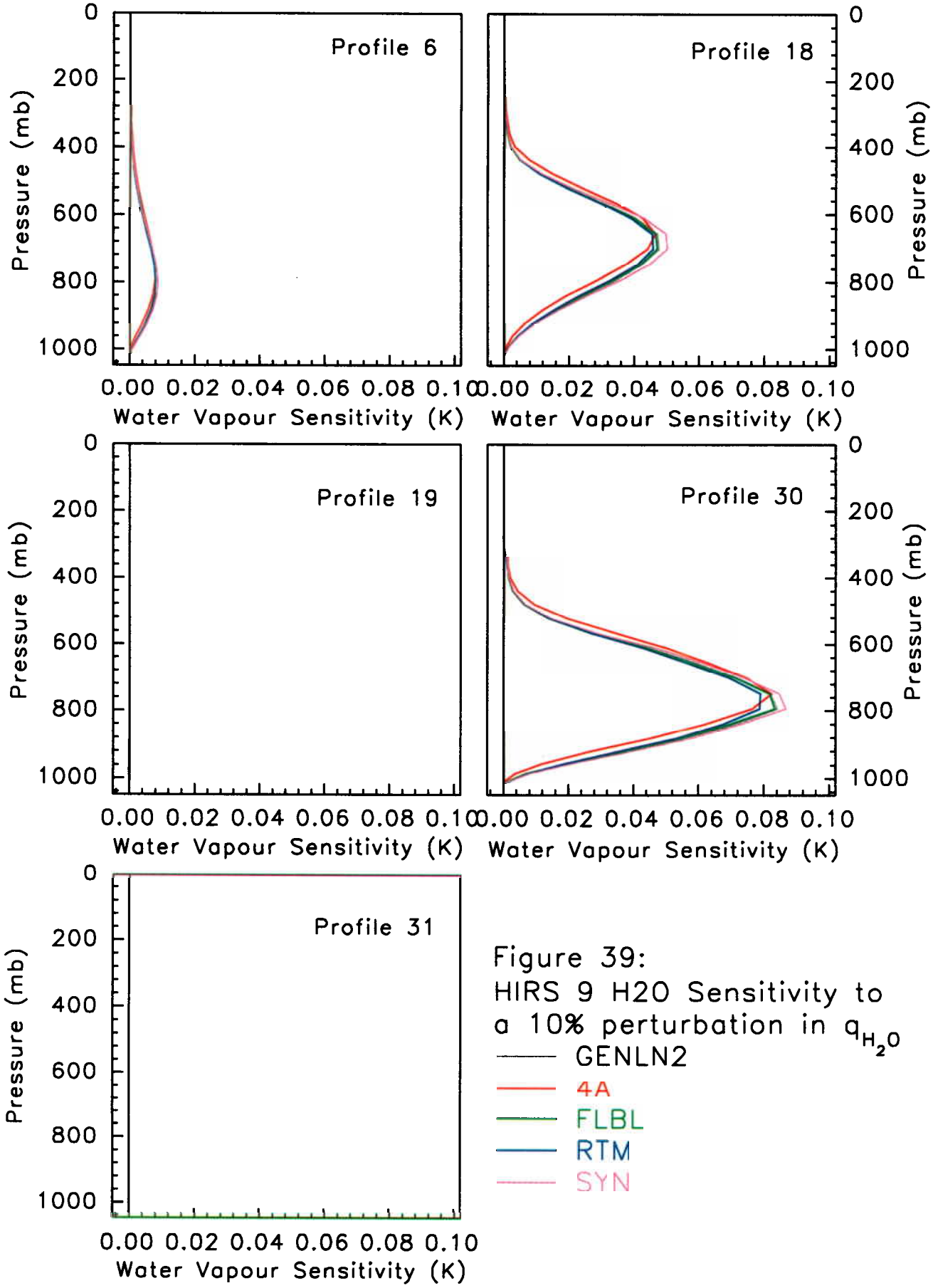

Figure 39:
HIRS 9 H2O Sensitivity to a 10% perturbation in q_{H_2O}

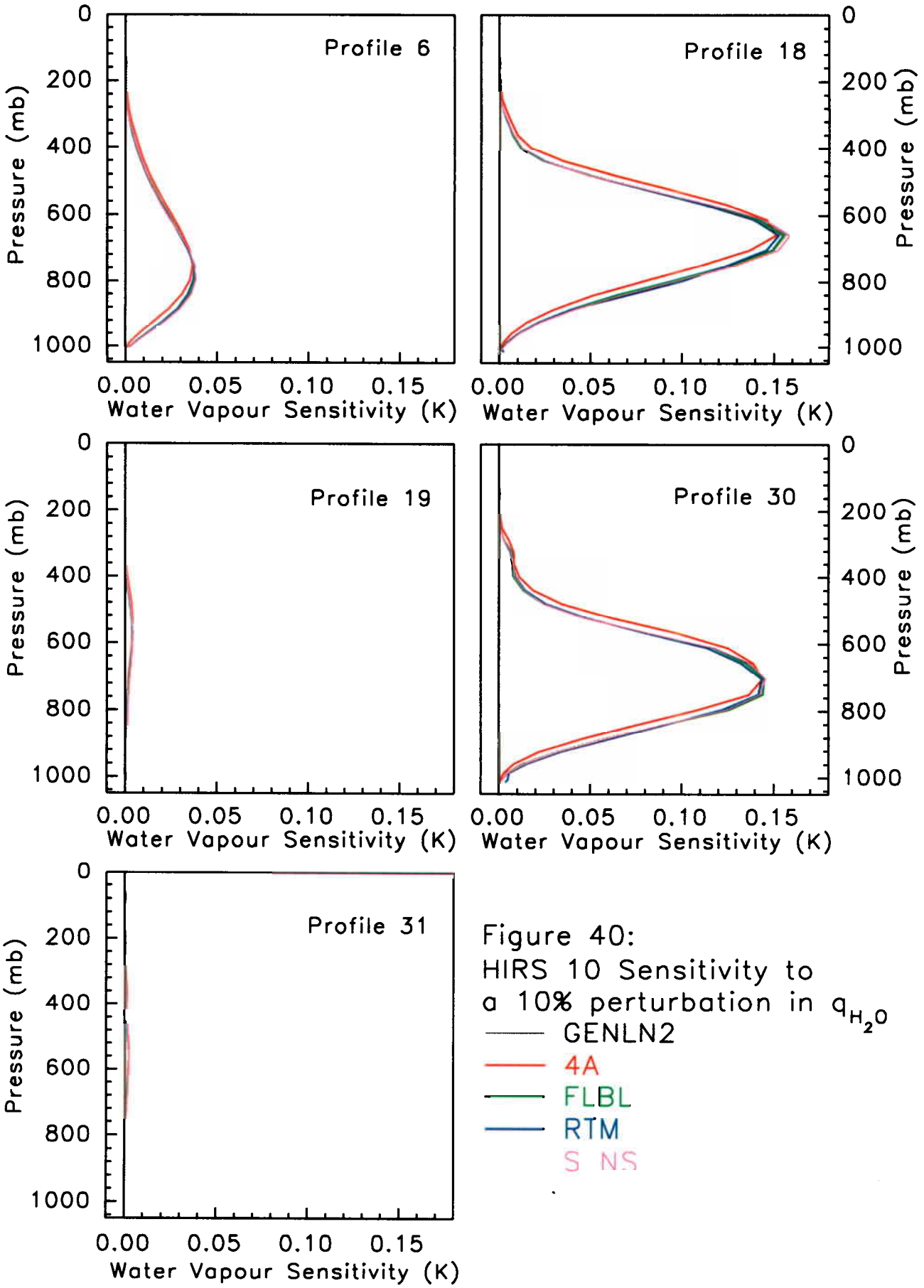

Figure 40:
HIRS 10 Sensitivity to a 10% perturbation in q_{H_2O}

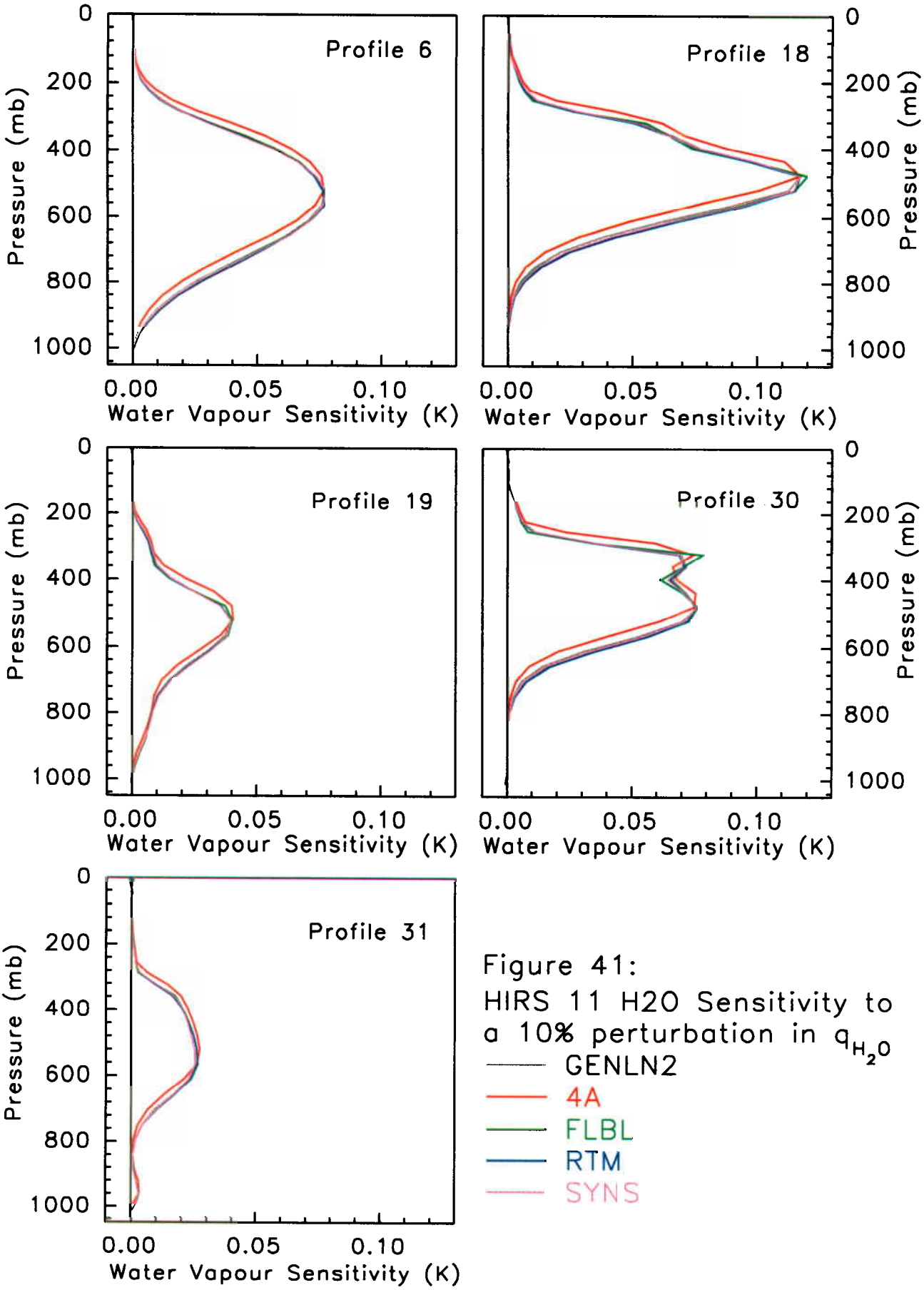

Figure 41:
HIRS 11 H2O Sensitivity to a 10% perturbation in q_{H_2O}

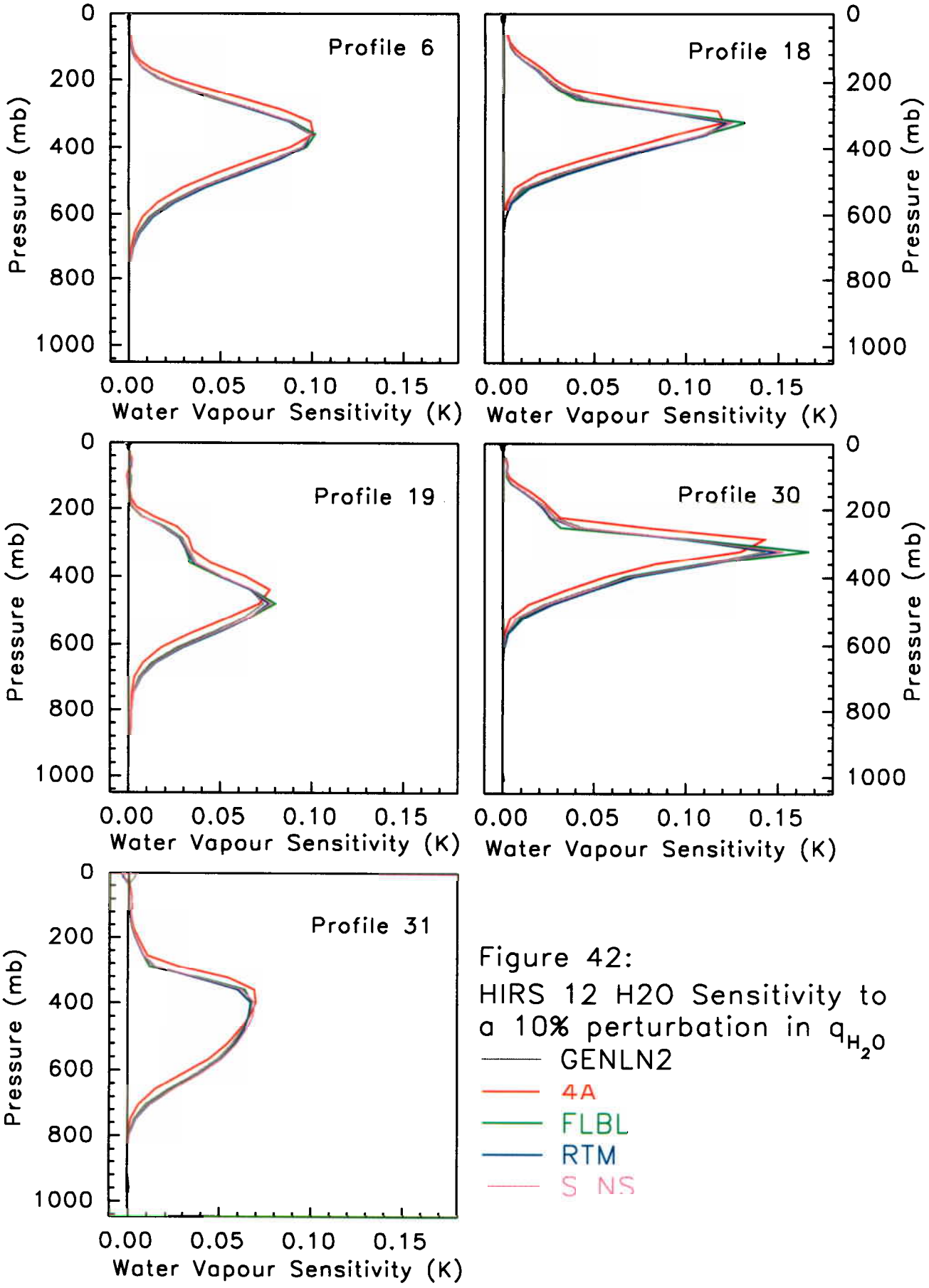

Figure 42:
HIRS 12 H2O Sensitivity to a 10% perturbation in q_{H_2O}

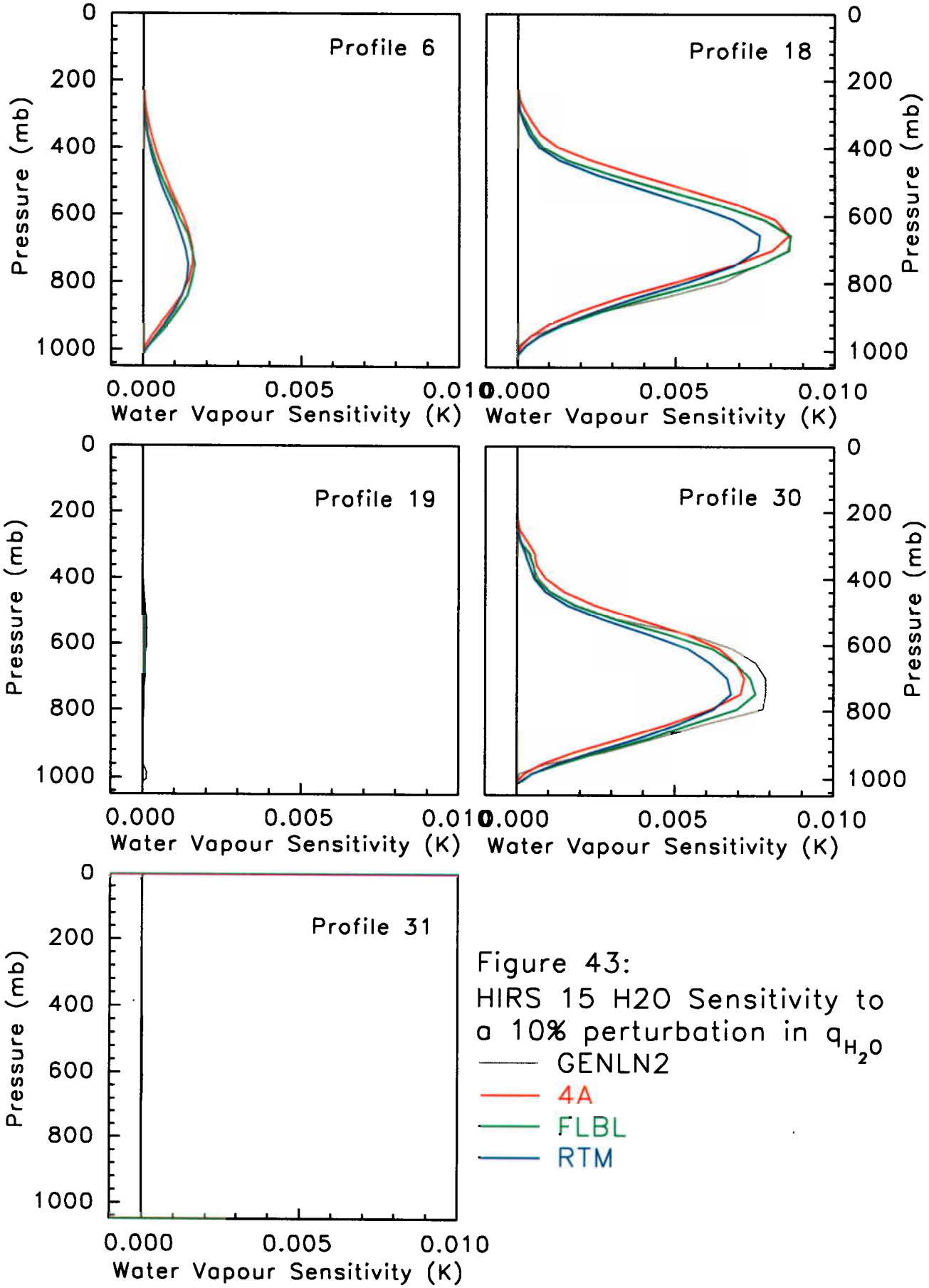

Figure 43:
HIRS 15 H2O Sensitivity to a 10% perturbation in q_{H_2O}

31) is nearly negligible. The curve for atmosphere 30 in HIRS-12 is somewhat bumpy and is likely due to a rather sharp dry region at the tropopause.

Figures 44 through to 46 are plots of the sensitivity of each channel/profile to atmospheric ozone. In general the models tend to follow each other reasonably well and the curves are generally smooth. Compared to HIRS-9; HIRS-2 and HIRS-5 are not very sensitive to ozone. The bumpiness in the lower troposphere observed in HIRS-9 and HIRS-5, atmosphere 31, are due to the bumpy ozone profile (figure 4). The ozone sensitivity curves are different from the others in that they have both a negative and a positive component.

V DISCUSSION

This study was driven by an intercomparison of fast forward models. Most fast models are constructed from LBL simulations of a representative group of atmospheres, and once constructed the bias of the fast model relative to its parent LBL for any set of atmospheres should be less than the instrument noise. When comparing fast models with different LBL parents, one has to take into account that the parent LBLs may differ. Ideally, if all the fast models were constructed from identical LBLs then the bias attributed to different LBLs would be zero and one would have a reliable indication of how well the fast models compare.

As it is, the LBLs do not agree with each other with infinite precision. Given that the LBL's differ, a target should be set for their agreement in the context of the HIRS instrument. It is generally accepted that fast models relative to the parent LBL should have a bias less than the channel's typical noise equivalent temperature, NEΔT (Saunders et al, 1999). It follows that the LBLs relative to a reference should have a bias such that when added to a fast model bias, is less than NEΔT. As LBLs are in principle the most accurate and precise models available, the target bias for them should be smaller, say ¼NEΔT. When the NEΔTs in table 4 and the biases in table 8 are compared only 15% of the biases meet this criterion.

The choice of a reference model is arbitrary, 4A could have equally been

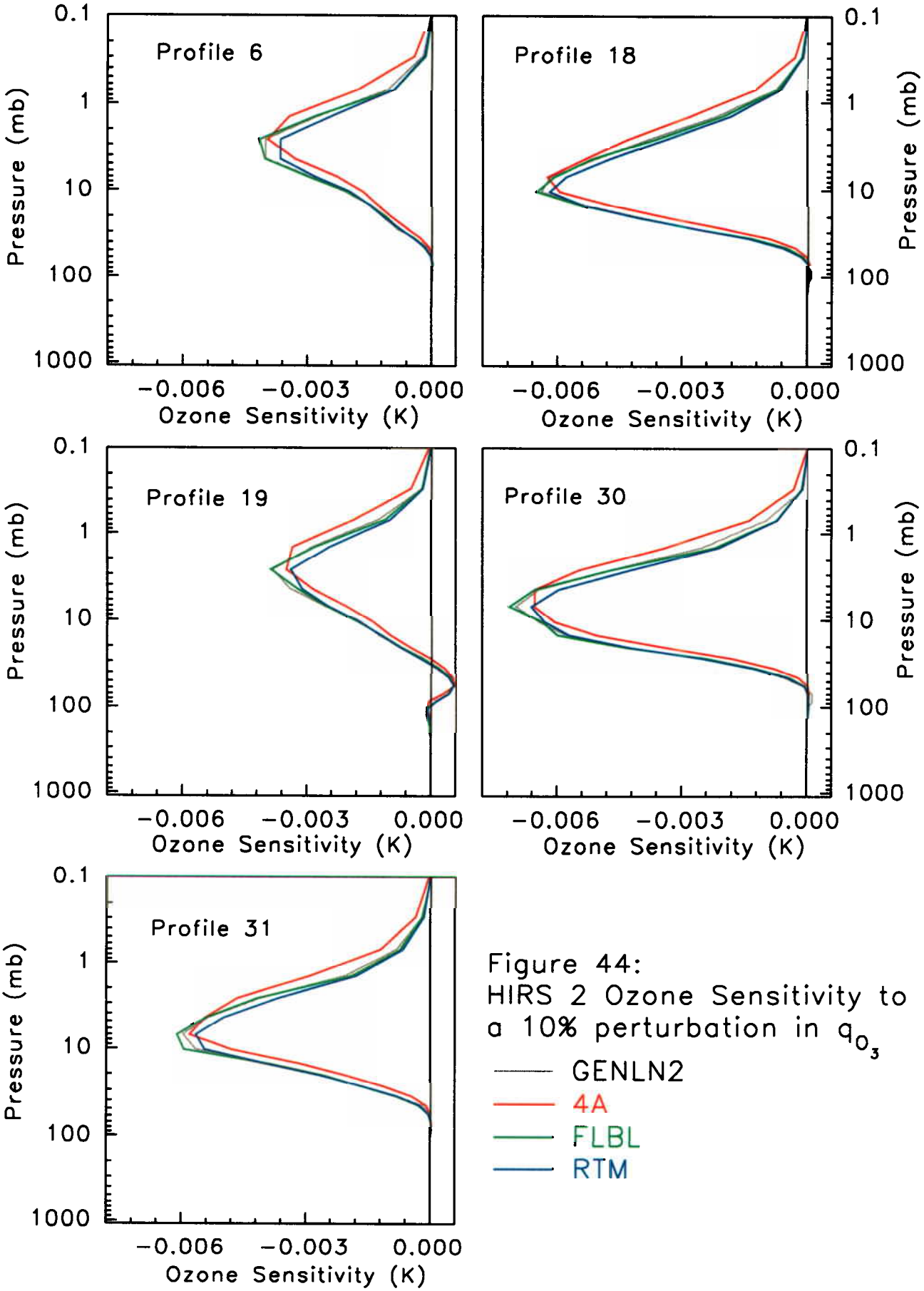

Figure 44:
HIRS 2 Ozone Sensitivity to a 10% perturbation in q_{O_3}

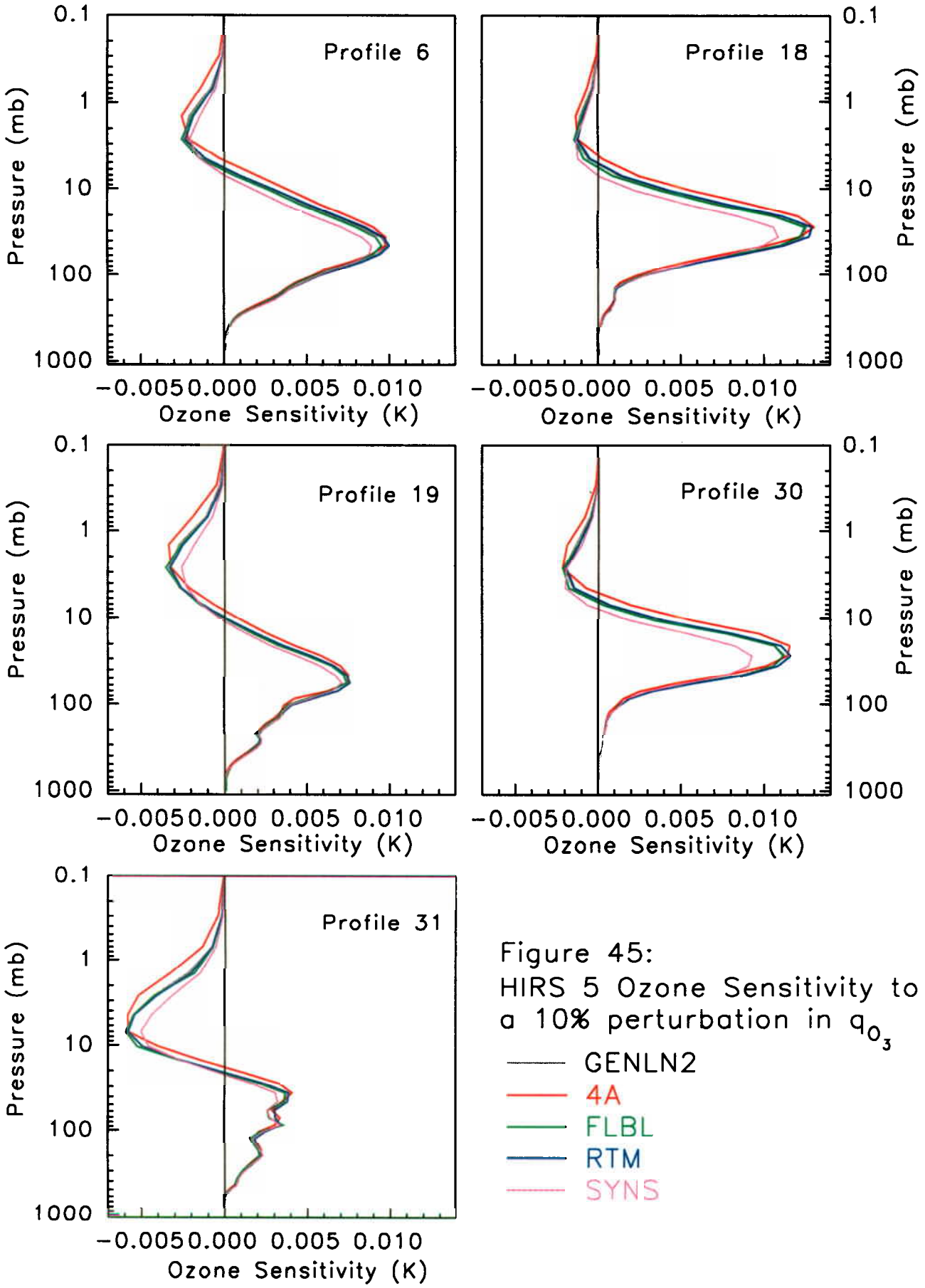

Figure 45:
HIRS 5 Ozone Sensitivity to a 10% perturbation in q_{O_3}

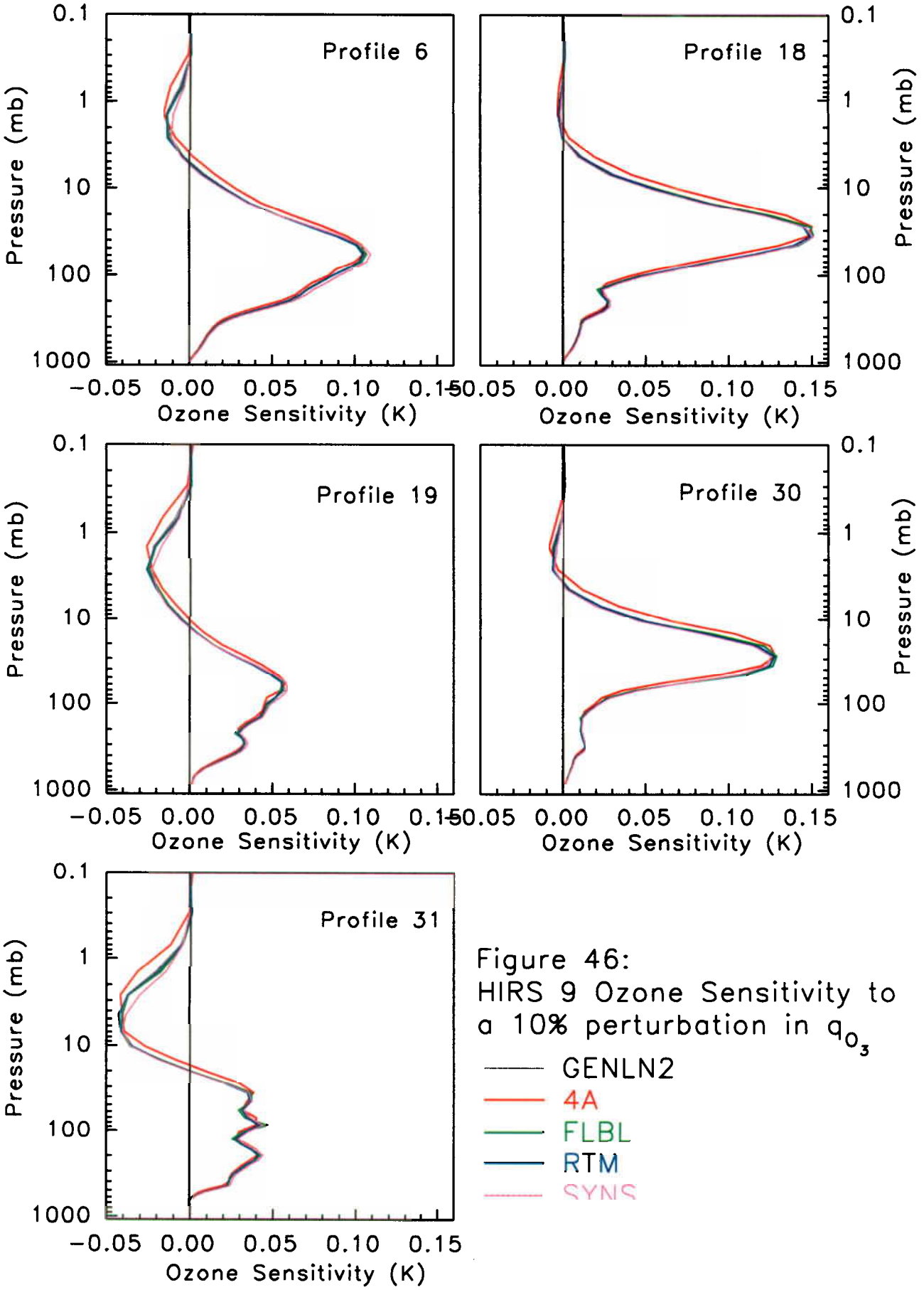

Figure 46:
HIRS 9 Ozone Sensitivity to a 10% perturbation in q_{O_3}

chosen. Table 10 lists the biases and standard deviations assuming 4A to be the reference model; the number of biases meeting the ½NEΔT criterion doubles. The increase comes mainly from HIRS-12, where it was previously noted that the reference model, GENLN2, was anomalous (figure 6).

The choice of ½NEΔT as a target for LBL agreement is also arbitrary. Perhaps it should be set to a smaller value in order to leave some leeway for a comparison with observed data.

	GEN2		FLBL		RTM		SYNS	
HIRS	Bias	std	Bias	std	Bias	std	Bias	std
2	0.063	0.037	-0.089	0.087	0.017	0.029	-0.186	0.120
5	0.084	0.025	-0.409	0.144	0.447	0.098	-0.120	0.130
9	-0.024	0.055	-0.036	0.027	0.093	0.038	0.462	0.608
10	-0.013	0.092	0.007	0.058	0.027	0.035	0.025	0.112
11	0.246	0.063	0.171	0.061	0.169	0.084	0.300	0.142
12	0.138	0.131	-0.006	0.089	-0.021	0.122	-0.018	0.159
15	-0.047	0.015	0.060	0.063	0.135	0.088		

Table 10: TOA brightness temperature bias of the 42 profiles with respect to 4A and its standard deviation as a function of channel and model.

One of the components missing in the intercomparison was a accurate and precise measurement of a real heterogenous atmospheric path and a simultaneous HIRS measurement. A few sets of these would have been worthwhile in order to establish a bias with respect to reality; that is—, provide an absolute validation of the LBLs. Unfortunately such a dataset where all the variables are precisely and accurately known does not exist. Partial datasets exist, ie; temperature and some of the constituents are known, however in general these datasets are not useful for the absolute validation of LBLs as the degree of accuracy of most operational sondes is not high enough. Obtaining a complete and accurate specification is very difficult.

Many of the curves in figure 6 appear to be systematically offset from the reference model and have small scale variations or noise. If all the correct physics is utilized, then one would expect the models to produce the same results; however one might also expect slight errors to arise due to different

numerical implementations of the same physics. Some of these deviations can be explained by differences in spectroscopy. Some examples are; the deviations in HIRS-2, HIRS-5 and HIRS-15 are probably related to the various CO_2 continuum parameterizations (table 1); the deviations in HIRS-12 may be related to the different parameterizations of the O_2 continuum; etc... The LBLs did not use the same absorber lists; hence some aberrations may be related to missing or additional absorbers. Without additional numerical experimentation it is impossible to define the impact of the different parameterizations.

The most significant difference appears to be related to a difference between the models and GENLN2 in the handling of water vapour. At least one of the other models uses the same line data and CKD2.1 as GENLN2; thus the difference does not appear to be due to the CKD versions used, nor does it appear to be due to line database used. Without more details one can only speculate as to the source of this discrepancy. It is possible that a there is significant difference in the implementation of CKD and/or there is a significant difference in the way the absorber amount component of optical depth is created.

Another potential source of noise is related to the method of evaluating the representative layer's values of pressure, temperature and absorber amount. These values are used to calculate the absorption coefficient and the optical depth. Under some conditions it has been noticed that the use of a mass-weighted p and T over a simple average determined by layer boundary levels has made a difference on the order of .1K which is of the same order as the small scale noise observed in figure 6.

In the past, atmospheric states have been supplied to the intercomparisons, but no requirement to compare the intermediate step of converting the atmospheric profiles to layers has been made. The differences between models is now sufficiently small that some of the anomalies may be explained by variations in the methods of layering. In future intercomparisons, it is recommended that the layer values of pressure, temperature, absorber amount, etc..., used for evaluating the optical depth be returned as a requested quantity or instead of supplying atmospheric profiles, the layer information be supplied. The latter

would bypass the front-end processing of the atmospheres in the LBL model.

The effective optical depth plots imply that the optical depths are noisy, implying that small ripples may exist on the transmittance curves which can not be seen but could affect the calculation of the Jacobian. Small ripples may explain the small differential spikes noted on the SYNSATRAD sensitivity curves. Most of the differences between the sensitivity curves are undoubtedly a reflection of the differences between LBL forward models. Presumably as the difference between the forward models shrink, so will the differences in the gradient model.

Comparing Jacobians from an LBL point of view was not particularly useful, except as a nice verification for 4A. 4A determined its Jacobians from an analytical differentiation of the 4A model.

Although not particularly useful in the context of comparing LBL models, the Jacobian database created from this exercise is useful for its information content. Differentiation of other models is realistically possible. Like the 4A model, SYNSATRAD and FLBL use lookup tables which are easily differentiable; whereas differentiation of GENLN2 and LBLRTM could be difficult since the differentiation would have to be done on a line-by-line basis. In addition, the sensitivity curves are useful standards for the fast forward models to compare against and as indicators of the various channels sensitivities in the context of instrument noise. For example; it is evident that HIRS-12 is not as sensitive to 10% changes in upper tropospheric moisture as one would desire since the peak sensitivity for a wet atmosphere at .15K is less than the NEΔT of .3K.

In summary, the LBL's generally compare favourably. However there is a significant systematic discrepancy between GENLN2 and the other models in HIRS-11 and HIRS-12. In addition, HIRS-5 has some indeterminate problems at this time.

VI FUTURE CONSIDERATIONS

In the future, an intercomparison in the context of modelling an instrument should be more rigid on a number of points.

i) all models should use the same absorber list,

ii) more attention should be paid to high resolution spectra, thus simulated high resolution spectra should be requested in addition to spectrally averaged quantities

iii) request layer values of p, T and u used to evaluate k and χ

iv) submit the attenuated atmospheric emission term for each layer; these profiles might be more useful in targeting regions in the atmosphere where problems occur than transmittance profiles.

v) supply a complete atmosphere; ie, well-defined pressure and temperature profiles, and mixing ratio profiles for all applicable absorbers, and corresponding instrument measurements.

Some possible spinoff studies would be;

i) the impact of the method of layering on RT quantities

ii) impact of various parameterizations of CO_2, O_2, N_2, etc...

ACKNOWLEDGMENTS

We gratefully acknowledge the work of Drs A. Chédin and R. Armante, Dr D.P. Edwards, Dr. J.R. Drummond, Drs S.A. Clough and M.J. Iacono, and Dr. S.A. Tjemkes for the development and maintenance of their LBL models, 4A and STRANSAC, GENLN2, GENASIS, LBLRTM and SYNSATRAD; and all the spectroscopists who contribute to the physics and databases so necessary to the field of atmospheric radiative transfer. We also thank C. Chouinard for his useful comments and M. Larocque for his preparation of the main database for dissemination and his work on the intercomparison website.

REFERENCES

Anderson, G.P., S.A. Clough, F.X. Kneizys, J.H. Chetwood and E.P. Shettle, *AFGL Atmospheric Constituent Profiles (0-120km)*. Rep. AFGL-TR-86-0110, Air Force Geophysics Lab., Hanscom AFB, MA, USA, 1986.

Clough, S.A. and M.J. Iacono, *Line-by-line Calculation of Atmospheric Fluxes and Cooling Rates. 2: Application to Carbon Dioxide, Ozone, Methane, Nitrous Oxide and the Halocarbons*. J. Geophys. Res., **100**, 16,519-16,535, 1995.

Clough, S.A., F.X. Kneizys, and R.W. Davies, *Line Shape and the Water Continuum*. Atmos. Res., **23**, 229-241, 1989.

Cousin, C., R. Le Doucen, C. Boulet, and A. Henry, *Temperature Dependence of the Absorption in the Region Beyond the 4.3μm Band Head of CO2. 2: N2 and O2 Broadening*. App. Opt., **24**(22), 3899-3907, 1985.

Edwards, D.P., *GENLN2: A General Line-by-line Atmospheric Transmittance and Radiance Model*. NCAR Tech. Note NCAR/TN-367+STR, 1992.

Garand, L., D.S. Turner, M. Larocque, J. Bates, S. Boukabara, P. Brunel, F. Chevallier, G. Deblonde, R. Engelen, M. Hollingshead, D. Jackson, G. Jedlovec, J.Joiner, T. Kleespies, D.S. McKague, L. McMillin, J.-L. Moncet, J.R. Pardo, P.J. Rayer, E. Salathe, R. Saunders, N.A. Scott, P. Van Delst and H. Woolf, *Radiance and Jacobian Intercomparison of Radiative Transfer Models Applied to HIRS and AMSU Channels*, 2000. (submitted to JGR)

Jacquinet-Husson, N., E. Arie, J. Ballard, A. Barbe, G. Bjoraker, B. Bonnet, L.R. Brown, C. Camy-Peyret, J.P. Champion, A. Chédin, A.Chursin, C. Clerbaux, G. Duxbury, J.M. Flaud, N. Fourrie, A. Fayt, G. Graner, R. Gamache, A. Goldman, Vl. Golovko, G. Guelachvili, J.M. Hartmann, J.C. Hilico, J. Hillman, G. lefevre, E. lellouch, S.N. Mikhailenko, O.V. Naumenko, V. Nemtchinov, D.A. Newnham, A. Nikitin, J. Orphal, D.C. Reuter, C.P. Rinsland, L. Vl. G. Tyuterev, R.H. Tipping, S. Urban, P. Varanasi and M. Weber, *The 1997 Spectroscopic GEISA Databank*, J. Quant. Spectrosc. Radiat. Transfer, **61**, 541-554, 1999.

Lafferty, Walter J., Alexander M. Solodov, Alfons Weber, Wm. Bruce Olsen, and Jean-Michel Hartmann, *Infrared Collision-Induced Absorption by N_2 Near 4.3μm for Atmospheric Applications: Measurements and Empirical Modelling*. App. Opt., **35**(30), 5911-5917, 1996.

Perrin, M.Y. and J.M. Hartmann, *Temperature-Dependent Measurements and Modeling of Absorption by CO_2-N_2 Mixtures in the Far Line-Wings of the 4.3μm CO_2 Band*, J. Quant. Spectrosc. Radiat. Transfer, **42**(4), 311-317, 1989.

Planet, W.G., *Data Extraction and Calibration of TIROS-N/NOAA Radiometers*. NOAA Tech. Memo. NESS 107-Rev. 1, U.S. Dept. of Commerce, Washington, DC, 58pp, 1988.

Ridgway, W.L., R.A. Moose and A.C. Cogley, *Atmospheric Transmittance/Radiance Computer Code FASCOD2*, AFGL-TR-81-0357, Air Force Geophysics Lab., Hanscom AFB, MA, USA 1981.

Rodrigues, R., K.W. Jucks, N. Lacome, Gh. Blanquet, J. Walrand, W.A. Traub, B. Khalil, R. Le Doucen, A. Valentin, C.Camy-Peyret, L. Bonamy, and J.-M. Hartmann, *Model, Software, and Database for Computation of Line-Mixing Effects in Infrared Q branches of Atmospheric CO_2. I. Symmetric Isotopomers*, J. Quant. Spectrosc. Radiat. Transfer, **61**(2), 153-184, 1999.

Rothman, L.S., C.P. Rinsland, A. Goldman, S.T. Massie, D.P. Edwards, J.-M. Flaud, A. Perrin, C. Camy-Peyret, V. Dana, J.-Y. Mandin, J. Schroeder, A. McCann, R.R. Gamache, R.B. Wattson, K.Yoshino, K.V. Chance, K.W. Jucks, L.R. Brown, V. Nemtchinov, and P. Varanasi, *The HITRAN Molecular Spectroscopic Database and HAWKS (HITRAN Atmospheric Workstation): 1996 Edition*. J. Quant. Spectrosc. Radiat. Transfer, **60**(5), 665-710, 1998.

Saunders, R.W., M. Matricardi and P. Brunel, *An Improved Fast Radiative Transfer Model for Assimilation of Satellite Radiance Observations*, Quart. J. Roy. Meteor. Soc. **125**, 1407-1425, 1999.

Scott, N.A. and A Chédin, *A Fast Line-by-Line Method for Atmospheric Absorption Computations: The Automated Atmospheric Absorption Atlas*. J. Applied. Meteor., **20**, 802-812, 1981.

Scott, N.A., *A Direct Method of Computation of the Transmission Function of an Inhomogeneous Gaseous Medium. PartI: Description of the Method and Influence of Various Factors*, J. Quant. Spectrosc. Radiat. Transfer, **14**, 691-704, 1974.

Soden, B., S. Tjemkes, J. Schmetz, R. Saunders, J. Bates, B. Ellingson, R. Engelen, L. Garand, D. Jackson, G. Jedlovec, T. Kleespies, D. Randel, P. Rayer, E. Salathe, D. Schwarzkopf, N. Scott, B. Sohn, S. de Souza-Machado, L. Strow, D. Tobin, D. Turner, P. van Delst and T. Wehr, *An Intercomparison of Radiation Codes for Retrieving Upper-Tropospheric Humidity in the 6.3-μm Band: A Report from the First GVaP Workshop*, Bull. Am. Meteorol. Soc., **81**, 797-808, 2000.

Strow, L.L. and D Reuter, *Effect of Line Mixing on Atmospheric Brightness Temperatures Near 15μm*, App. Opt., **27**(5), 872-878, 1988.

Thibault, F., V. Menoux, R. Le Doucen, L. Rosenmann, J.-M. Hartmann, and Ch. Boulet. *Infrared Collision-Induced Absorption by O_2 Near 6.4μm for Atmospheric Applications: Measurements and Empirical Modelling*. App. Opt., **36**(3), 563-567, 1997.

Timofeyov, Y.M. and M.V. Tonkov, *Effect of the Induced Oxygen Absorption Band on the Transformation of Radiation in the 6 micron Region of the Earth's Atmosphere*, Izvetiya, Atmos. Oceanic Phys., **14**, 437-441, 1978.

Tjemkes, S.A. and J. Schmetz, *Synthetic Satellite Radiances using the Radiance Sampling Method*, J. Geophy. Res., **102**(D2), 1807-1818, 1997.

Turner, D.S. and C.B. Chouinard, *An Attempt to Understand and Correct Some of the Errors of Forward Radiative Transfer Models*. Technical Proceedings of the Ninth International TOVS Study Conference, Igls, Austria, 20-26 February, 499-508, 1997.

Turner, D.S., J.R. Drummond, Z.Z. Yu and J. Cormier, *GENASIS: A line-by-line Radiative Transfer Tool for the Atmospheric Sciences*, 30th Canadian Meteorological and Oceanographic Society, Toronto, Ont., Canada, 26-31 May, 1996.

Turner, D.S., *Absorption Coefficient Estimation Using A Two Dimensional Interpolation Procedure*. J. Quant. Spectrosc. Radiat. Transfer, **53**(6), 633-637, 1995.

APPENDIX I

The intercomparison atmospheric state set was chosen to be diverse in terms of temperature, ozone and water vapour. The first six states in the subset are the AFLG reference states (Anderson et al, 1986). The rest of the states were extracted from a working set of 189 states which was developed at MSC (Turner, 1997). Each atmospheric state in the working set consists of an altitude profile, pressure profile, temperature profile and volume mixing ratio profiles for H_2O, CO_2, O_3, N_2O, CO, CH_4, O_2 and N_2. The volume mixing ratios of CO_2, O_2 and N_2 are fixed to 360ppmv, .209 and .781, respectively and the volume mixing ratio profiles of N_2O, CO and CH_4 are set to one of the AFGL reference states according to their latitude-longitude tag[10].

The next 12 states were selected by binning the 'column temperature' of each temperature profile into one of 12 bins. One state is drawn from each of the bins to represent that bin. The procedure was repeated to draw 24 more states based on total column ozone and total column water, 12 of each. The water vapour profiles were checked for saturation and any level found to exceed 95% relative humidity was reset to 95% relative humidity. This procedure resulted in a set of states with a wide range of temperature, ozone and water vapour. In order to maintain diversity, the final list was checked to ensure there are no duplicate states. If a duplicate was found, then a different state was drawn from the bin.

The column temperature C_T is defined as;

$$C_T = \frac{1}{T_o} \sum_{j=2}^{N_{lev}} (T_j - T_j^{ref}) (p_j - p_{j-1})$$

The reference temperature profile, T^{ref} is the US standard temperature profile (AFGL 6).

---

[10] The original states temperature, H_2O and O_3 profiles were extracted from retrieved SAGEII data and MSC NWP simulations. As there were lat/long coordinates associated with them, suitable AFGL profiles for the other absorber could be assigned to the state.

The water vapour and ozone column amounts are defined as

$$C_{H2O} = \frac{1000\,L R_{gas} T_o}{N_o p_o g_o} \sum_{j=2}^{N_{lev}} (q_j - q_{j-1})\,(p_j - p_{j-1}) \quad \textit{and} \quad C_{O_3} = \frac{100\,R_{gas} T_o}{M_{dry} P_o T_o} \sum_{j=2}^{N_{lev}} (c_j - c_{j-1})\,(p_j - p_j - 1)$$

where q is the specific humidity (g/kg), c is the ozone volume mixing ratio (ppmv), T_o is the standard pressure (273.15K) p_o is the standard pressure (1013.25mb), M_{dry} is the mass of dry air (28.964g/mol), R_{gas} is the gas constant (8.3143J/K/mol), g_o is the acceleration due to gravity 9.80616m/sec^2, L is Loschmidt's number (2.68684x10^{19}molecules/cm^3) and N_o is Avagadro's number (6.02217x10^{23}molecules/mol).

Some models use specific mass, q, instead of volume mixing ratio, c, as a variable. To convert from one to the other the following formula was supplied,

$$q_{gas} = \frac{c_{gas} M_{gas}}{(1 - c_w) M_{dry} + c_w M_w}$$

where M_{dry} is the molecular weight of dry air (28.964g/mol), M_{gas} is the molecular weight of the absorber (18g/mol for H_2O, 44g/mol for CO_2, etc...), c_{gas} is the absorber's volume mixing ratio and c_w is the volume mixing ratio of H_2O.

APPENDIX II

HIRS-2		BT(X) - BT(GENLN2)						BT(X) - BT(GENLN2)						BT(X) - BT(GENLN2)				
PROF	GENLN2 (K)	4A (K)	FLBL (K)	RTM (K)	SYNS (K)	PROF	GENLN2 (K)	4A (K)	FLBL (K)	RTM (K)	SYNS (K)	PROF	GENLN2 (K)	4A (K)	FLBL (K)	RTM (K)	SYNS (K)
1	220.224	-.096	-.270	-.070	-.428	15	218.451	-.058	-.171	-.059	-.223	29	219.840	-.084	-.289	-.051	-.291
2	228.171	-.087	-.200	-.086	-.348	16	215.727	-.078	-.196	-.041	-.357	30	220.656	-.095	-.215	-.044	-.409
3	219.470	-.013	-.016	.003	-.061	17	219.967	-.086	-.268	-.056	-.334	31	225.899	-.096	-.266	-.030	-.325
4	232.732	-.070	-.113	-.066	-.269	18	221.328	-.092	-.228	-.063	-.422	32	220.748	-.091	-.217	-.059	-.412
5	217.054	.014	.020	.034	.072	19	222.917	-.035	-.014	-.004	-.165	33	222.000	-.091	-.213	-.065	-.410
6	223.890	-.062	-.126	-.061	-.252	20	218.134	-.081	-.178	-.035	-.406	34	215.230	-.001	.050	.034	-.013
7	222.787	-.119	-.339	-.062	-.393	21	223.009	-.061	-.135	-.056	-.251	35	235.475	-.067	-.152	-.094	-.221
8	229.937	-.039	-.054	-.043	-.135	22	222.042	-.091	-.225	-.065	-.423	36	237.978	-.120	-.365	-.126	-.487
9	221.042	-.094	-.244	-.057	-.379	23	217.238	-.078	-.173	-.029	-.359	37	221.213	-.019	-.017	-.020	-.071
10	235.227	-.100	-.306	-.148	-.353	24	219.887	-.032	-.152	.001	-.029	38	217.622	-.042	-.085	-.051	-.151
11	224.126	-.048	-.170	-.085	-.171	25	231.148	-.080	-.143	-.091	-.263	39	220.255	-.029	-.087	-.039	-.091
12	211.673	.048	.220	.123	.166	26	220.176	-.090	-.284	-.069	-.385	40	228.329	-.038	-.052	-.041	-.134
13	208.509	.013	.111	.089	.047	27	219.183	-.092	-.239	-.071	-.379	41	237.405	-.062	-.168	-.112	-.206
14	231.840	-.058	-.047	-.044	-.227	28	219.517	-.087	-.276	-.061	-.351	42	230.368	-.049	-.096	-.063	-.172

Table IIa: The relative TOA brightness temperature of the LBL models (excluding GENLN2) with respect to GENLN2 as a function of profile and the absolute brightness temperature of GENLN2 for HIRS-2.

HIRS-5		BT(X) - BT(GENLN2)						BT(X) - BT(GENLN2)						BT(X) - BT(GENLN2)				
PROF	GENLN2 (K)	4A (K)	FLBL (K)	RTM (K)	SYNS (K)	PROF	GENLN2 (K)	4A (K)	FLBL (K)	RTM (K)	SYNS (K)	PROF	GENLN2 (K)	4A (K)	FLBL (K)	RTM (K)	SYNS (K)
1	245.687	-.079	-.589	.448	-.272	15	242.266	-.077	-.515	.422	.043	29	245.550	-.054	-.434	.442	-.324
2	245.802	-.076	-.571	.381	-.310	16	244.832	-.096	-.464	.433	-.106	30	246.788	-.069	-.489	.417	-.344
3	235.825	-.059	-.480	.364	-.135	17	245.992	-.073	-.530	.460	-.322	31	230.040	-.139	-.330	.228	-.598
4	243.979	-.082	-.554	.314	-.272	18	247.726	-.067	-.765	.516	-.162	32	247.052	-.086	-.618	.451	-.205
5	230.708	-.051	-.352	.326	-.092	19	229.826	-.087	-.311	.231	-.241	33	245.108	-.085	-.583	.429	-.270
6	240.157	-.085	-.649	.412	-.202	20	245.962	-.094	-.553	.446	-.112	34	237.089	-.070	-.643	.433	.092
7	226.314	-.179	-.355	.290	-.481	21	239.157	-.079	-.632	.406	-.151	35	239.545	-.095	-.524	.262	-.281
8	230.235	-.063	-.205	.112	-.186	22	248.545	-.082	-.827	.521	-.129	36	235.838	-.133	-.304	.185	-.376
9	231.557	-.122	-.383	.315	-.457	23	247.109	-.087	-.632	.468	-.230	37	233.861	-.069	-.374	.307	-.082
10	235.032	-.119	-.373	.254	-.216	24	243.448	-.054	-.412	.387	-.271	38	230.848	-.101	-.613	.410	-.116
11	235.379	-.101	-.601	.410	.058	25	244.178	-.085	-.539	.355	-.304	39	229.388	-.078	-.342	.279	-.057
12	234.003	-.055	-.611	.436	.014	26	245.458	-.087	-.493	.445	-.248	40	232.108	-.065	-.243	.171	-.149
13	236.202	-.077	-.568	.487	-.133	27	246.258	-.080	-.574	.452	-.269	41	235.189	-.090	-.301	.180	-.089
14	242.384	-.084	-.582	.313	-.154	28	246.247	-.049	-.436	.440	-.310	42	232.256	-.079	-.376	.197	-.149

Table IIb: The relative TOA brightness temperature of the LBL models (excluding GENLN2) with respect to GENLN2 as a function of profile and the absolute brightness temperature of GENLN2 for HIRS-5.

HIRS-9		BT(X) - BT(GENLN2)						BT(X) - BT(GENLN2)						BT(X) - BT(GENLN2)				
PROF	GENLN2 (K)	4A (K)	FLBL (K)	RTM (K)	SYNS (K)	PROF	GENLN2 (K)	4A (K)	FLBL (K)	RTM (K)	SYNS (K)	PROF	GENLN2 (K)	4A (K)	FLBL (K)	RTM (K)	SYNS (K)
1	275.705	.007	-.046	.124	1.014	15	265.519	-.072	-.063	.052	1.049	29	275.492	.061	.007	.185	.902
2	267.822	.071	.051	.171	.598	16	267.685	-.060	-.092	.058	.896	30	278.114	.034	-.075	.188	1.064
3	248.214	.085	.063	.155	.239	17	278.237	.019	.002	.169	1.014	31	241.920	.041	-.035	.126	-.579
4	262.603	.085	.049	.164	.319	18	287.469	-.017	-.049	.117	1.434	32	278.579	-.084	-.112	.050	1.218
5	238.303	.070	.043	.114	.131	19	235.381	.081	.006	.113	-.276	33	274.076	-.061	-.114	.086	1.038
6	261.935	.067	.043	.149	.548	20	273.604	-.092	-.099	.038	1.058	34	259.679	.025	.050	.128	.894
7	240.460	.019	-.063	.092	-.481	21	259.737	.040	.013	.134	.551	35	256.091	.034	.003	.114	.080
8	234.026	.027	-.018	.063	-.349	22	288.271	-.052	-.075	.075	1.489	36	246.480	.042	-.030	.086	-.550
9	242.439	.073	-.014	.140	-.339	23	280.193	-.111	-.118	.040	1.253	37	243.279	.059	.037	.117	.169
10	247.286	.003	-.044	.047	-.095	24	261.408	.022	.009	.114	.652	38	245.907	.052	.021	.137	.243
11	254.834	-.013	-.018	.062	.719	25	266.822	.095	.067	.189	.523	39	236.247	.040	-.002	.090	.020
12	250.805	.092	.081	.202	.516	26	274.145	.002	-.026	.141	.957	40	236.604	.038	-.020	.079	-.239
13	256.813	.058	.053	.195	.643	27	277.163	-.019	-.080	.122	1.147	41	243.153	-.001	-.030	.038	-.095
14	259.377	.082	.063	.161	.328	28	275.430	.111	.044	.214	.965	42	238.650	.055	-.005	.078	-.261

Table IIc: The relative TOA brightness temperature of the LBL models (excluding GENLN2) with respect to GENLN2 as a function of profile and the absolute brightness temperature of GENLN2 for HIRS-9.

HIRS-10		BT(X) - BT(GENLN2)						BT(X) - BT(GENLN2)						BT(X) - BT(GENLN2)				
PROF	GENLN2 (K)	4A (K)	FLBL (K)	RTM (K)	SYNS (K)	PROF	GENLN2 (K)	4A (K)	FLBL (K)	RTM (K)	SYNS (K)	PROF	GENLN2 (K)	4A (K)	FLBL (K)	RTM (K)	SYNS (K)
1	289.467	.079	.040	.089	.021	15	280.765	-.017	-.002	.009	.051	29	282.910	.268	.116	.190	-.010
2	287.125	.011	.022	.046	.073	16	282.888	-.046	.000	.004	.081	30	286.324	.191	.061	.156	-.036
3	269.670	-.054	.000	.005	.066	17	287.867	.171	.110	.163	.006	31	249.960	-.045	.002	.005	-.007
4	281.249	.012	.016	.031	.056	18	301.527	.181	.118	.155	.023	32	293.002	-.012	.001	.030	.051
5	256.302	-.036	.003	.000	.063	19	251.346	-.041	.001	.001	.064	33	287.787	.067	.026	.066	.028
6	282.969	-.030	.013	.024	.067	20	288.125	-.057	.003	.006	.086	34	279.474	-.036	-.001	.013	.012
7	246.923	-.044	.001	.001	-.003	21	280.903	-.034	-.007	.012	.035	35	270.355	-.040	.001	.010	.025
8	242.422	-.048	.000	.001	.044	22	304.751	.074	.050	.082	.110	36	253.527	-.014	-.001	.003	.001
9	257.284	-.036	-.001	-.002	.036	23	294.337	-.004	-.027	.012	.046	37	260.563	-.051	.001	.000	.058
10	257.237	-.024	.001	.000	.018	24	276.548	-.005	.030	.033	.080	38	268.769	-.070	-.002	.002	.042
11	273.396	-.059	-.005	.001	.043	25	282.083	.137	.055	.098	.005	39	253.265	-.032	.003	.001	.061
12	274.583	-.058	-.004	.005	.035	26	285.070	.132	.069	.132	.022	40	248.717	-.059	.002	.001	.067
13	277.206	-.047	.002	.007	.038	27	290.265	.066	.031	.088	-.001	41	252.611	-.019	.000	.000	.040
14	279.803	-.047	.000	.013	.069	28	284.812	.290	.127	.219	-.007	42	254.485	-.052	.003	.002	.071

Table IId: The relative TOA brightness temperature of the LBL models (excluding GENLN2) with respect to GENLN2 as a function of profile and the absolute brightness temperature of GENLN2 for HIRS-10.

HIRS-11		BT(X) - BT(GENLN2)						BT(X) - BT(GENLN2)						BT(X) - BT(GENLN2)				
PROF	GENLN2 (K)	4A (K)	FLBL (K)	RTM (K)	SYNS (K)	PROF	GENLN2 (K)	4A (K)	FLBL (K)	RTM (K)	SYNS (K)	PROF	GENLN2 (K)	4A (K)	FLBL (K)	RTM (K)	SYNS (K)
1	261.045	-.221	-.087	-.123	-.029	15	260.282	-.270	-.118	-.142	-.110	29	253.626	-.200	-.127	-.189	-.121
2	260.096	-.224	-.065	-.081	.041	16	263.685	-.238	-.091	-.106	-.034	30	261.180	-.284	-.206	-.235	-.126
3	252.227	-.297	-.070	-.045	.079	17	253.875	-.172	-.070	-.110	-.075	31	242.771	-.169	-.038	-.019	.422
4	255.719	-.272	-.098	-.095	.070	18	261.034	-.222	-.104	-.174	-.124	32	268.658	-.253	-.076	-.101	-.027
5	246.111	-.245	-.060	-.043	.079	19	242.513	-.237	-.065	-.037	.148	33	262.383	-.264	-.110	-.154	-.059
6	254.949	-.317	-.044	-.028	.067	20	267.929	-.220	-.028	-.015	.067	34	255.445	-.342	-.060	-.037	-.007
7	240.299	-.217	-.073	-.067	.384	21	259.057	-.318	-.096	-.085	.036	35	249.669	-.362	-.063	-.016	.194
8	237.822	-.110	-.025	-.015	.146	22	263.870	-.225	-.070	-.086	-.092	36	245.141	-.205	-.061	-.043	.327
9	246.788	-.284	-.088	-.075	.247	23	267.879	-.232	-.037	-.020	.005	37	249.542	-.240	-.059	-.041	.081
10	247.786	-.241	-.076	-.056	.202	24	251.311	-.182	-.073	-.077	-.010	38	253.605	-.375	-.115	-.074	.102
11	254.897	-.361	-.071	-.043	.035	25	253.367	-.263	-.099	-.145	-.028	39	243.832	-.232	-.047	-.025	.088
12	254.737	-.358	-.095	-.080	.007	26	254.888	-.212	-.074	-.092	-.053	40	243.904	-.099	-.021	-.015	.132
13	257.141	-.296	-.053	-.026	.095	27	261.234	-.206	-.072	-.114	-.070	41	245.614	-.168	-.039	-.024	.103
14	256.052	-.318	-.091	-.082	.040	28	255.404	-.193	-.141	-.216	-.155	42	245.590	-.209	-.028	-.004	.184

Table IIe: The relative TOA brightness temperature of the LBL models (excluding GENLN2) with respect to GENLN2 as a function of profile and the absolute brightness temperature of GENLN2 for HIRS-11.

HIRS-12		BT(X) - BT(GENLN2)						BT(X) - BT(GENLN2)						BT(X) - BT(GENLN2)				
PROF	GENLN2 (K)	4A (K)	FLBL (K)	RTM (K)	SYNS (K)	PROF	GENLN2 (K)	4A (K)	FLBL (K)	RTM (K)	SYNS (K)	PROF	GENLN2 (K)	4A (K)	FLBL (K)	RTM (K)	SYNS (K)
1	245.473	-.105	-.233	-.296	-.313	15	246.288	-.061	-.166	-.221	-.271	29	238.299	-.482	-.460	-.577	-.549
2	244.195	-.095	-.207	-.234	-.257	16	247.685	-.067	-.141	-.184	-.279	30	247.620	-.310	-.454	-.437	-.446
3	239.418	-.085	-.104	-.116	-.090	17	237.499	-.447	-.426	-.514	-.495	31	234.651	-.084	.020	.074	.165
4	242.122	-.176	-.262	-.308	-.255	18	245.522	-.212	-.334	-.412	-.404	32	252.543	.078	-.046	-.083	-.186
5	234.969	-.140	-.062	-.054	-.022	19	233.406	-.145	-.071	-.047	.009	33	246.345	-.057	-.120	-.179	-.255
6	238.473	-.127	-.128	-.152	-.163	20	250.367	.085	-.053	-.041	-.171	34	239.406	-.067	-.081	-.058	-.127
7	231.572	-.170	.018	.032	.147	21	245.446	-.030	-.103	-.088	-.097	35	236.504	-.137	-.127	-.132	-.070
8	232.313	-.017	.028	.066	.127	22	247.914	-.142	-.284	-.393	-.383	36	234.959	-.153	-.065	-.049	-.057
9	235.151	-.172	-.096	-.092	-.026	23	250.589	.045	-.113	-.126	-.228	37	237.196	-.120	-.061	-.040	-.047
10	237.235	-.129	-.067	-.059	-.036	24	236.800	-.374	-.385	-.423	-.383	38	243.051	-.029	.009	.021	.153
11	239.610	-.105	-.010	.025	-.026	25	237.563	-.264	-.248	-.325	-.321	39	233.637	-.139	-.026	.006	.018
12	241.520	-.042	-.052	-.056	-.014	26	237.049	-.410	-.388	-.464	-.476	40	238.165	.029	.064	.099	.171
13	240.855	-.113	-.093	-.064	-.075	27	245.007	-.138	-.227	-.285	-.349	41	236.899	-.090	.030	.082	.098
14	241.847	-.095	-.158	-.191	-.197	28	240.262	-.409	-.421	-.534	-.514	42	235.038	-.105	.043	.139	.153

Table IIf: The relative TOA brightness temperature of the LBL models (excluding GENLN2) with respect to GENLN2 as a function of profile and the absolute brightness temperature of GENLN2 for HIRS-12.

HIRS-15		BT(X) - BT(GENLN2)					BT(X) - BT(GENLN2)					BT(X) - BT(GENLN2)		
PROF	GENLN2 (K)	4A (K)	FLBL (K)	RTM (K)	PROF	GENLN2 (K)	4A (K)	FLBL (K)	RTM (K)	PROF	GENLN2 (K)	4A (K)	FLBL (K)	RTM (K)
1	256.975	.042	.166	.266	15	251.144	.046	.137	.200	29	257.273	.065	.194	.326
2	255.008	.039	.125	.208	16	254.739	.048	.167	.219	30	258.721	.063	.188	.312
3	241.233	.038	.073	.134	17	258.216	.050	.189	.320	31	231.689	.088	.052	.101
4	250.419	.043	.085	.167	18	263.221	.032	.212	.353	32	258.198	.035	.159	.232
5	233.855	.040	.054	.102	19	231.184	.048	.037	.082	33	255.616	.047	.155	.245
6	248.054	.037	.105	.191	20	256.156	.044	.161	.214	34	244.617	.035	.096	.174
7	227.626	.094	.068	.125	21	246.307	.037	.099	.176	35	242.036	.052	.042	.110
8	229.830	.039	.003	.032	22	263.636	.023	.197	.311	36	236.430	.080	.046	.092
9	234.881	.071	.081	.136	23	258.588	.035	.167	.234	37	237.186	.044	.060	.108
10	235.697	.062	.051	.103	24	252.073	.046	.131	.206	38	235.202	.037	.069	.143
11	240.052	.040	.083	.154	25	252.447	.056	.123	.231	39	231.242	.043	.044	.089
12	240.884	.033	.076	.150	26	256.474	.047	.177	.285	40	232.643	.042	.020	.056
13	244.946	.049	.128	.197	27	258.300	.042	.178	.281	41	234.866	.047	.021	.062
14	247.903	.036	.073	.148	28	258.674	.057	.196	.333	42	232.522	.038	.010	.055

Table IIg: The relative TOA brightness temperature of the LBL models (excluding GENLN2) with respect to GENLN2 as a function of profile and the absolute brightness temperature of GENLN2 for HIRS-15.